

# S-Band CubeSat Patch Antenna

ECE 499

August 11, 2025



University  
of Victoria



**Group ID:** 01

**Faculty supervisor:** Levi Smith

**Co-supervisor (if any):** Levente Buzas

**Team Information:**

Name	V Number
Logan Dring	V00984802
Jordan Bona	V00969093
Jonathan Boyce	V00967622
Darius Clayton	V010122665



## **Acknowledgment**

Thank you to Levente Buzas and the rest of the team at UVIC CfAR for the opportunity and resources to work on this project. As well a special thanks to Dr. Levi Smith for advising our team through all stages of the antenna design. Thank you to our friends and family for supporting us through this project and our years of study. Lastly, thank you to the University of Victoria for preparing us to complete this degree capstone project.

## **Executive Summary**

This report details the end-to-end design, simulation, and validation of a high-performance S-band patch antenna for the University of Victoria's PolarLink CubeSat platform. Addressing the need for a compact, lightweight, and efficient communication system for low Earth orbit (LEO) research, the project's primary objective was to develop an antenna capable of operating within the 2.0-2.3 GHz S-band frequency range. The final design is a square stacked patch hybrid feed antenna with mismatched patch sizes and corner truncation, engineered to achieve a wide bandwidth and circular polarization. The design was optimized using full-wave electromagnetic simulations with Ansys HFSS. The prototype, fabricated on an FR-4 substrate, was physically tested against key performance specifications using a VNA and anechoic chamber. The antenna demonstrated an impedance bandwidth that was shifted slightly down in frequency from the required range but still met the VSWR requirement within the band. An antenna gain ranging of 6.3 dBi was achieved while an average axial ratio of 4.58 dB was recorded within the frequency band. The final results showed the antenna successfully met the gain, HPBW and mechanical constraints but failed to operate within the specified frequency band and fell short of the desired axial ratio. Likewise, the final space-flight version will require fabrication with a Rogers 4003C to meet efficiency requirements and material selection to meet outgassing requirements. The semi-successful outcomes from both simulation and testing validate the design as a viable communication solution for the PolarLink mission, with specific recommendations for future work outlined in the report.

# Table of Contents

1	Introduction.....	1
1.1	Background.....	1
1.2	Project Statement .....	1
1.3	Scope of Work .....	2
1.4	Motivation.....	2
1.5	EGBC Code of Ethics .....	3
2	Objectives .....	3
3	Design Specifications.....	4
4	Literature Survey .....	7
4.1	Patch Antennas.....	7
4.1.1	General Characteristics .....	7
4.1.2	Patch Antenna Shapes.....	8
4.1.3	Methods To increase Bandwidth .....	8
4.1.4	Methods to Achieve Circular Polarization.....	12
4.2	Current Market Analysis.....	15
4.3	Design Decisions .....	16
5	Team Duties & Project Planning .....	17
5.1	Team Roles .....	17
5.2	Project Challenges .....	18
6	Design Methodology & Analysis.....	18
6.1	Design 1: Single Rectangular Patch Antenna Design and Simulations .....	18
6.2	Design 2: Single Circular Patch Antenna Design and Simulations .....	25
6.3	Design 3: Extremely Electromagnetically Coupled Patch Antennas.....	30
6.4	Final Configurable Design: CubeSat S-Band EMCP Antenna.....	31
6.5	Analysis 1: Direct and Coupled Patch Size .....	32
6.6	Analysis 2: Impedance Matching via Probe Location .....	33
6.7	Analysis 3: Air Gap Height.....	34
6.8	Analysis 4: Truncated Corners to Achieve Circular Polarization.....	35
6.9	Analysis 5: Accounting for the Real World.....	36
6.9.1	Achieving the Air Gap in the Model.....	36
6.9.2	Manufacturing Considerations in the Model .....	37
6.10	PCB Design.....	39

7	Design & Prototype.....	40
7.1	Design Overview .....	40
7.2	Key Features .....	41
7.2.1	Mismatched Direct and Coupled Patch Sizes .....	41
7.2.2	Probe Location Impedance Matching .....	41
7.2.3	Large Air Gap .....	42
7.2.4	Corner Truncation.....	42
7.2.5	Substrate Material .....	43
7.2.6	Mechanical Considerations.....	43
7.3	Final Design Parameters .....	44
7.4	Performance Parameters .....	44
7.5	Design Shortcomings – Contributing Factors.....	45
7.5.1	EE-1: Bandwidth.....	45
7.5.2	EE-11: Axial Ratio.....	46
7.5.3	EE-12: Efficiency.....	46
7.6	Parts Required for Fabrication.....	46
8	Testing & Validation.....	47
8.1	Physical Test Plans .....	47
8.1.1	Bandwidth, Input Impedance, VSWR, and Efficiency Test Plan .....	47
8.1.2	Half-Power Beamwidth, Gain, and Axial Ratio Test Plan .....	48
8.1.3	Mass Measurement .....	49
8.1.4	Anechoic Chamber Setup .....	50
8.2	Software Simulations of Final Design .....	51
8.3	Physical Test Results .....	56
8.3.1	Bandwidth, Input Impedance, VSWR, and Efficiency Results .....	56
8.3.2	Half-Power Beamwidth, Gain, and Axial Ratio Results.....	60
8.3.3	Antenna Weight .....	64
9	Cost Analysis .....	65
9.1	Direct Cost Breakdown.....	65
9.2	Indirect Cost Breakdown .....	66
9.3	ROI Calculation .....	67
9.4	Cost-Reduction Strategies.....	67
10	Conclusion & Recommendations .....	68
10.1	Conclusion .....	68

10.2	Recommendations.....	68
11	References.....	70
	Appendix A: EMCO 3164-05 Calibration Certificate .....	71
	Appendix B: Project Website.....	74

# 1 Introduction

## 1.1 Background

To address limitations of traditional satellites, Defense Research and Development Canada (DRDC) is exploring low Earth orbit (LEO) satellite technologies to design a flexible, resilient, and secure space-based network capable of supporting diverse mission needs [1]. CfAR's approved proposal PolarLink will utilize a single CubeSAT, a class of satellite with standardized size and form factor, in sun synchronous orbit with a payload consisting of radio frequency (RF) and optical communication equipment intended for the facilitation of research [2]. Due to its low-profile, compact size, and light weight the preferred type of radio antenna for the CubeSAT will be a patch antenna, a very thin patch of conducting material placed on a dielectric substrate [1].

## 1.2 Project Statement

In response to Canada's Space Low Earth Orbit Architecture initiative (SpaceLEO), the University of Victoria Center for Aerospace Research (CfAR) has proposed the implementation and development of PolarLink a single CubeSat with the purpose of aiding research in the artic region. PolarLink requires the development of a communication system consisting of a radio transceiver and one or more patch antennas. Our team has been tasked with the development and initial testing of an S band patch antenna to facilitate the communication of the CubeSAT with multiple domestic and/or international commercial constellations, as well as several remote terminals across northern Canada (see figure 1). The patch antenna is to transmit and receive signals within the 2-4 GHz frequency range, also known as the S-band.

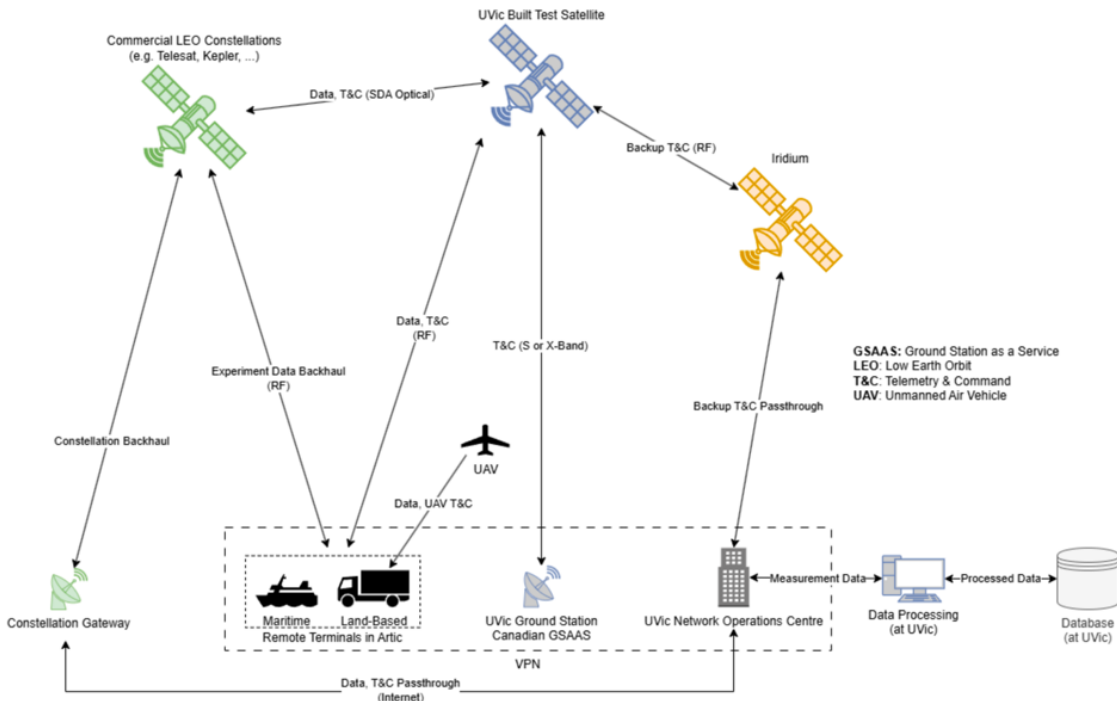


Figure 1.1: PolarLink technology demonstration high level concept.

## **1.3 Scope of Work**

This project focuses on the end-to-end design and validation of a compact S-band patch antenna intended for use on PolarLink's CubeSat platform. The scope of work encompasses the following key tasks:

### **1. Literature Review and Current Market Analysis:**

A comprehensive review of existing academic and industry literature on microstrip patch antennas, with a focus on S-band applications for small satellites. This includes identifying commercial off-the-shelf (COTS) solutions, evaluating their performance, and assessing design trade-offs relevant to CubeSat integration.

### **2. Full-Wave Electromagnetic Simulation (HFSS):**

High-fidelity, full-wave simulations using Ansys HFSS will be done to analyze the antenna's performance. Furthermore, iterative optimization will be done to ensure the antenna meets S-band communication requirements and the design requirements.

### **3. PCB Design in Altium Designer:**

The design of the patch antenna layout will be done using Altium Designer, ensuring compliance with CubeSat mechanical and electrical interface standards as well the project design constraints. The design will incorporate Rogers 4003C substrate material, 50 Ohms impedance matching features, and a single female SMA connector placement.

### **4. Fabrication of the Patch Antenna:**

A fabrication facility will be coordinated with to manufacture the PCB-based patch antenna design from the developed Gerber files.

### **5. Mounting Solution Development:**

A mechanical mounting solution will be chosen that secures the antenna to the CubeSat body while maintaining signal performance.

### **6. Testing of Antenna in Anechoic Chamber and with Vector Network Analyzer (VNA):**

Antenna performance testing in a radio frequency (RF) anechoic chamber and with a VNA will be performed to validate simulation results. Measurements will include gain, half power beam width, and antenna efficiency.

## **1.4 Motivation**

Designing an S-band patch antenna for a CubeSat presents a compelling opportunity to apply theoretical knowledge in electromagnetics, RF design, and space systems to a practical, real-world engineering challenge. CubeSats are rapidly transforming space exploration and communication due to their affordability and modularity, and reliable antenna systems are critical to their performance [1]. This project offers the chance to contribute to the advancement of small satellite technology by addressing the unique constraints of space communication such as size, weight, and efficiency, while gaining

hands-on experience with modern design tools like HFSS and Altium as well as access to the specialized equipment and tools at CfAR. The interdisciplinary nature of the work, bridging PCB design, RF simulation, and space application, makes it both intellectually rewarding and highly relevant to current industry needs.

Our proposed patch antenna seeks to meet the functionality of current market satellite communication systems at a fraction of the cost, allowing for the development of CubeSats to be further accessible to the wider public. This facilitates the democratization of space by allowing the opportunity for new players to utilize the final frontier instead of being restricted by costs.

## 1.5 EGBC Code of Ethics

Inherently due to the collaboration of this project with CfAR, all involved team members will adhere to the Engineers & Geoscientists of British Columbia (EGBC) Code of Ethics.

- Regarding principle 2 of the code of ethics all team members will utilize our course material and demonstrated previous knowledge pertaining to antennas and electromagnetics within its capabilities. For decisions outside of our capabilities we will rely on educated assistance from credible literature as well as our advisors at CfAR and our faculty advisor Dr. Smith.
- Regarding principle 3 of the code of ethics all work encompassed within this project will abide by any common law and applicable enactments including those of local Government, the International Telecommunication Union, and the National Spectrum Authorities.
- Regarding principle 11 of the code of ethics all individuals who have contributed professional work will be clearly identified. This information will be made available in our work breakdown structure and relavent project files.
- Regarding principle 12 of the code of ethics all work and documentation of the project will be given its proper care and due diligence.
- Lastly, regarding principle 13 of the code of ethics all team members will act at all times with fairness, courtesy and good faith towards all professional personnel including CfAR and the greater UVic body as well in accordance with the public interest.

## 2 Objectives

- To establish clear roles and responsibilities for each team member
- To Develop a Work Breakdown Structure (WBS) and Gantt chart to outline key milestones and timelines.
- To perform an extensive literature review on patch antennas to understand fundamental principles, design challenges, and recent advancements.
- To conduct a comprehensive market analysis of commercially available S-band antennas suitable for CubeSat applications.
- To utilize HFSS (High-Frequency Structure Simulator) to simulate potential antenna designs that align with mission constraints.

- To select the most promising antenna design based on its ability to meet or exceed project requirements.
- To refine the selected design through iterative HFSS simulations to optimize performance parameters.
- To complete the PCB layout of the S-band patch antenna using Altium Designer, ensuring compliance with electrical and mechanical specifications.
- To coordinate with fabrication services to manufacture the final PCB version of the antenna.
- To develop a reliable and space-constrained mounting solution for integrating the patch antenna into the CubeSat structure.
- To validate the performance of the fabricated antenna in an anechoic chamber and with a vector network analyzer to ensure it satisfies all technical constraints.
- To prepare a project poster and develop a dedicated website to effectively communicate the design process and results.

### 3 Design Specifications

The S band patch antenna is to meet the electrical and mechanical success criteria outlined in the project's requirements and constraints in Table 3.1 and Table . The results of our project will be utilized by CfAR to direct future development of PolarLink's communication system.

*Table 3.1: Electrical Specifications*

ID	Shall Statement	Method of Verification	Success Criteria
EE-1	The antenna shall be designed for operation in the 2025-2110 MHz and 2200-2290 MHz frequency range.	Test	Requirement EE-5 is verified.
EE-2	The antenna shall be a passive rectangular or circular patch antenna using printed circuit board (PCB) technology on Rogers 4003C substrate, or an array comprised of such antenna elements.	Design Review	Review of design documents shows that the requirement is satisfied.
EE-3	The antenna shall be designed to have a nominal input impedance of 50 Ohms over its frequency range of operation in EE-I.	Design Review	Review of design documents shows that the requirement is satisfied.
EE-4	The antenna electrical interface shall be a single female, SMA type connector located on the side opposite to the radiating element.	Design Review	Review of design documents shows that the requirement is satisfied.

EE-5	The antenna shall have a VSWR of 1.5:1 or better over its frequency range of operation in EE-I, as measured at the SMA connector.	Test	Measurement with a calibrated VNA indicates the desired VSWR at the connector.
EE-6	The antenna shall be able to handle at least 5 W of RF power.	Analysis	Theoretical analysis or simulations justify that desired power level is ok (e.g. no excessive dielectric heating, arcing).
EE-7	The antenna half-power beamwidth HPBW shall be at least 60 degrees.	Test	Anechoic chamber measurement with calibrated VNA support the desired HPBW.
EE-8	The antenna shall be circularly polarized, with the direction of circularity being either left hand circular polarization (LHCP) or righthand circular polarization (RHCP).	Test	Review of design documents shows that the requirement is satisfied.
EE-9	During production it shall be possible to configure the antenna for left hand circular polarization (LHCP) or righthand circular polarization (RHCP), using the same main printed circuit board element.	Design Review	Review of design documents shows that the requirement is satisfied.
EE-10	The antenna shall have at least 6 dBi gain along its direction of maximum radiation, which shall be aligned with the boresight of the antenna.	Test	Anechoic chamber
EE-11	The axial ratio of the antenna within its half power beam width (HPWB) shall be at most 3dB.	Analysis	Simulations of the axial ratio indicate that the requirement is met.
EE-12	The efficiency of the antenna shall be at least 90% or better over its frequency range of operation in EE-I.	Test	Analysis based on data from with calibrated VNA supports the desired efficiency.

Table 3.2: Mechanical Specifications

ID	Shall Statement	Method of Verification	Success Criteria
ME-1	The antenna shall be compatible with the Mechanical Interface Control Document (ICD) in Appendix A.	Fit Check	A 3D STEP model exported from Altium passes a SolidWorks fit check.

ME-2	The antenna shall comply with NASA guidelines for selecting all non-metallic materials based on available outgassing data [3]. The antenna shall not utilize any non-metallic materials with a Total Mass Loss (TML) greater than 1.0 percent or a Collected Volatile Condensable Material (CVCM) value of greater than 0.1 percent.	BOM Review	Review of bill of materials (BOM) shows that there are no parts of concerns.
ME-3	The antenna weight shall not exceed 100 grams.	Test	Weighing of antenna in its final configuration shows that requirement is met.
ME-4	The antenna shall comply with the CubeSat standard (see appendix B).	Design Review	Review of design documents shows that the requirement is satisfied.

During development of the project, it was discussed with the project supervisors and the team to alter some requirements considering feasibility and time constraints. A summary of the changes has been provided in

*Table 3.3: Revision to Design Specifications*

ID	Revision	Justification
EE-2	The antenna shall be a passive rectangular or circular patch antenna using printed circuit board (PCB) technology on Rogers 4003C <b>or FR-4</b> substrate, or an array comprised of such antenna elements.	It was observed that for the S-Band frequencies described in EE-1, that a FR-4 substrate could be used without compromising other design objectives and for a fraction of the price.
EE-5	The antenna shall have a VSWR of <b>1.5:1</b> <b>1.92:1</b> or better over its frequency range of operation in EE-I, as measured at the SMA connector.	With the narrow band behaviour of patch antennas, achieving a VSWR of 1.5:1 is possible but not for the entire frequency range. A VSWR of 1.92:1 corresponds to a return loss of -10dB which is another common convention for bandwidth.
EE-9	<b>During Prior to</b> production, it shall be possible to configure the antenna for left hand circular polarization (LHCP) or righthand circular polarization (RHCP), using the same main printed circuit board element.	The initial prototype focuses on achieving left hand circular polarization. However, future renditions of the antenna can be made to achieve this requirement by altering the PCB design.

EE-11	The <b>nominal</b> axial ratio of the antenna within its half power beam width (HPWB) shall be at most 3dB.	The axial ratio of a patch antenna is heavily dependant on the geometry which is tuned for a given frequency. Over the entire band, the axial ratio will change and worsen as the frequency changes.
ME-2	The <b>final</b> antenna shall comply with NASA guidelines for selecting all non-metallic materials based on available outgassing data [3]. The antenna shall not utilize any non-metallic materials with a Total Mass Loss (TML) greater than 1.0 percent or a Collected Volatile Condensable Material (CVCM) value of greater than 0.1 percent.	As will be discussed later, the prototype antenna uses nylon components. Nylon is not acceptable for space due to its outgassing performance. The final design will use ceramic components. The effects of nylon versus ceramic on antenna performance has been deemed negligible using HFSS.

## 4 Literature Survey

The following section will outline the basic structure and capabilities of patch antennas and outline alterations that can be made to the basic design to meet our design specifications. Solutions will be presented and their viability for this project will be assessed.

### 4.1 Patch Antennas

Patch Antennas are an example of a low-profile, low-cost and easily manufacturable antenna that are popular for high-performance aircraft, spacecraft and satellite applications. Major operational disadvantages of these antennas include their narrow bandwidth on the range of a few percent, low efficiency, low power, and poor polarization purity [2]. Single square or circular patch antennas are easy to design and can achieve the gain, HPBW, efficiency, and feed requirements of this project. The bandwidth and circular polarization requirements, however, require special topology or configurations to achieve and will be discussed in this section.

#### 4.1.1 General Characteristics

Patch antennas are also known as microstrip antennas and consist of very thin ( $t \ll \lambda_o$ , where  $\lambda_o$  is the free-space wavelength) patch of conducting material is placed on a dielectric substrate (with relative permittivity  $\epsilon_r$ ) above a ground plane.

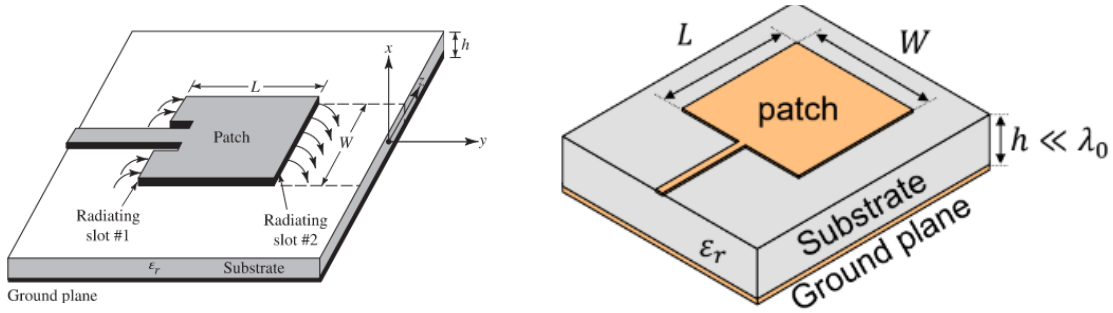


Figure 4.1: Patch (Microstrip) Antenna General Layout [2]

#### 4.1.2 Patch Antenna Shapes

Several patch shapes are presented in Figure

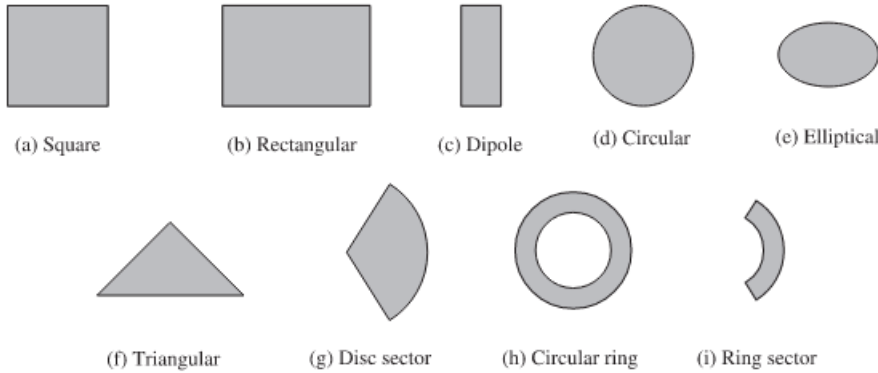


Figure 4.2: Patch Shapes [2]

Different patch shapes are used to allow:

- Wider bandwidths
- Reduced Sizes
- Circular Polarization
- Low Coupling Between Elements

The two most popular patch shapes (and the two we are constrained to for this project) are the circular and rectangular.

#### 4.1.3 Methods To increase Bandwidth

The frequency range of operation for a rectangular patch antenna is defined by the fractional bandwidth given by:

$$FBW = \frac{f_{high} - f_{low}}{f_r} * 100\% \quad (1)$$

For our case the fractional bandwidth can be calculated as

$$FBW = \frac{2290MHz - 2025MHz}{2157.5MHz} * 100\% \quad (2)$$

$$FBW = 12.28\% \quad (3)$$

This is an extremely high FBW for a patch antenna as the FBW for a generic rectangular or circular patch antenna is generally at most five percent [2] [3]

An approximate expression for the bandwidth (for  $VSWR \leq 2, |\Gamma| \leq \frac{1}{3}$  and  $h < 0.15\lambda_o$ ) for the rectangular patch is given by:

$$BW = \frac{16}{3\sqrt{2}} \left[ \frac{\epsilon_r - 1}{\epsilon_r^2} \right] \frac{h}{\lambda_o} \left( \frac{W}{L} \right) = 3.771 \left[ \frac{\epsilon_r - 1}{\epsilon_r^2} \right] \frac{h}{\lambda_o} \left( \frac{W}{L} \right) \quad (4) [3]$$

As the bandwidth of generic rectangular and circular patch antennas are inherently small (in the range of 2-5%) it is necessary to consider techniques to increase the bandwidth [1].

Some of the methods to increase the bandwidth for a patch antenna include:

1. Increasing the substrate height
2. Implementing an array of differently sized patches to achieve dual/multi band operation [4]
3. Electromagnetically coupled patches [5]

The first method, increasing the height of the substrate, is only capable of increasing the fractional bandwidth by at most a few percent above 5% and comes at the cost of lowered efficiency due to an increase in surface wave effects [1]. The marginal increase in bandwidth, higher material cost, and significantly lowered efficiency associated with this method make it unsuitable for the purposes of this project. The other two methods described will be expanded upon in the following sections

#### **4.1.3.1 Patch Antenna Arrays**

Generally, patch antenna arrays are utilized to increase the gain of a microstrip patch antenna, as single element patch antennas are inherently capable of at most 10dB of gain [6]. However, given the patches in the array are of varying sizes, an array can be used to illicit bandpass behaviour [4]. This application of arrays is of more interest in our scenario

as increasing gain is of less concern than increasing bandwidth. When designing two patch array for dual band operation, the patches can be sized to resonate at different desired frequencies but must also be sufficiently large spacing or a dedicated matching network in place to suppress mutual coupling between the patches that will detune the antenna.

The inter-element spacing for fixed beam arrays is generally selected to be less than a free space wavelength  $\lambda_o$  to avoid grating lobes (creating lobes that point away from the broadside direction) and greater than  $\frac{\lambda_o}{2}$  to provide enough room for the feed lines that connect the patches [6]. Given our central resonant frequency of  $f_r = 2157.5 \text{ MHz}$  the free space wavelength is given by:

$$\lambda_o = \frac{c}{f} = \frac{(3 * 10^8)}{(2157.5 * 10^6)} = 0.1379 \text{ [m]} = 13.7899 \text{ [cm]}$$

Given that our antenna designed is constrained to a 10cmx10cm area and the width of our patch is determined from the constrained resonant frequency, we are unable to use an array due to size constraints. The width of the patches required to operate around in the S-band are around 40mm as described in the design sections of the report.

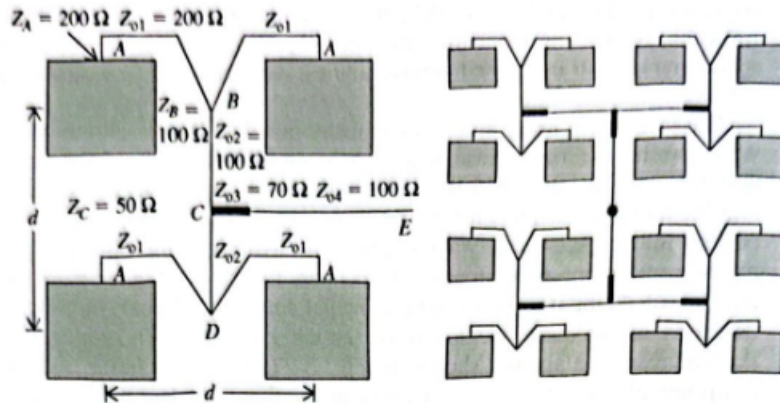


Figure 4.3: 4 element array with Feed Network impedance specifications (left) and 16 element array formed from sub arrays (right) [6]

#### 4.1.3.2 Electromagnetically Coupled Patches (EMCPs)

Our preferred method of increasing the bandwidth involves a multilayered structure in which two patches are stacked on top of each other as shown in Figure . Patch antennas with this configuration are often referred to as electromagnetically coupled patches (EMCPs) and been shown to be broadband radiators due to the nature of the electromagnetic coupling between patches on each layer [5].

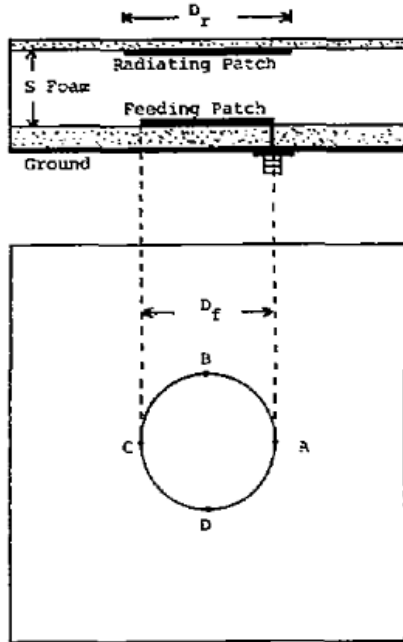


Figure 4.4: Stacked circular patch antenna Configuration [5]

In Figure , it is shown that the design consists of two circular patches of radius  $D_f$  and  $D_r$  separated by a distance  $S$ . The top patch is the radiating patch and is captively excited by the lower feeding patch which is in turn fed by a coaxial line. The space between the radiating and feeding patches is an air gap or filled with a material with a low dielectric constant like foam to support the radiating patch and provide proper separation between the patches.

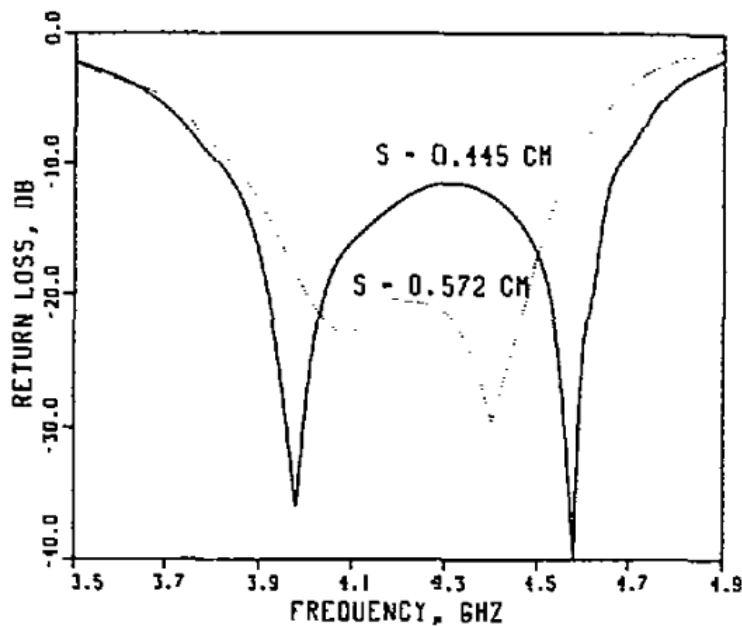


Figure 4.5: Return loss for stacked circular patch design [5]

As can be seen in Figure , the return loss of the EMCP design is characterized by two resonant frequencies that depend on the separation between the resonant and feeding patches. It can be seen that the upper resonant frequency shifts downward and the lower frequency shifts upward as the separation increases making bandwidth tuning based on patch dimensions difficult. Increasing the gap between the two patches decreases the capacitive coupling between the two patches causing the direct fed patch to dominate and results in more broadband, as opposed to dual band, behaviour. This idea will be expanded upon in later sections of the report. It is also important to note that methods for achieving circular polarization such as corner trimming are compatible [5].

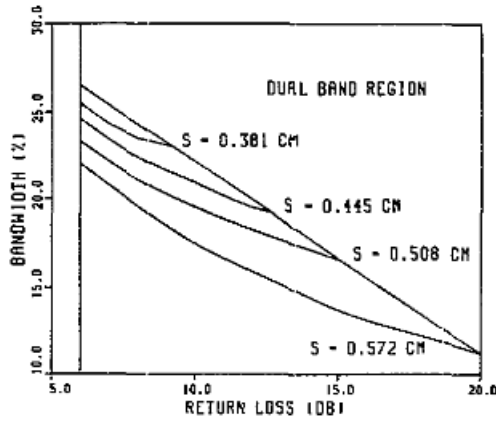


Figure 4.6: Bandwidth vs Return Loss for two-layer EMCP [5]

#### 4.1.4 Methods to Achieve Circular Polarization

As stated in section 3, the antenna is to be configured for circular polarization. On a patch antenna, several methods can be deployed to achieve circular polarization. These methods take advantage of dual feeds and the geometry of the patch itself. The goal is to create orthogonal fields separated by  $90^\circ$  such that if we trace the sum of these fields for a fixed moment in space over time, the vector traces a circle, hence the name circular polarization [1]

##### 4.1.4.1 Dual Feed Arrangement

In this arrangement a perfectly square patch is fed on two adjacent edges. The signals present on the edges are of the same source signal but a  $90^\circ$  phase change has been introduced. In theory, two orthogonal signals with a time-phase delay of  $90^\circ$  theoretically results in perfect circular polarization. Figure shows a rectangular patch using this arrangement, but a circular patch can also be used [1]. The physical geometry of the patch is simple if this solution is used. The complexity is introduced in the phase delay. A microstrip coupler can be designed to take advantage of transmission line properties and create the  $90^\circ$  phase delay. However, transmission line properties are dependent on frequency and since the operating frequency range of this antenna will span 265 MHz, unideal phase delays could occur.

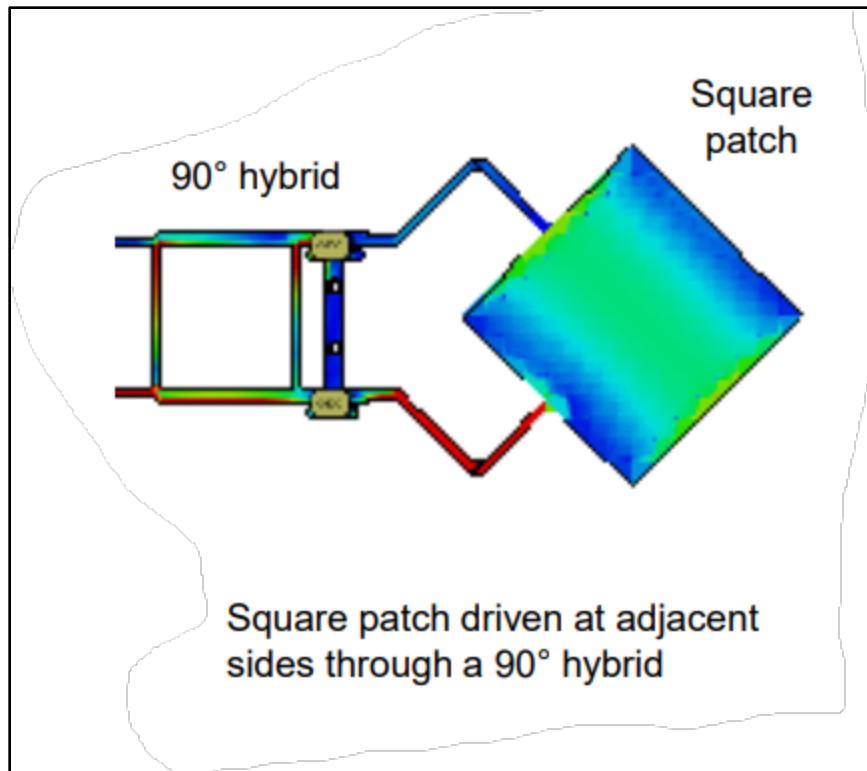


Figure 4.7: Dual Feed Square Patch Circularly Polarized Antenna

#### 4.1.4.2 Diagonal Feed Arrangement

Using a rectangular patch, the desired quadrature effect can be attained by designing the dimensions of the rectangular patch. If  $W$  and  $L$ , shown in Figure 4.8, slightly differ different TM modes are excited [1]. However, this method cannot achieve a large bandwidth easily.

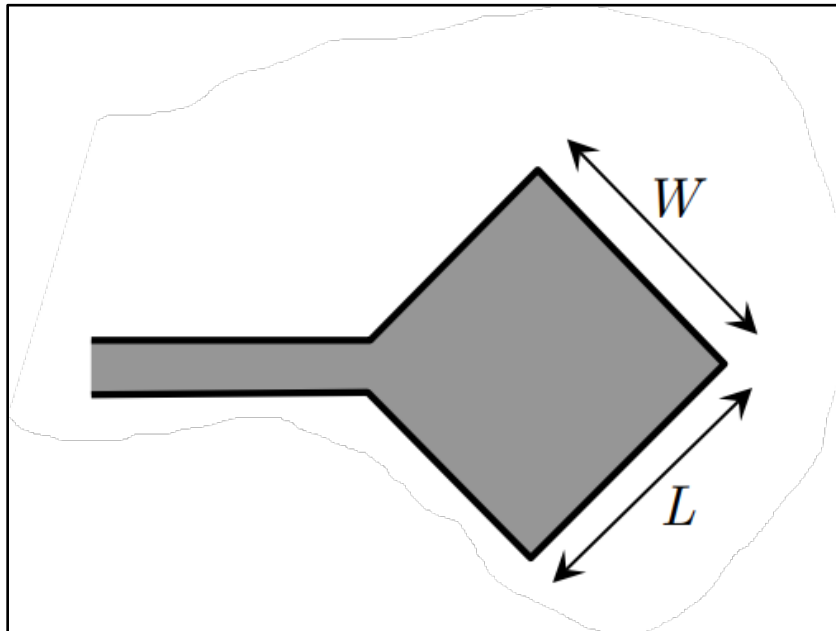


Figure 4.8: Nearly Rectangular Circularly Polarized Patch Antenna Fed from Corner

#### 4.1.4.3 Removal of Material Arrangements

For a single fed circular or square patch fed from the edge, the polarization can be influenced by removing material either in the form of slot in the middle of the patch or trimming the corners of the patch. Every version of this arrangement applied is shown in Figure 4.9 [1]. For each of these methods, the removal impacts the overall quality of the antenna. The quality factor, bandwidth, and efficiency are interrelated for a patch antenna. As such, there is no complete freedom to independently optimize any one quantity, and trade-offs must be considered to develop design an antenna with features that will fulfill the requirement of the project. The relations between the total quality factor, bandwidth, and efficiency are shown below:

$$FBW = \frac{1}{Q_t} \quad (5)$$

$$e_{cdsw} = \frac{\frac{1}{Q_{rad}}}{\frac{1}{Q_t}} = \frac{Q_t}{Q_{rad}} \quad (6) [7]$$

Where  $Q_{rad}$  is the quality factor due to radiation, FBW is the fractional bandwidth, and  $e_{cdsw}$  is the radiation efficiency of the antenna

By removing material, the total quality factor is changed. This change can be approximated as follows

$$\text{For square patches: } \frac{\Delta S}{S} = \frac{1}{2Q_t} \quad (7)$$

$$\text{For circular patches: } \frac{\Delta S}{S} = \frac{1}{1.841Q_t} \quad (8)$$

For the remainder of the analysis, a square patch with truncated corners will be considered due to its simplicity, but these results can be replicated for a circular patch and slot with ease. Re-writing the square patch equation we attain

$$Q_t = \frac{W \times L}{2 \times (C^2 \times 2)}; C = \text{length of corner removed} \quad (9)$$

By observation, the quality decreases as more material is removed.

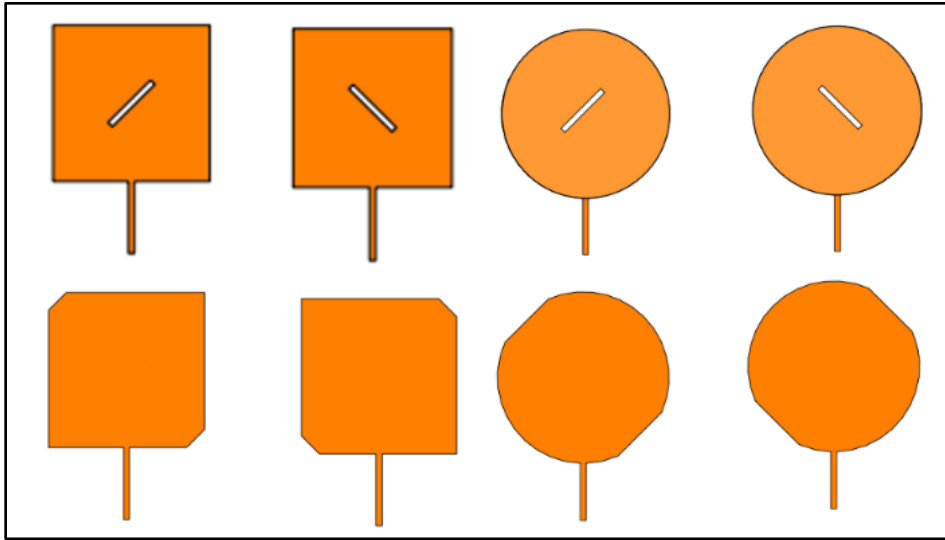


*Figure 4.9: Single Feed Circularly Polarized Patch Antennas [1]*

This method does have considerable disadvantages as the  $90^\circ$  phase difference is achieved by exciting orthogonal modes at different frequencies. Material is removed to alter the resonant frequencies causing radiation at different times. As one can imagine, this results in a worse bandwidth. Methods to balance a low axial ratio and wide bandwidth are explored more in section 6.8.

## 4.2 Current Market Analysis

The following outlines seven current market patch antennas that are compatible with the 1U CubeSats as well as function in the S-band of frequencies. While each product was evaluated for its relevance and performance, their specifications were found to be insufficient in meeting the project specifications outlined in Section 3.

*Table 4.1: Current Markey Solutions 1*

Item #	Product	Manufacturer	Part #	Cost	Connector Type	Substrate	Mounting	Dimensions - LxWxH (mm)	Mass (g)
1	S-band Patch Antenna	Cubecom	SANT	N/A	SMP	N/A	Multiple	85x110x6.2	83
2	Single Patch Antenna	IQSpacecom	202013	\$5,309.00	SMA (f)	Rogers Laminate	Flat - 4 screws	70x70x3.4	39
3	S-Band Dual Patch Antenna	IQSpacecom	202192	\$7,340.00	SMA (f)	Rogers Laminate	Flat - 4 screws	100x81x3.4	62
4	S-Band Patch Antenna	ISISPACE	100091	N/A	SMA (f)	N/A	Flat - 4 screws	80x80x5.5	<50
5	Wide Bandwidth S-Band Patch Antenna	EXA Aerospace	SSA01	\$3,501.00	SMA, MCX or Ufl	Rogers 4350	N/A	96.5x69.7x4.8	60
6	Wide Bandwidth Amplified S-band Patch Antenna	EXA Aerospace	SSA02	\$14,959.00	SMA, MCX or Ufl	Rogers 4350	Flat - 8 screws	97x80x4.8	60

7	S-Band CubeSat Antenna	AAC Clyde Space	Pulsar-Sant	N/A	SMA (f)	N/A	N/A	N/A	<50
---	------------------------	-----------------	-------------	-----	---------	-----	-----	-----	-----

Table 4.2: Current Market Solutions 2

Item #	Frequency Range	Input Impedance	HPBW	Patch Shape / Configuration	Max Gain	Polarization	VSWR / Return Loss	Axial Ratio	RF Power (Max)
1	2.2 - 2.29 GHz	50 Ω	90°	Rectangular - Single Patch	6 dBi	LHCP / RHCP	> 13dB Return Loss	<3dB	5W
2	2.2 - 2.29 GHz	50 Ω	80°	Rectangular - Single Patch	6 dBi	RHCP	1.25 - 1.8	N/A	2W
3	Tx (2.2-2.27), Rx (2.04 -2.09) GHz	50 Ω	80°	Rectangular - Dual Patch	7 dBi	RHCP	< 2	N/A	2W
4	2.2 - 2.29 GHz	50 Ω	100°	Rectangular - Single Patch	6.5 dBi	RHCP	> 13dB Return Loss	<3dB	2W
5	2.025 - 2.120 GHz, 2.200 - 2300 Ghz	50 Ω	N/A	Rectangular - Single Patch	6.5 dBi	RHCP	<1.85	N/A	N/A
6	2.025 - 2.120 GHz, 2.200 - 2300 Ghz	50 Ω	N/A	Rectangular - Single Patch	24 dBi	RHCP	< 1.8	N/A	N/A
7	2.2 - 2.3 GHz, 2.4 - 2.45 GHz	N/A	60°	Circular - Quad Patch	7 dBi	LHCP / RHCP	N/A	N/A	N/A

### 4.3 Design Decisions

The gain, standing wave ratio, and half power beamwidth specified in the requirements of our project are easily achievable for a standard circular or rectangular patch design. As such, we had to deviate from the standard designs presented in [1] to achieve circular polarization, an efficiency of 90%, and a bandwidth that contains the bands of 2025-2110 MHz and 2200-2290 MHz.

To increase the bandwidth, it is optimal to maximize the thickness of the substrate (h), but increasing h also decreases efficiency at an unacceptable rate. To alleviate this problem, an array consisting of two different patches tuned to two different frequencies corresponding to the bands of 2025-2110 MHz and 2200-2290 MHz seemed like a promising solution. However, an array design could not be fit onto the 10cmx10cm allocated area of the CubeSat. As such, the ECMP design was necessary to provide sufficient bandwidth without causing efficiency issues.

To achieve circular polarization, the simplest method is to slightly change the shape of a perfect square or circle patch. Methods involving changing the feeding network introduce more complexity and require their own analysis and simulation. By limiting our variation to the amount of material removed, we could perform simulations to determine the correct amount of material removed. The truncated corner method was chosen to allow for greater flexibility of the probe location.

Finally, it is important to note that the design of circular patch antennas are inherently more difficult because of their geometry. After designing a simple circular patch antenna and not achieving great results (as shown later in the report), we focused on rectangular patch designs.

## 5 Team Duties & Project Planning

The S-Band CubeSat Patch Antenna development group consisted of a four-member team with responsibilities divided to utilize each member's strengths and to maintain an efficient workflow. Duties were assigned at the start of the semester but were adjusted accordingly to meet with demands and delays.

### 5.1 Team Roles

Team Member	Role	Key Deliverables	Significance to Project
<b>Darius Clayton</b>	Antenna Modelling Lead	Developed initial and refined patch antenna designs in ANSYS HFSS based on project requirements.	Provided the foundational geometry for performance simulations, ensuring designs were physically realizable and aligned with specifications.
<b>Logan Dring</b>	Simulation and Optimization Lead	Conducted parametric sweeps in HFSS, varying patch dimensions, substrate properties, and feed positions to maximize gain, bandwidth, and impedance matching.	Enabled identification of the optimal design parameters, directly influencing final antenna efficiency and performance.
<b>Jordan Bona</b>	PCB Design and Fabrication Lead	Translated the optimal simulated design into an Altium PCB layout, ensuring manufacturability and adherence to design tolerances.	Produced a fabrication-ready design, bridging the gap between theoretical simulations and physical realization.
<b>Jonathan Boyce</b>	Testing and Validation Lead	Performed performance testing using a Vector Network Analyzer (VNA) and anechoic chamber measurements; compared measured data with simulations.	Verified that the fabricated antenna met design specifications and documented real-world performance for validation purposes.

## 5.2 Project Challenges

### Challenge 1 – Meeting Bandwidth Requirements within Size Constraints

The first major challenge arose during the modelling phase: achieving the required bandwidth with the limited patch dimensions available. This constraint led to extensive research into broadband patch antenna designs. The solution was the adoption of a stacked patch configuration, which provided the necessary bandwidth without exceeding the allowable dimensions.

### Challenge 2 – Achieving Circular Polarization

During the design phase, producing circular polarization within the size limits proved challenging. To address this, truncated corners were added to the patch geometry, which effectively generated the orthogonal modes necessary for circular polarization while maintaining impedance match.

### Challenge 3 – Achieving Acceptable Bandwidth and Circular Polarization through Simulation

During the simulation phase, multiple parametric sweeps were required to balance bandwidth and circular polarization. This proved time-intensive and delayed downstream tasks, as manufacturing depended on finalized, validated simulation results. To overcome this bottleneck, the team collectively prioritized simulation efforts, reallocating time and resources to expedite parameter optimization while maintaining accuracy.

### Challenge 4 – Delays in Manufacturing

The final challenge occurred after the PCB design was completed and submitted for fabrication. Manufacturing delays pushed the expected delivery beyond the original August 1 deadline. The team obtained an extension to August 11, which allowed sufficient time for fabrication, assembly, and subsequent testing without compromising data quality.

## 6 Design Methodology & Analysis

The following sections present the different designs tested throughout the project and analysis of the final design. The reasons behind the evolution of each design are presented and the parameters that were varied to optimize the final design were explored. All discussed results are from Ansys HFSS simulations and were used to guide the design process. This report does not claim that the performance shown can be achieved with a physical antenna matching any of the test cases.

### 6.1 Design 1: Single Rectangular Patch Antenna Design and Simulations

To better understand the limitations of a basic rectangular single patch design, a basic prototype was designed and simulated.

The design process proposed by Balanis was used for this project [1]. To start it is important to assess the known parameters given by the constraints outlined in the objectives section of the report. These parameters are given below in Table

*Table 6.1: Known parameters for Rectangular Patch Antenna Design*

Parameter	Symbol	Value
Resonant Frequency $f_r$ (taken to be the average of frequency range)	$f_r$	2157.5 MHz
Dielectric Constant, $\epsilon_r$ , of Rogers 4003C substrate [8]	$\epsilon_r$	3.55

At this point, the parameters of interest that need to be determined are shown in Table 6.2 below.

*Table 6.2: Unknown parameters for Rectangular Patch Design*

Parameter	Symbol
Width of Patch	W
Length of Patch	L
Height of Substrate	h

From this point, a first order approximation for an optimal width for a given center frequency was used [1]:

$$W = \frac{c}{2f_r} \sqrt{\frac{2}{\epsilon_r + 1}}$$

$$W = \frac{(3 * 10^8)}{2(2157.5 * 10^6)} \sqrt{\frac{2}{3.55 + 1}}$$

$$W = 0.046094569 [m]$$

$$W \approx 4.61 [cm]$$

Before any further parameters of interest can be calculated the height of the substrate was then chosen. While there is no exact equation to choose this quantity, there is a design trade-off between the bandwidth and the efficiency. We followed the general rule of thumb and chose an h which sits in the given interval [2]:

$$0.003\lambda_o \leq h \leq 0.05\lambda_o$$

Where,

$$\lambda_o = \frac{c}{f_r} = \frac{(3 * 10^8)}{(2.1575 * 10^9)} = 0.1390498[m] \approx 13.9\text{cm}$$

Meaning that our substrate height, h, should be in the interval

$$0.0417\text{cm} \leq h \leq 0.695\text{cm}$$

For the initial design **h = 0.1575 cm** was chosen. It was noted later that the substrate height is restricted and influenced by what is available from vendors and what is cost efficient.

Taking fringing into account, the effective dielectric constant was calculated to be

$$\epsilon_{ref} = \frac{\epsilon_r + 1}{2} + \frac{\epsilon_r - 1}{2} \left[ 1 + 12 \frac{h}{W} \right]^{-\frac{1}{2}}$$

$$\epsilon_{ref} = \frac{3.55 + 1}{2} + \frac{3.55 - 1}{2} \left[ 1 + 12 \frac{0.001575\text{m}}{0.0461\text{m}} \right]^{-\frac{1}{2}} = 3.789$$

Now the quantities  $\Delta L$  were determined to calculate the length of the patch

$$\Delta L = 0.412h \frac{(\epsilon_{ref} + 0.3) \left( \frac{W}{h} + 0.264 \right)}{(\epsilon_{ref} - 0.258) \left( \frac{W}{h} + 0.8 \right)}$$

$$\Delta L = 0.412 * 0.001575 \frac{(3.789 + 0.3)(29.26984 + 0.264)}{(3.789 - 0.258)(29.26984 + 0.8)} = 7.3805 * 10^{-4} [\text{m}]$$

The length of the patch was then approximated to be

$$L = \frac{c}{2f_r\sqrt{\epsilon_{ref}}} - 2\Delta L = \frac{3 * 10^8}{2 * (2.1575 * 10^9) * \sqrt{3.55}} - 2 * (7.38 * 10^{-4}) = 3.54[\text{cm}]$$

Once the main patch dimensions were determined, the base input impedance  $Z_{in}$  of the patch antenna were calculated using the length L and the width W. This impedance

calculation assumes that the coax feed probe is positioned at the edge of the substrate length ( $X_p = 0$ ).

$$Z_{in} = 90 \frac{\epsilon_r^2}{\epsilon_r - 1} \left( \frac{L}{W} \right)^2 = 90 \left( \frac{3.55^2}{3.55^2 - 1} \right) \left( \frac{3.54cm}{4.61cm} \right)^2 = 57.6437 [\Omega]$$

The design constraints outline that the nominal input impedance of the antenna is to be  $50\Omega$  to match the impedance of the coax feed. Using this impedance along with the input impedance calculated above, the location along the patch length where the probe feed should be placed to achieve a matched feed was determined as follows:

$$Z_{in(\Delta x_p)} = Z_{in(\Delta x_p=0)} \cos^2 \left( \frac{\pi \Delta x_p}{L} \right)$$

Rearranging and solving for  $\Delta x_p$  gives:

$$\Delta x_p = \cos^{-1} \sqrt{\frac{Z_{in(\Delta x_p)}}{Z_{in(\Delta x_p=0)}}} * \left( \frac{L}{\pi} \right)$$

$$\Delta x_p = \cos^{-1} \sqrt{\frac{50\Omega}{57.6437\Omega}} * \left( \frac{3.54cm}{\pi} \right) = 0.41998 [cm]$$

The figures below are snapshots of results obtained by modelling the rectangular patch antenna described above in Ansys HFSS [9].

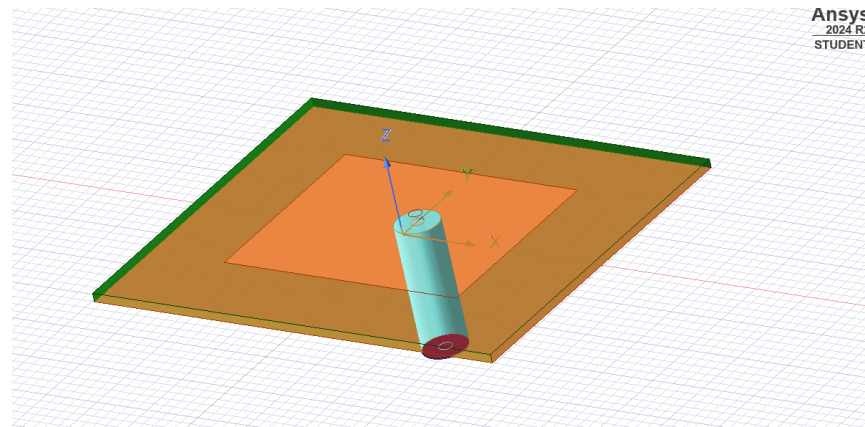


Figure 6.1: Ansys HFSS 3D model of rectangular patch antenna prototype

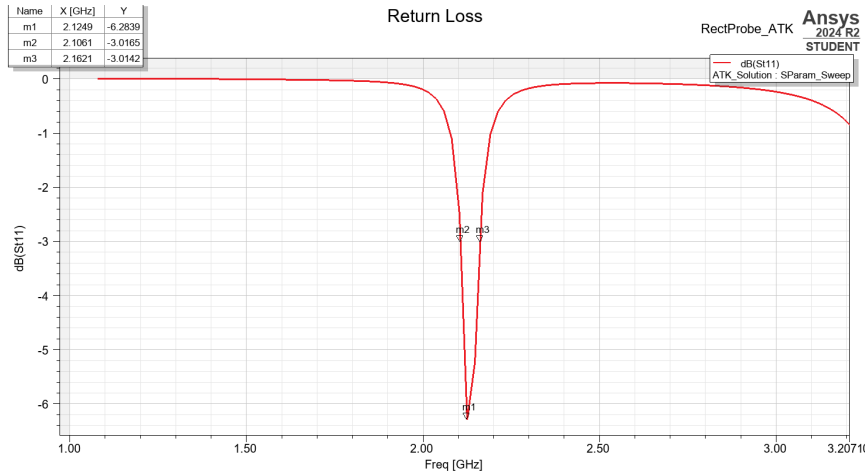


Figure 6.2: Return loss of rectangular patch antenna prototype with bandwidth shown

From Figure we can see that the return loss of this design is not even close to achieving the bandwidth and VSWR requirements for the project. To achieve the VSWR requirement, the entire bandwidth is required to have a return loss of -10dB or less.

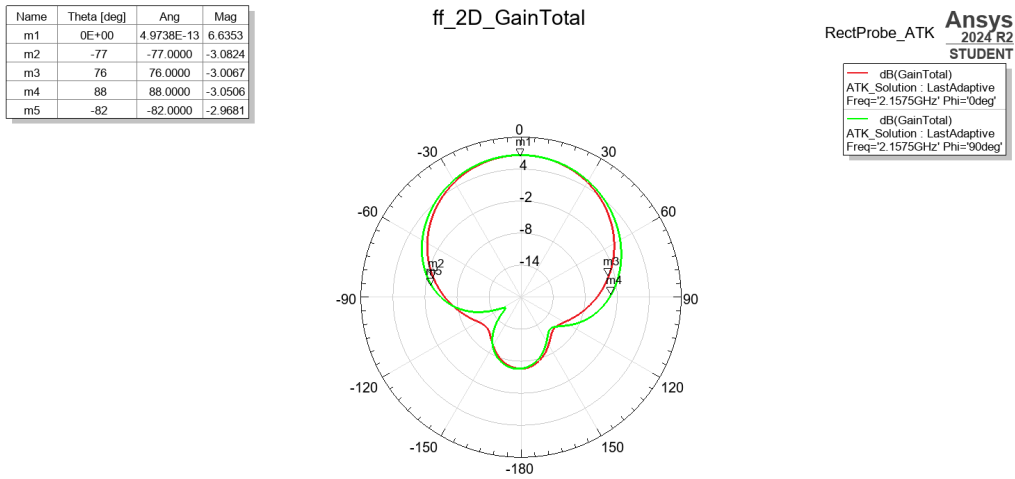


Figure 6.3: 2D polar gain plot of rectangular patch antenna prototype showing HPBW

Figure shows that the gain in the broadside direction sits at 6.6353 dBi and exceeds the 6dBi requirement. It also shows that the power at 30° on either side of the broadside direction exceeds 4dB which is less than 3dB from the 6.6dB maximum, meaning that the design exceeds the 60° HPBW requirements.

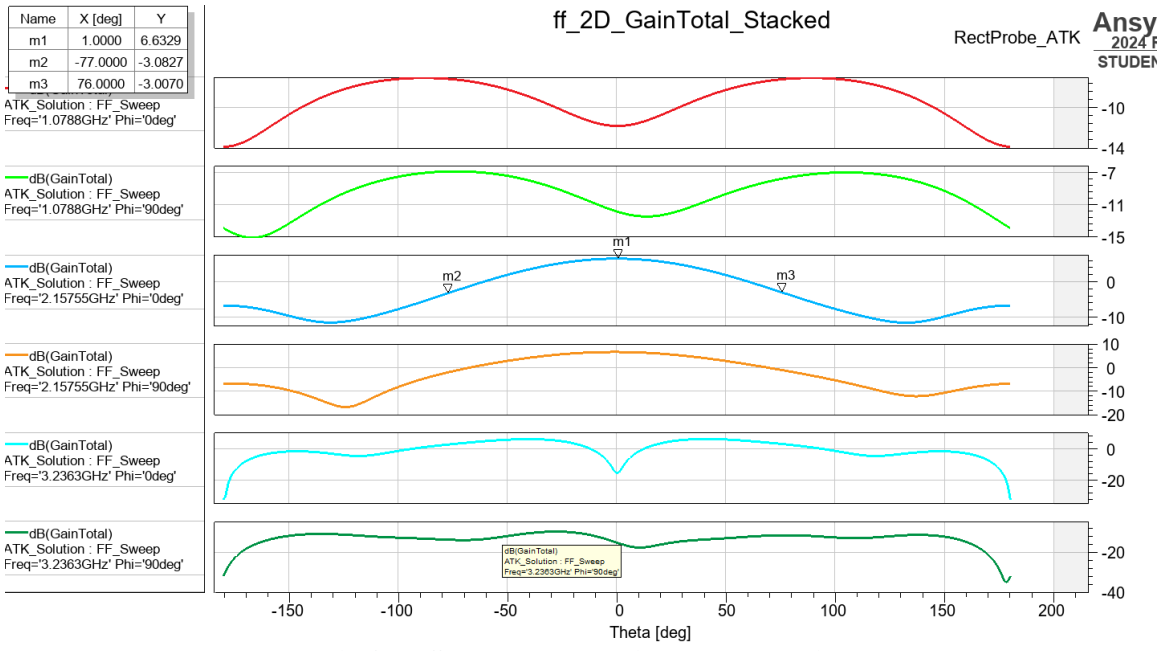


Figure 6.4: 2D Gain Plot for Different Frequency with HPBW Measured at Resonant Frequency

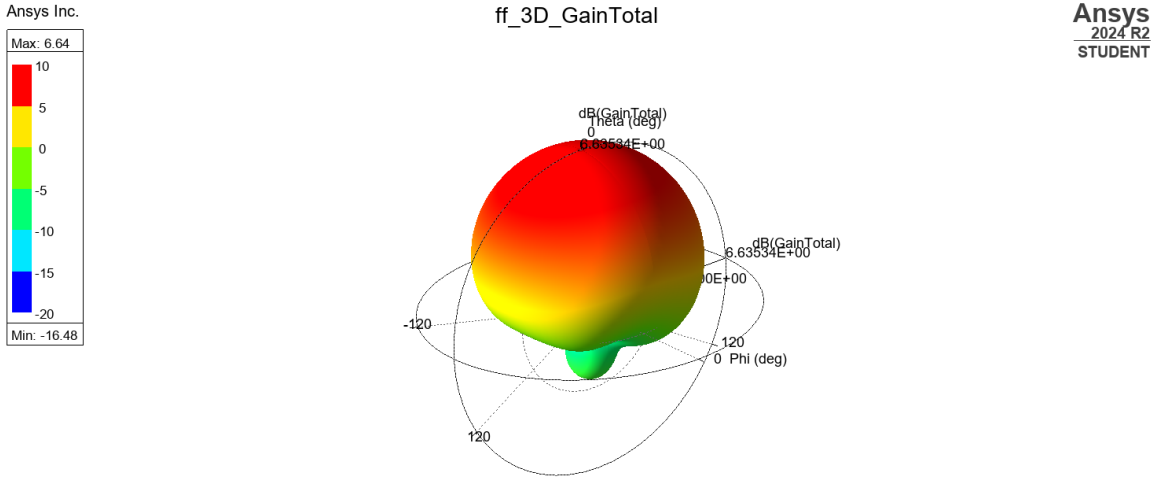


Figure 6.5: 3D Gain Plot for Rectangular Patch Antenna Prototype

Figure shows the radiation pattern of the prototype antenna. The pattern is mostly ideal as most of the power is radiated in the broadside direction with a peak of 6.64dB that exceeds our constraints.

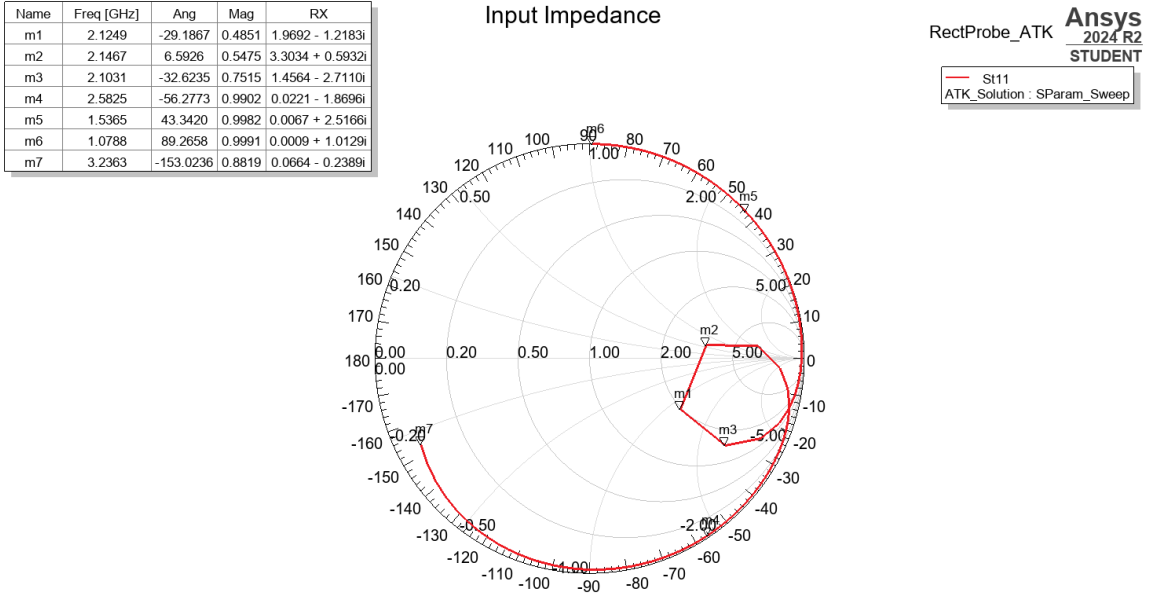


Figure 6.6: Input Impedance at Varying Frequencies Shown on Smith Chart

Figure shows the input impedance for various frequencies. From this plot we can see that our antenna is far from matched as the origin of the graph is not intersected. This indicates that some further analysis of the probe placement is needed to achieve fewer reflections and a better voltage standing wave ratio (VSWR) and reflection coefficient.

It is important to note that no measures were put in place to make this initial design circularly polarized so the polarization was linear. The performance of this initial design qualified whether or not the project constraints were met, and its summary is found in Table 6.3.

Table 6.3: Performance Evaluation of Rectangular Patch Design

Quantity	Meet Constraints?
Bandwidth/VSWR	NO
Gain in broadside direction	YES
HPBW	YES
Input Impedance	NO
Axial Ratio	NO
Efficiency	NO

## 6.2 Design 2: Single Circular Patch Antenna Design and Simulations

In a similar fashion to the last section, to better understand the limitations of a basic circular single patch design, a basic prototype was designed and simulated.

The specified design parameters are the same as in the rectangular patch design scenario, including the substrate height which was chosen to be  **$h = 0.1575 \text{ cm}$** . Again, the standard design approach was followed [1].

With the specified parameters, the necessary effective radius  $a_e$  was calculated:

$$a_e = \frac{1.8412c}{2\pi f_{r,110}\sqrt{\epsilon_r}}$$

$$a_e = \frac{1.8412(3 * 10^8)}{2\pi(2157.5 * 10^6)\sqrt{3.55}}$$

$$a_e = 0.021626058 \text{ [m]}$$

$$a_e = 2.16 \text{ [cm]}$$

Then the patch radius  $a$  was determined, from its relation to the effective radius  $a_e$ :

$$a_e = a \sqrt{1 + \frac{2h}{\pi a \epsilon_r} \left[ \ln \left( \frac{\pi a}{2h} \right) + 1.7726 \right]}$$

To solve this, the value of  $a$  was approximated in the square root with  $a_e$

$$a = \frac{a_e}{\sqrt{1 + \frac{2h}{\pi a_e \epsilon_r} \left[ \ln \left( \frac{\pi a_e}{2h} \right) + 1.7726 \right]}}$$

This result can then be refined through an iterative procedure. However, we instead be used following first order approximation in the interest of time:

$$a = \frac{F}{\sqrt{1 + \frac{2h}{\pi \epsilon_r F} \left[ \ln \left( \frac{\pi F}{2h} \right) + 1.7726 \right]}}$$

Where h is in cm and

$$F = \frac{8.791 * 10^9}{f_r \sqrt{\epsilon_r}}$$

$$F = \frac{8.791 * 10^9}{(2157.5 * 10^6) \sqrt{3.55}}$$

$$F = \frac{8.791 * 10^9}{(2157.5 * 10^6) \sqrt{3.55}}$$

$$F = 2.162585562$$

Thus:

$$a = \frac{2.162585562}{\sqrt{1 + \frac{2 * 0.1575}{\pi(3.55)(2.162585562)} \left[ \ln \left( \frac{\pi(2.162585562)}{2 * 0.1575} \right) + 1.7726 \right]}} = 2.09726 [cm]$$

Next, the input impedance for the coax probe fed circular patch antenna was found. This calculation of input impedance assumes an edge feed ( $\rho' = a_e$ ):

$$R_{in}(\rho' = a_e) = \frac{1}{G_t} = \frac{1}{G_{rad} + G_c + G_d}$$

$$G_{rad} = \frac{(k_0 a_e)^2}{120 D_0} = \frac{(45.18657 * 0.0216)^2}{120 * (6)} = 0.001323 [S]$$

Note: We assumed the use of a copper ground plane with  $\sigma = 5.8 * 10^7 S/M$

$$\begin{aligned} G_c &= \frac{(\epsilon_{mo} \pi (\mu_0 f_r)^{-\frac{3}{2}})}{4h^2 \sqrt{\sigma}} [(ka_e)^2 - m^2] = \\ &= \frac{(1\pi(\pi(4\pi*10^{-7})(2.1575*10^9))^{-\frac{3}{2}})}{4(0.001575)^2 \sqrt{5.8*10^7}} [(85.14 * 0.0216)^2 - 1] = 4.9836 * 10^{-6} [S] \end{aligned}$$

$$\begin{aligned} G_d &= \frac{\epsilon_{mo} \tan \delta}{4\mu_0 h f_r} [(ka_e)^2 - m^2] = \\ &= \frac{(1 * 0.0027)}{4(4\pi * 10^{-7})(0.001575)(2.1575 * 10^9)} [(85.14 * 0.0216)^2 - 1] = 3.765 * 10^{-4} [S] \end{aligned}$$

Finally, the input resistance was calculated:

$$R_{in}(\rho' = a_e) = \frac{1}{0.001323 [S] + 4.9836 * 10^{-6} [S] + 3.765 * 10^{-4} [S]} = 757.576 [\Omega]$$

With  $R_{in}(\rho' = a_e)$  computed we then found the feed point distance  $\rho_0$ . As in the rectangular patch design example the antenna input impedance should be  $50 \Omega$  to match the coax feed:

$$R_{in}(\rho' = \rho_0) = R_{in}(\rho' = a_e) \frac{J_1^2(k\rho_0)}{J_1^2(ka_e)}$$

$$J_1(k\rho_0) = \frac{R_{in}(\rho' = \rho_0)}{R_{in}(\rho' = a_e)} * J_1^2(ka_e) = \sqrt{\frac{50\Omega * 0.3386}{757.576\Omega}} = 0.14949$$

We have:

$$J_1(k\rho_0) = 0.14949$$

From the Bessel function table, we get:

$$k\rho_0 = 0.38$$

This gives:

$$\rho_0 = \frac{0.38}{k} = \frac{0.38}{85.14} = 0.446 [cm]$$

This design was again simulated using Ansys HFSS and the results are shown in the figures below.

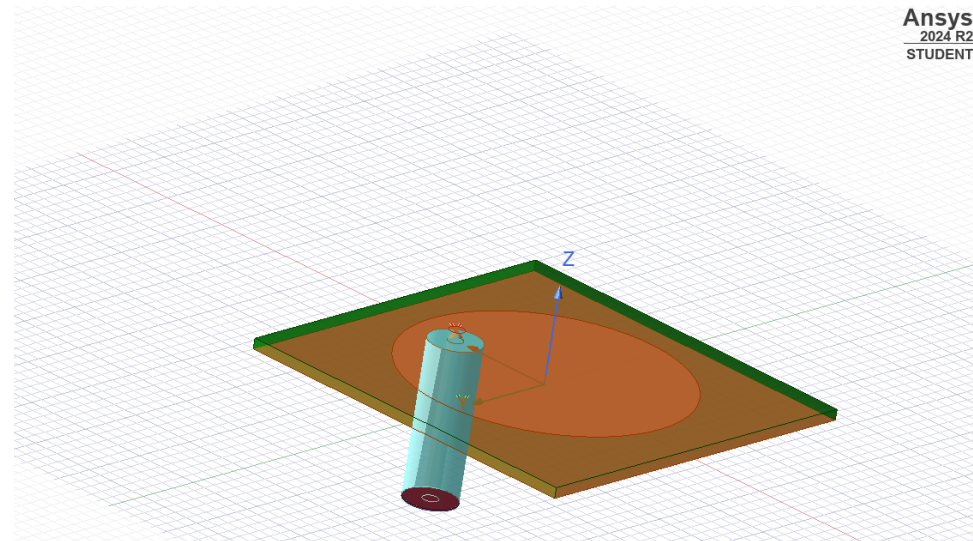


Figure 6.7: 3D Model of Circular Patch Prototype

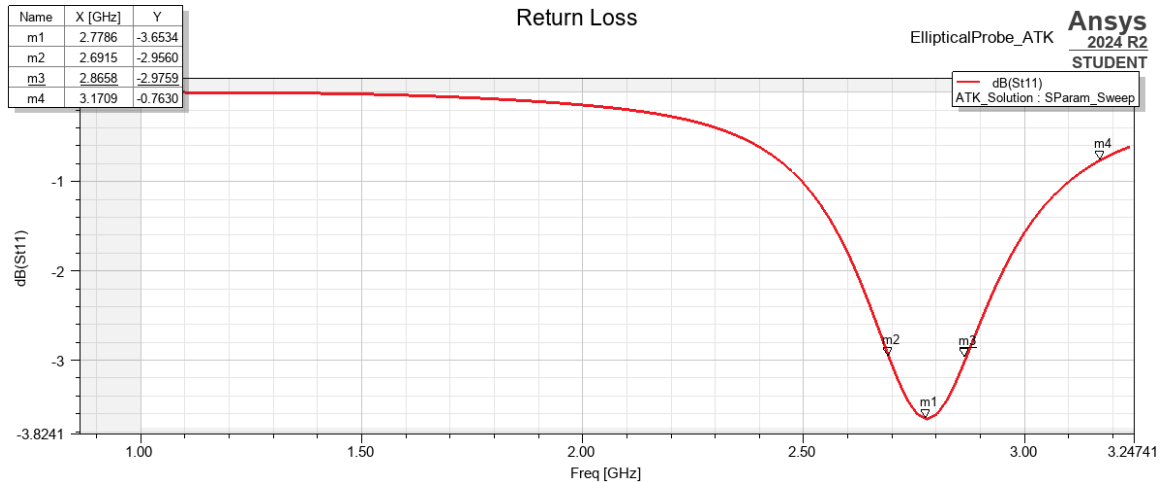


Figure 6.8: Return Loss of Circular Patch Prototype with Bandwidth Shown

As can be seen in Figure , the resonant frequency did not sit at the desired 2.1575 GHz and the bandwidth was much narrower than what is necessary due to impedance matching issues and the inherently narrow bandwidth characteristics of circular patch designs. The resonant frequency not being where we want it was a result of the first order approximation used to determine the radius of the patch.

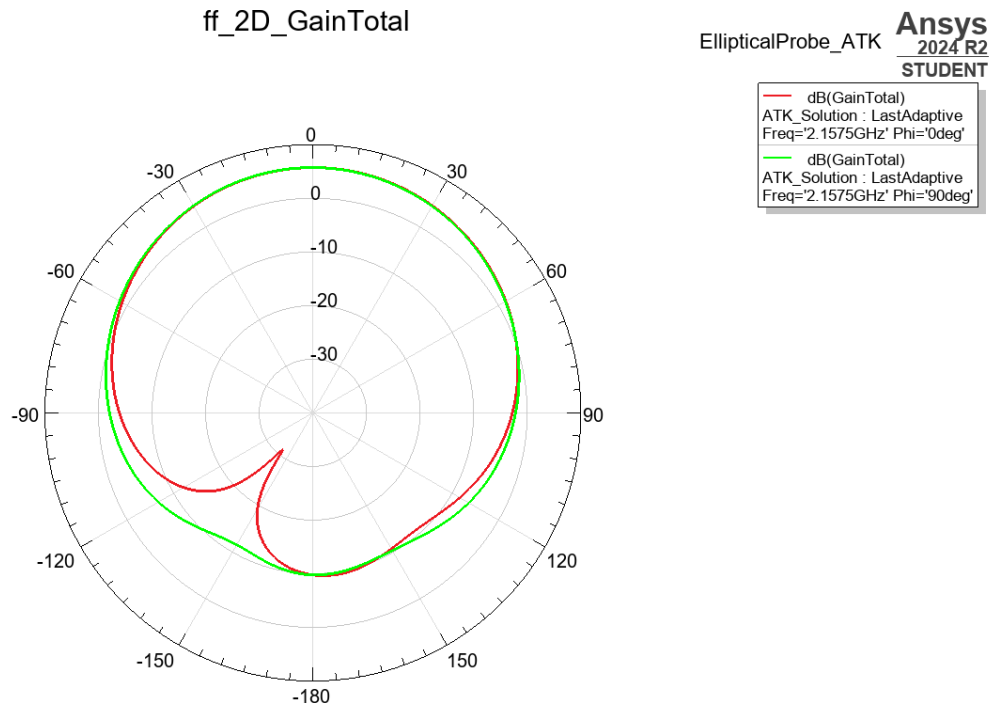


Figure 6.9: 2D Polar Gain Plot of Circular Patch Prototype

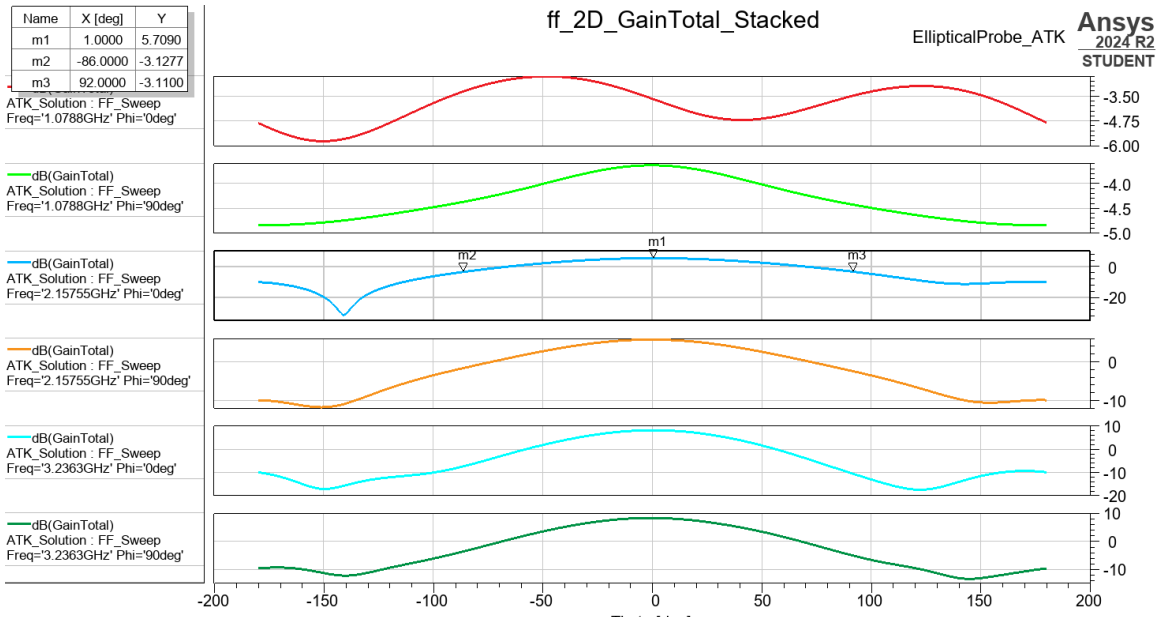


Figure 6.10: 2D Gain Plot for Circular Patch Prototype

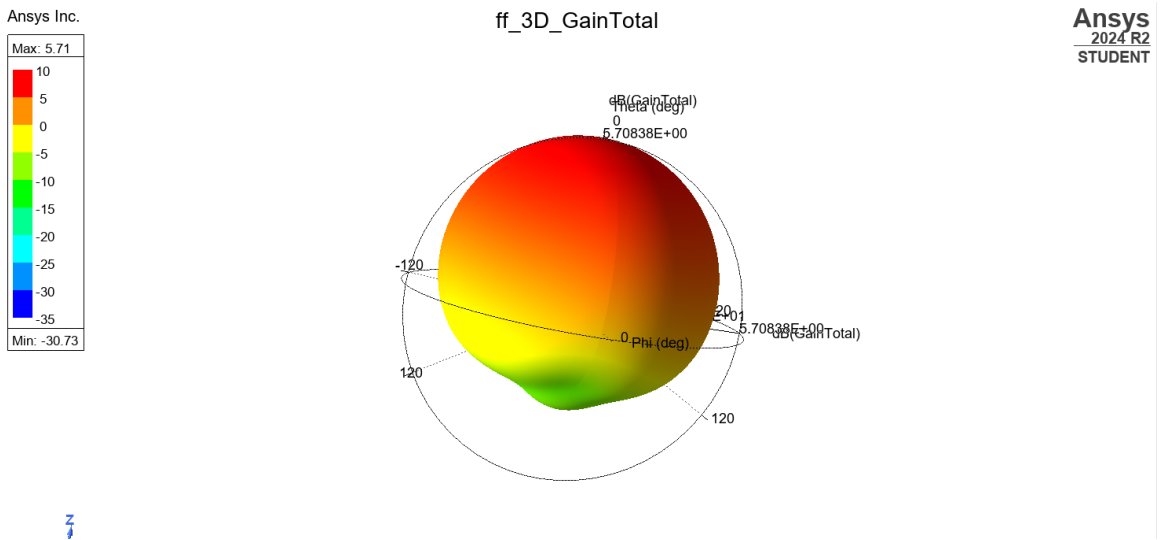


Figure 6.11: 3D Gain Plot for Circular Patch Prototype

As can be seen in Figure , the maximum gain sat slightly below our 6dB requirement at only 5.7dB. This was likely due to reflection losses due to the poor impedance matching presented in the next figure.

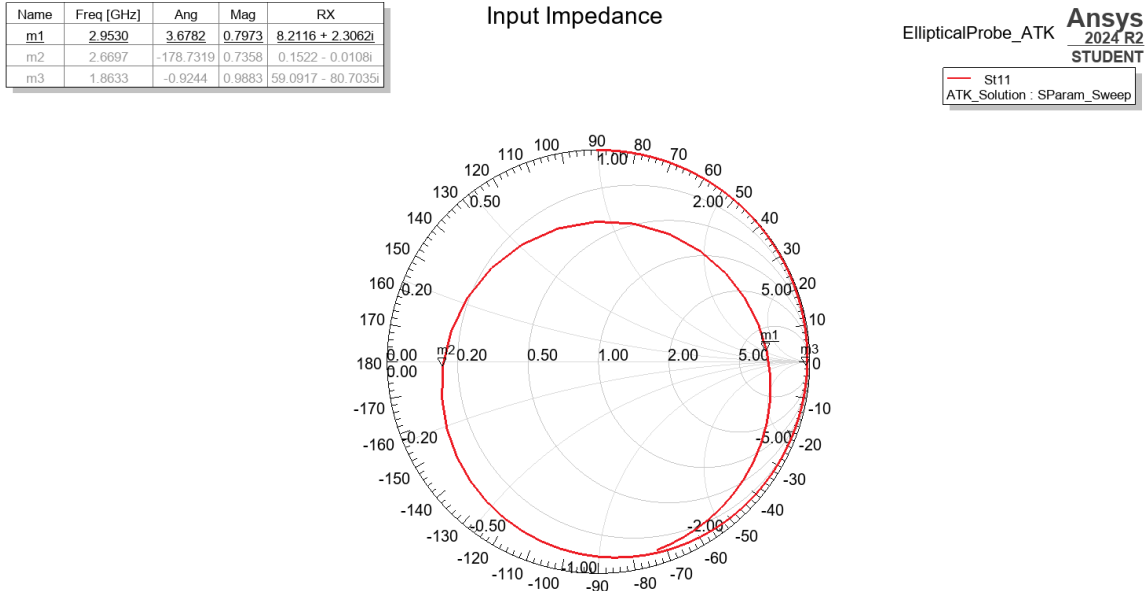


Figure 6.12: Input Impedance Smith Chart Plot for Circular Patch Prototype

As is evident from the less than desirable results presented, the design process for a circular patch antenna is a lot more complicated than that of the rectangular patch and first order approximations cannot be relied upon to give well performing designs. As a result, the rectangular patch geometry was adopted for the project.

Similarly, the performance of the circular patch antenna was summarized as Table 6.4.

Table 6.4: Performance Evaluation of Circular Patch Design

Quantity	Meet Constraints?
Bandwidth/VSWR	NO
Gain in broadside direction	NO
HPBW	NO
Input Impedance	NO
Axial Ratio	NO
Efficiency	NO

### 6.3 Design 3: Extremely Electromagnetically Coupled Patch Antennas

After initial prototyping of the antenna described in section 6.1, it was observed that a broader band was needed. One method of improving bandwidth that was investigated was a coupled patch configuration as investigated in section 4.1.3.2. Keeping in mind the original mechanical constraints of a 5mm height, the air gap between the patches was quite small leading to large amounts of coupling. A HFSS model of the described antenna can

be found in Figure 6.13. As mentioned previously, this leads to a dual-band response of the antenna as is demonstrated in Figure 6.14.

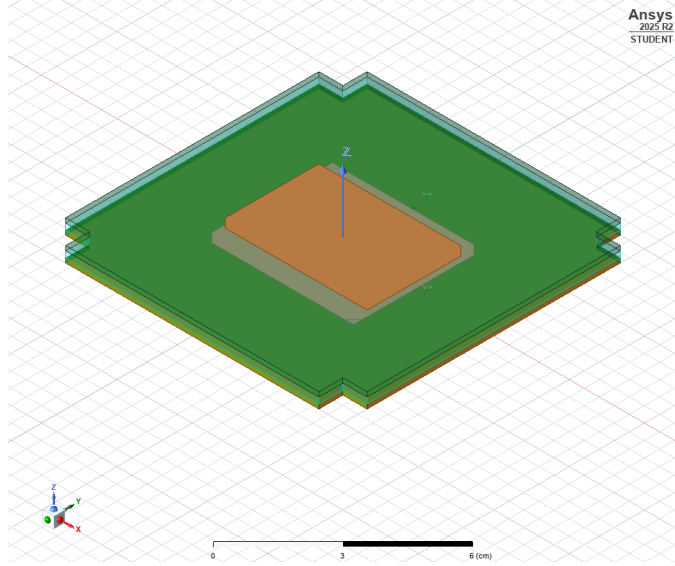


Figure 6.13: Extremely Electromagnetically Coupled Patch Antenna

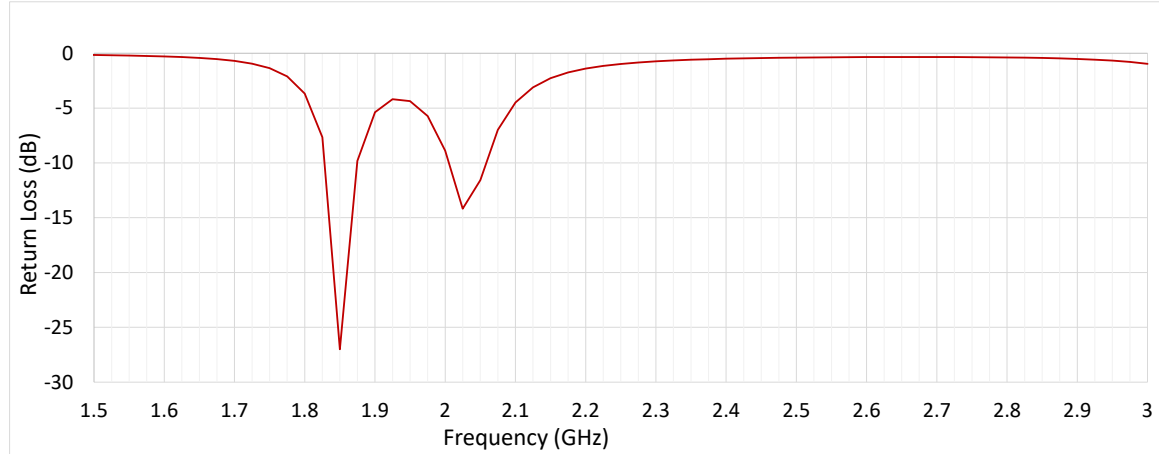


Figure 6.14: Return Loss of an EMCP with a Gap Of 1mm

## 6.4 Final Configurable Design: CubeSat S-Band EMCP Antenna

The design explored in section 6.3 was unable to produce the desired results. However, it was observed that by increasing the gap height beyond the mechanical constraints, the performance of the antenna improved significantly. After showing such results to the supervisors, the mechanical constraint was loosened in lieu of the allowed tuna can volume for CubeSats. Figure 6.15 shows how the allowable volume can be leveraged for the needed design.

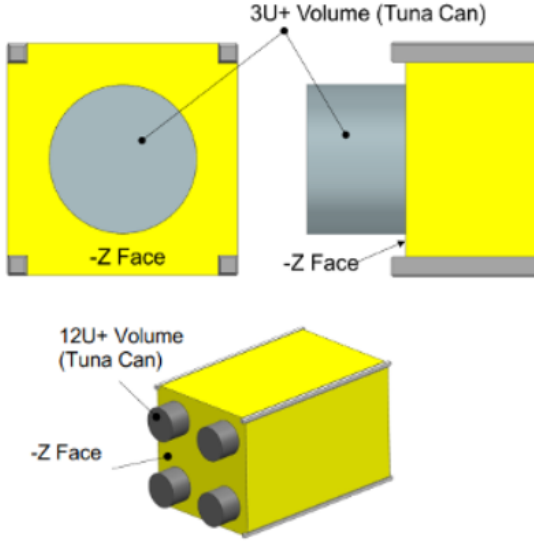


Figure 6.15: Additional "Tuna Can" Volume [10]

With the design method and configuration decisions finalized, a new model of the antenna was created in HFSS. The model included a  $50\ \Omega$  female SMA port, ground plane with configurable trimmed edges, configurable patches both driven and coupled, standoffs to space the two patches which adjust with gap height, an upper circular substrate to match the tuna can requirements, and all the mounting holes needed to accurately model the antenna described in section 7.

## 6.5 Analysis 1: Direct and Coupled Patch Size

With an antenna configuration proposed in section 6.4, there are now two patch dimensions which will influence the operation. This section will explore the effects that each patch has on the return loss of the antenna.

The driven patch which directly contacts the probe of the SMA connector dominates the coupled patch in terms of the antenna's resonant frequency. Using the model described in section 6.4, all parameters were kept constant except the driven patch size. Simulating such a parametric sweep yields the results shown in Figure 6.16. Intuitively, a larger patch corresponds to larger wavelengths ergo smaller frequencies.

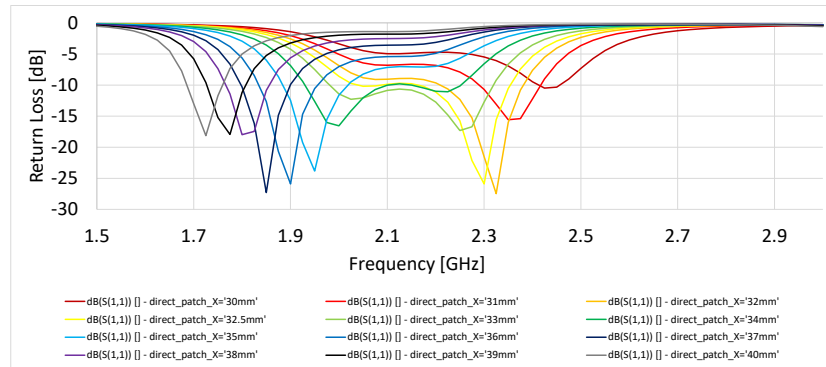


Figure 6.16: Return Loss vs Frequency for Varied Driven Patch Sizes

In contrast, the coupled patch size was found to only influence bandwidth characteristic. Since the coupled patch is present in the antenna, it introduces a second resonant frequency. As was discussed in section 4.1.1, the dimensions of a patch determine its resonant frequency. However, the effect of the coupled patch's length does not change the overall resonant frequency of the antenna to the same extent the driven patch did. Instead, how close the secondary resonant frequency was to the primary, impacted whether the bandwidth resembled dual band or broadband behaviour. To analyse this phenomenon in more detail a similar parametric sweep was ran. This time the coupled patch dimensions were varied while all others were kept constant to achieve the datasets shown in Figure 6.17.

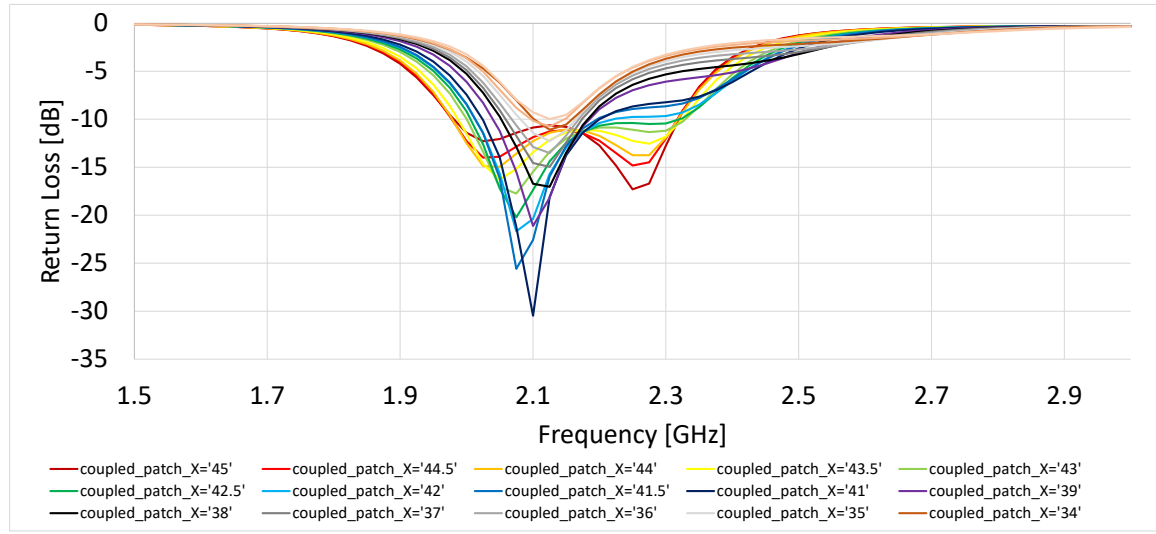


Figure 6.17: Return Loss vs Frequency for Varied Coupled Patch Sizes

## 6.6 Analysis 2: Impedance Matching via Probe Location

Since the patch would use most of the allocated space with its size needing to be approximately 3-4 cm per section 6.1, the design choice was made to achieve impedance matching via probe location as opposed to implementation of any matching networks. Using the transmission line equivalent models of a probe fed and proximity coupled antenna, the equivalent model of the proposed antenna can be represented by the circuit shown in Figure 6.18 [2].

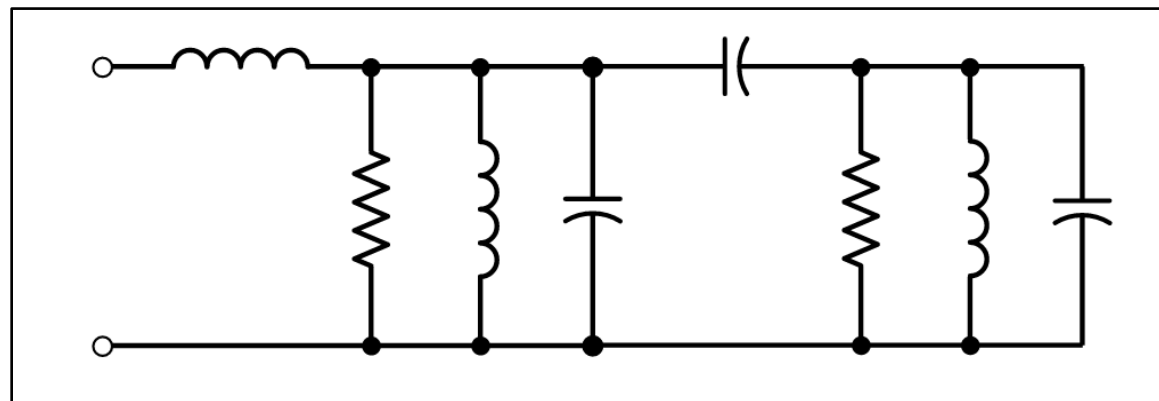


Figure 6.18: Transmission Line Equivalent Model of the Chosen Configuration [2]

In this lumped model representation, the first impedance network corresponds to the driven patch. Each of these reactances are dictated by how much of the patch the signal needs to travel. This fact can be taken advantage of, and the input impedance of the antenna can be tuned to improve the bandwidth. It was observed in the datasets shown in Figure 6.19 that with a fixed driven and coupled patch size, the probe location could be altered to improve the bandwidth but does not change the resonant frequency or bandwidth characteristic the same way the patch dimensions do.

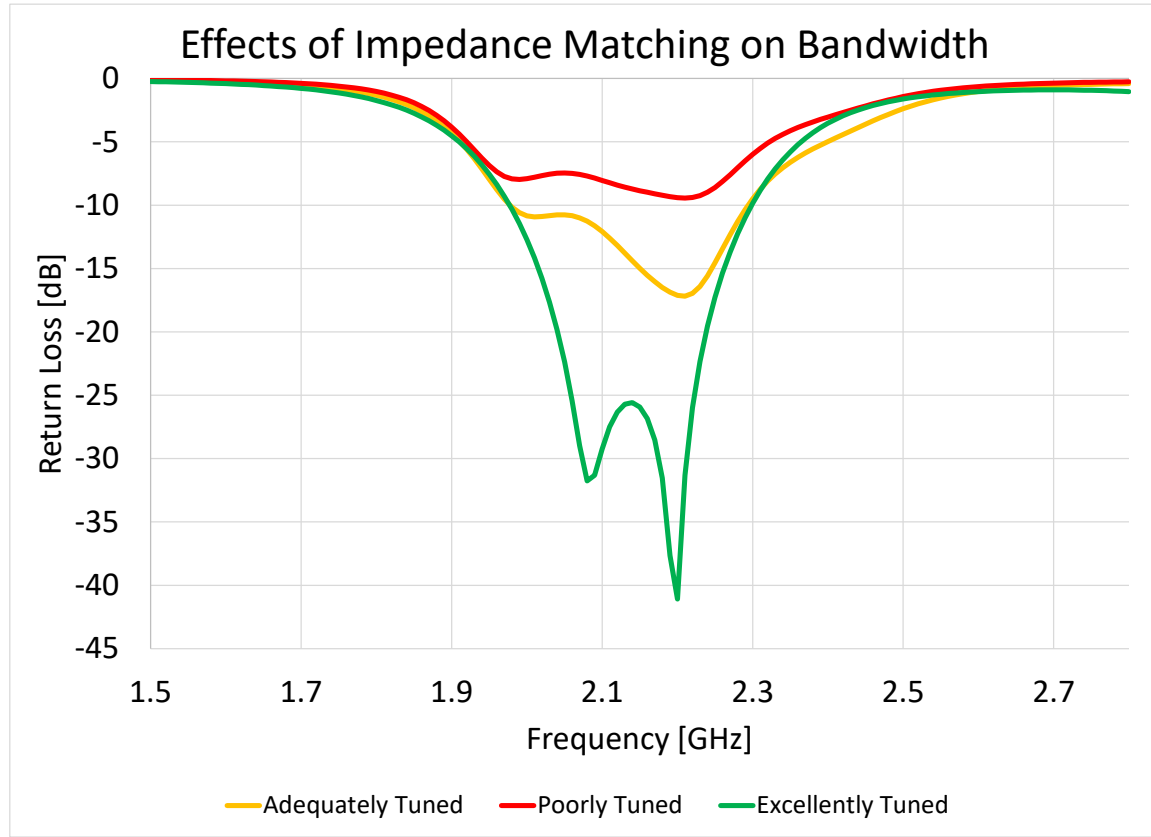


Figure 6.19: Return Loss vs Frequency for Different Probe Locations

## 6.7 Analysis 3: Air Gap Height

Because of the chosen stacked patch configuration, the gap height is an important parameter. When the coupled patch is closer to the driven patch, a performance best characterised as dual band is achieved. This can occur due to even and odd modes being excited in the two patches as they are close enough to exhibit microwave coupler behaviour [11]. With strong coupling, two distinct resonant frequencies are observed. As the coupling is reduced due to increased gap height, this behaviour changes. Since the patches are no longer close enough to generate distinct even and odd modes, the waves begin to “overlap” as do the resonant frequencies. This is how such antennas can achieve broadband performance. To explore what gap height achieves what performance, a parametric sweep of the height was ran while keeping all other parameters constant. The results of such a simulation are shown in Figure 6.20.

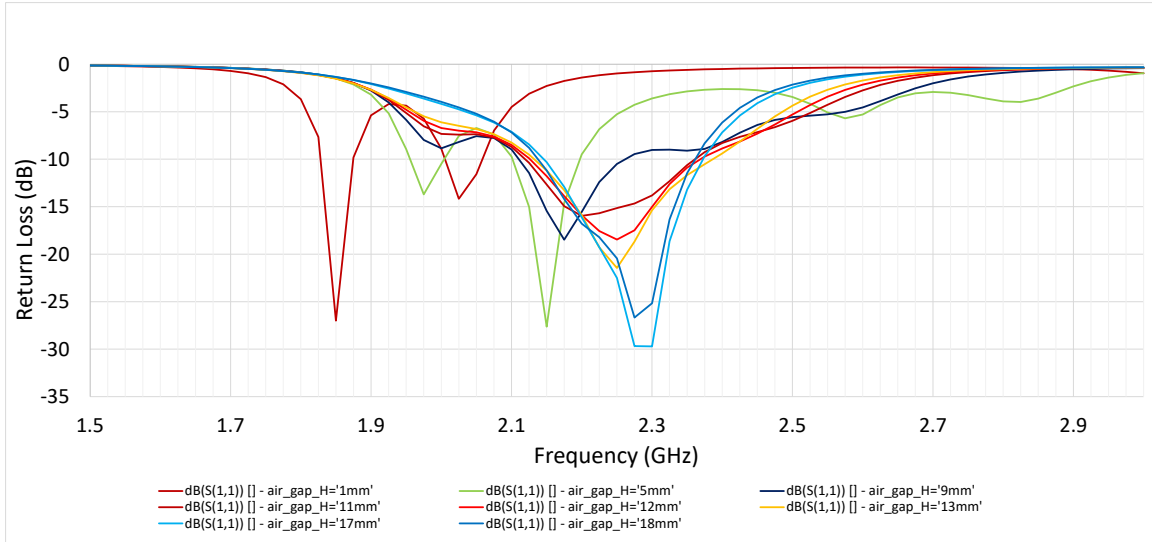


Figure 6.20: Return Loss vs Frequency for Varied Air Gap Height

## 6.8 Analysis 4: Truncated Corners to Achieve Circular Polarization

As was decided in section 4.3, the truncated corners method was chosen to achieve circular polarization. Although the implementation of this method both in the model and PCB manufacturing is simple, it made the detailed design work complex. If we recall the analysis of this method, complications regarding the bandwidth arise when trying to achieve good circular polarization. This phenomenon gave way to two extremes:

Case 1: Good bandwidth (Return Loss < -10dB over the entire band), but poor polarization (Axial Ratio up to 10dB)

Case 2: Mediocre bandwidth (Return Loss < -10dB for only portions of the band), but good polarization (Axial Ratio < 3dB for most of the band)

Figure 6.21 and Figure 6.22 demonstrate the exclusivity of attaining the desired bandwidth or axial ratio.

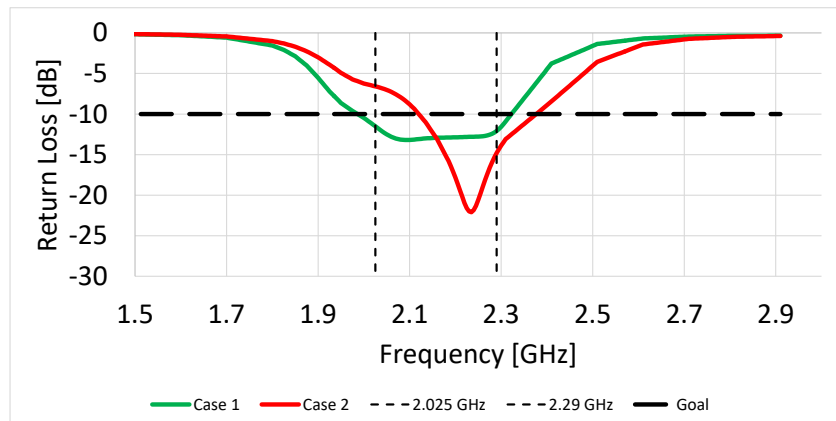


Figure 6.21: Return Loss vs Frequency for Case 1 and Case 2

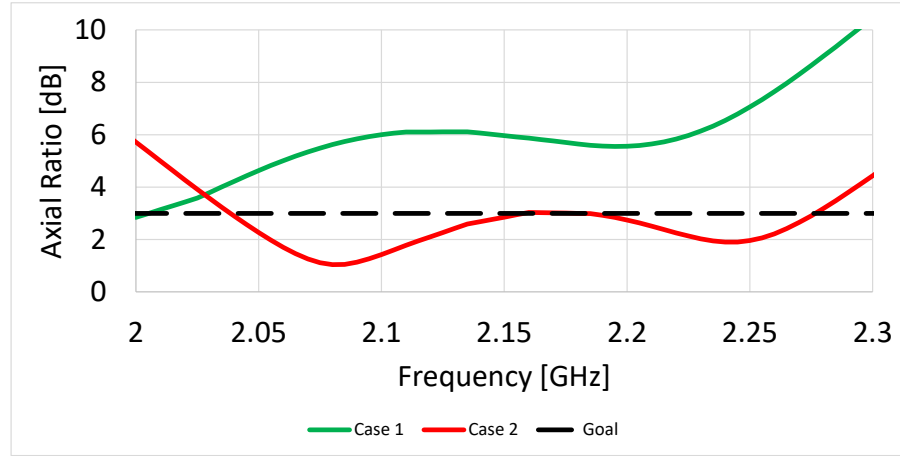


Figure 6.22: Axial Ratio vs Frequency for Case 1 and Case 2

It was apparent that an engineering trade-off was required in this instance. Using an excel spreadsheet and the equation for polarization loss, the effects of the axial ratio could be investigated [12]:

$$P_L = 0.5 \times \left[ 1 + \frac{(1 - AR_{TX}^2) \times (1 - AR_{RX}^2) \cos 2\theta + 4 \times AR_{TX}^2 \times AR_{RX}^2}{(1 + AR_{TX}^2) \times (1 + AR_{RX}^2)} \right] \quad (10)$$

Where  $AR_{TX}$  and  $AR_{RX}$  are the axial ratios of the transmitting and receiving antennas as linear numbers, and  $\Theta$  is the polarization angle between the antennas. Assuming an earth station antenna with equal axial ratio requirements (< 3dB), an axial ratio of 7.85 dB still resulted in less than 1.5 dB of polarization loss even under worst case angle misalignment. Thus, the design choice was made to favor bandwidth over polarization in our design meaning performance more like Case 1 rather than Case 2.

## 6.9 Analysis 5: Accounting for the Real World

This section describes the methods and steps taken in attempt to make the model closer to its real-world implementation. These steps served two-purposes. The first being to validate all of our past findings. If introducing a non-ideality to the antenna caused vastly different results, it would be noted that previous simulations would have to be redone

### 6.9.1 Achieving the Air Gap in the Model

Since the technology to levitate PCBs does not exist, a mechanical component would need to be used to achieve the desired gap. For our design, the use of standoffs was considered. This allowed us to minimize the amount of material in between the two patches thus keeping the average permittivity between them as low as possible. The standoffs needed to be non-conductive to preserve the antenna's performance. Nylon and ceramic were considered as both materials are non-conductive and are readily available from vendors. While the low cost of nylon is attractive, it does not meet NASA guidelines for non-metallic materials. Depending on the exact chemical composition of the nylon, it has a total mass loss (TML) of ~1.75% and a collected volatile condensable material (CVCM) of ~0.07% [13]. Since nylon loses too much mass under vacuum, it is not acceptable for

implementation in space. Thus, ceramic was considered for the final design of the antenna. However, due to the increased cost of ceramic standoffs, nylon standoffs were still used in the prototype. The effects of the different materials were simulated in HFSS to ensure the testing data from the prototype would still be valid. The comparison of these results can be found in Figure 6.23.

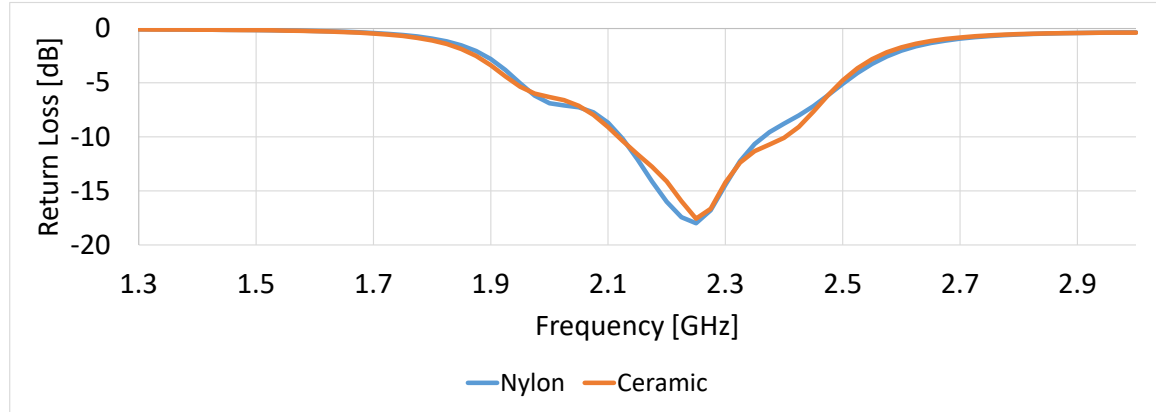


Figure 6.23: Return Loss vs Frequency for Different Standoff Materials

It was observed that minimal differences are incurred. It should be noted that if wider standoffs with larger outer diameters are used, the amount of material would begin to increase the permittivity in between the two patches and worsen the performance of the antenna.

### 6.9.2 Manufacturing Considerations in the Model

PCB Manufacturers do not often offer the capability of having the ground plane be present right to the edge of the substrate. As such a configurable parameter was created to influence the amount of ground plane would be trimmed from the edges. The final implementation of this trim can be seen in Figure 7.1. To verify the reduction of ground plane material would not sway our results, a simulation was run with different amounts of trim resulting in the datasets shown in Figure 6.24 and Figure 6.25.

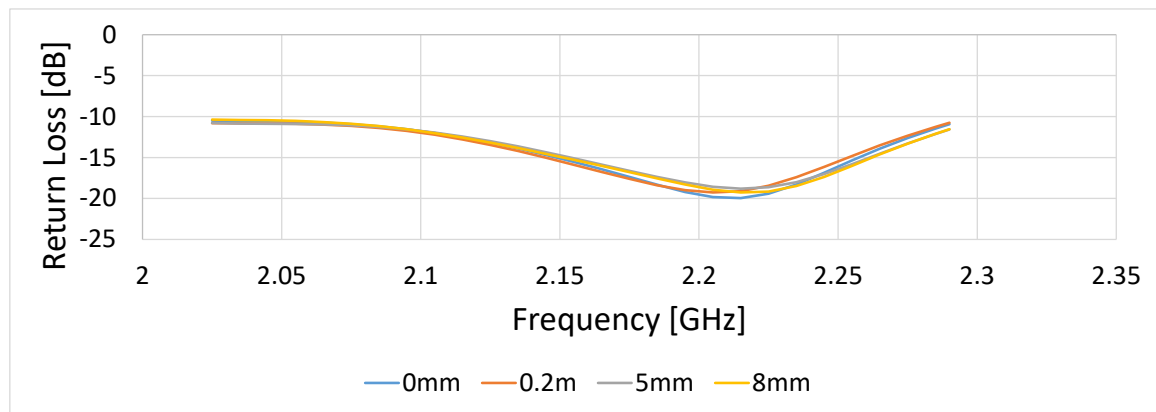


Figure 6.24: Return Loss vs Frequency in Operation Band for Different Amounts of Removed Ground Plane

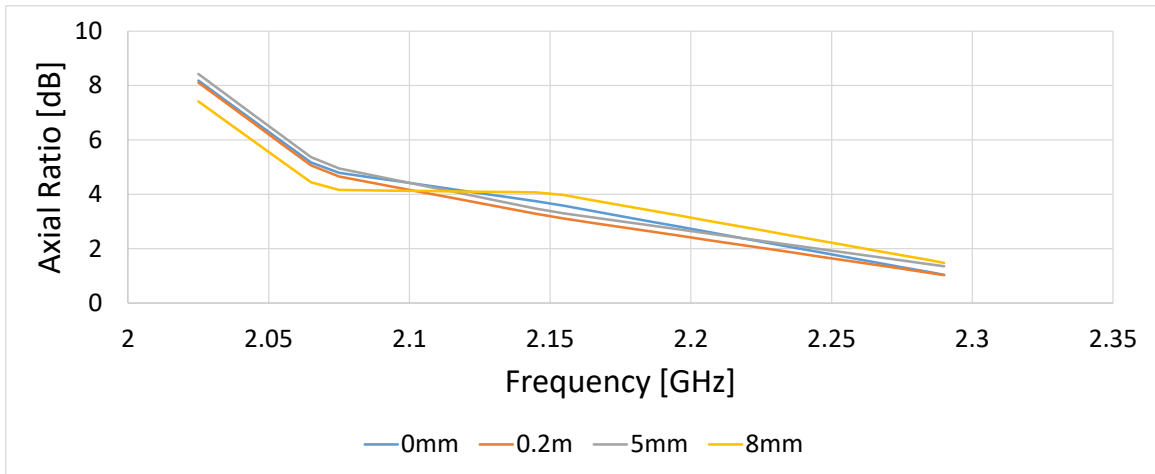


Figure 6.25: Axial Ratio vs Frequency in Operation Band for Different Amounts of Removed Ground Plane

Concerning the results within the 2.025 – 2.29 GHz band, the different amounts of removed ground plane had negligible effects on the performance.

An additional manufacturing consideration was related to the SMA connector mounting. A low-cost method was used to connect the SMA to the PCB. This method is explained in more detail in section 7.2.6.2. After connecting the SMA in such a fashion, it was expected to have a slight amount of excess solder present on the driven patch. To account for such a circumstance, a “blob” of conductive material was added to the HFSS model, and its effects were observed in Figure 6.26 and Figure 6.27.

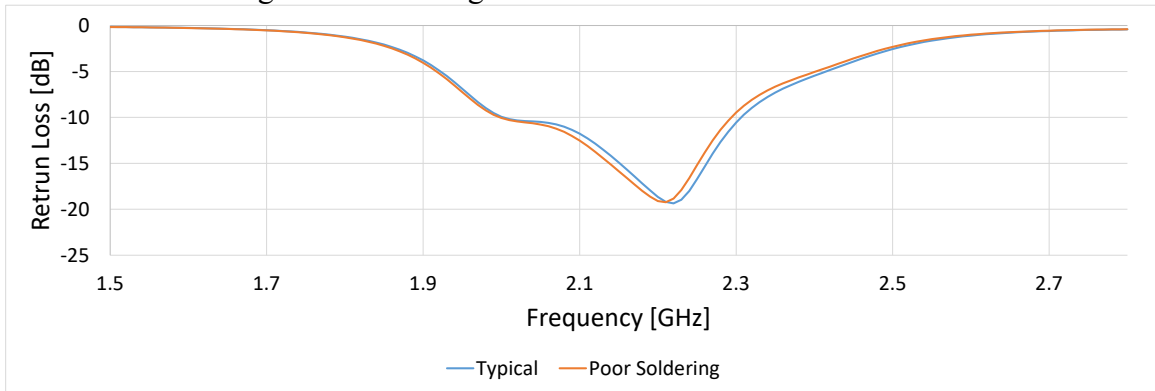


Figure 6.26: Effects of Poor Soldering on Bandwidth

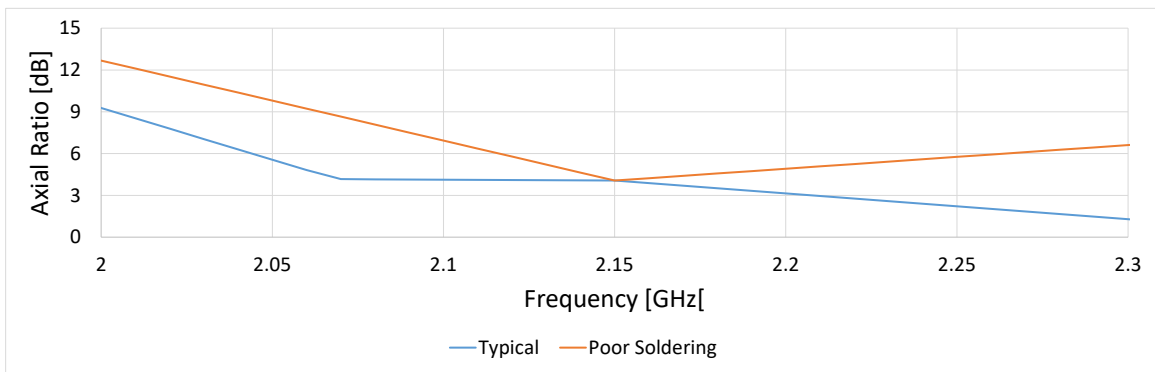


Figure 6.27: Effects of Poor Soldering on Axial Ratio

The effects on bandwidth were minimal as the lump of solder does not impact the geometry of the patches to any significant extent. However, the axial ratio was seen to be impacted as the presence of the solder can impact how the electric fields are generated during transmission. This highlights the importance of quality manufacturing and that flattening the solder improves performance.

## 6.10 PCB Design

The PCB design for the upper and lower patches was done in Altium designer. The process was unconventional but overall, relatively simple. The PCB design process consisted of the following major steps:

1. Export top view of HFSS model as 2D dwg/dxf file
2. Use AutoCAD to modify layer names and remove unneeded layers from drawing file for ease of importing to Altium.
3. Create new project and pcb/schematic files in Altium
4. Import dxf/dwg file to Altium and ensure patch outlines are mapped to top copper layers, board outlines are mapped to a mechanical layer and ground plane outline is mapped to bottom copper layer.
5. Create board outline and board cutouts from 2D board shape
6. Create copper solid regions for patches and polygon pour for ground plane using convert entities from imported CAD lines
7. Obtain manufacturer footprint for SMA connector and create pads on ground plane and non-plated through hole for center conductor.
8. Create solder mask cutouts for radiating patches to ensure copper is exposed
9. Run DRC and Generate Gerber and Drill files (1-layer for upper board, 2-layer for bottom board)

## 7 Design & Prototype

### 7.1 Design Overview

The finalized design is a square stacked patch hybrid feed antenna with corner truncation. It features a smaller lower (direct) patch and larger upper (coupled) patch which are proximity-coupled to facilitate a large bandwidth. An airgap which acts as a low-permittivity dielectric between the upper and lower substrate exists to further tune the patch coupling and increase bandwidth. The lower patch is fed directly via the inner conductor of a female SMA connector in alignment with the project requirements. The finalized HFSS antenna model is shown below in Figure 7.1 and Figure 7.2.

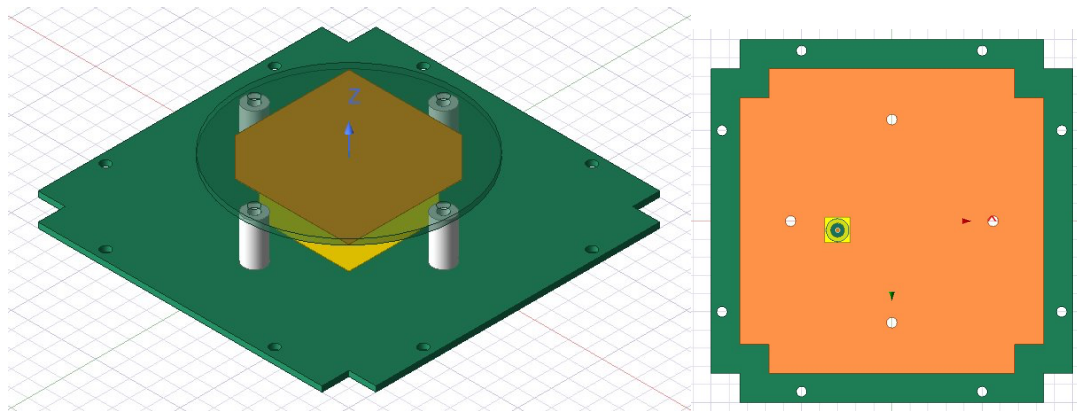


Figure 7.1: Model of Final Design Used for Simulation: Isometric View (Left), Bottom View (Right)

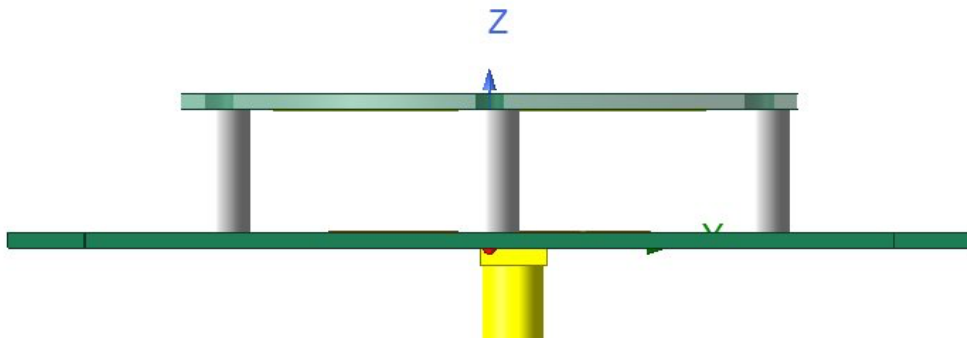


Figure 7.2: Model of Final Design Used for Simulation (Side View)

The design consists of separate PCBs for the upper and lower patches which are mechanically distanced from one another by standoffs. The lower patch is contained on a 2-layer PCB. On its top layer is the exposed lower radiating patch while the ground plane forms the bottom copper layer. A through-hole (THT) female SMA connector is mounted on the bottom side of the lower PCB. The THT SMA center conductor feeds through a non-plated through hole in the board and is soldered to the top patch. The ground pins of

the SMA are shaved down and soldered to surface pads on the bottom ground plane. The fabricated prototype is shown below in Figure 7.3.

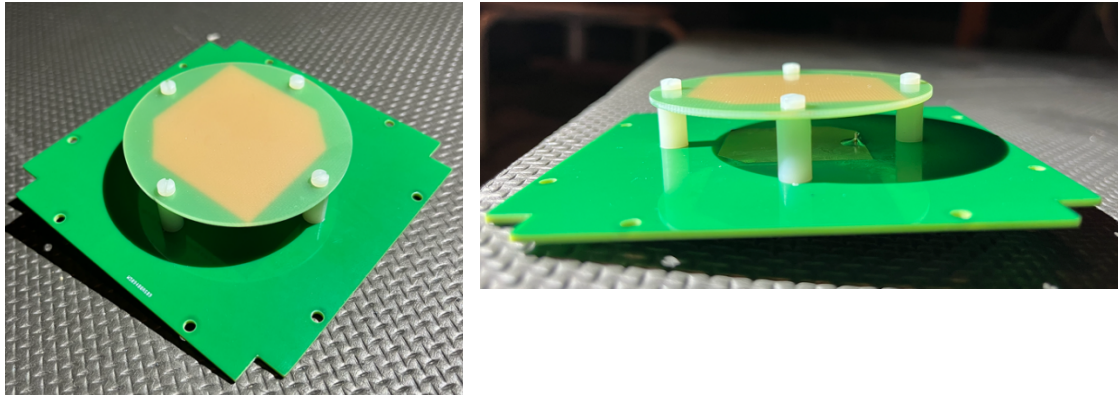


Figure 7.3: Isometric (left) and Side (right) View of Physical Prototype

## 7.2 Key Features

The key features of the design and justification for their implementation in meeting the project constraints are provided in this section:

### 7.2.1 Mismatched Direct and Coupled Patch Sizes

Differing upper (44.8mm) and lower (33.3mm) patch sizes were selected to enhance dual-band operation and increase the overall impedance bandwidth. The main factor underlining the center frequency at which a patch antenna operates is its dimensions. Therefore, offsetting the two patch lengths from each other allowed them to target different center frequencies. In the outlined design, the upper patch 11.5mm larger to extend the range of operation to lower frequencies which helped meet the uplink frequency requirement. Oppositely, the lower patch targeted higher frequencies extending the impedance pass band over the downlink transmission frequency range. In the design, a lower return loss was favored in the downlink band to minimize reflection back to the signal generator in the CubeSat.

### 7.2.2 Probe Location Impedance Matching

The input impedance of the antenna was controlled by the feed location of the probe within the patch area. Feeding the patch at its center results in a very low impedance (near  $0\ \Omega$ ) since the electric field is weakest and current is maximum, while feeding the patch at its edge results in a large impedance (near open circuit). Additionally, changing the feed location in the x-plane versus y-plane alters the active dominant mode which can assist dual-mode behaviour to achieve circular polarization. An optimal feed location of  $x = -15\text{mm}$  and  $y = 2.5\text{mm}$  was selected (see Figure 7.4) to achieve an antenna input impedance of near  $50\Omega$  and to increase excitation of the  $\text{TM}_{010}$  mode.

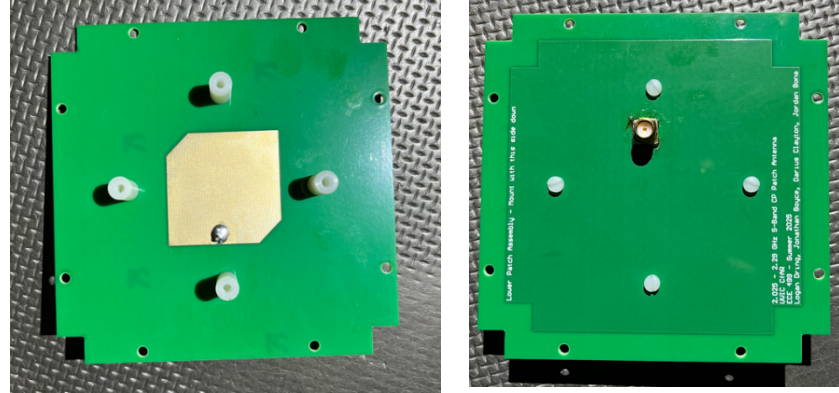


Figure 7.4: Top (right) and Bottom (left) of Bottom Board

### 7.2.3 Large Air Gap

A large air gap acting as a low permittivity dielectric between the radiating patches was required to achieve the frequency range of operation. The airgap height controlled the electromagnetic coupling strength between the upper and lower patches. Increasing the height weakened the coupling strength and induced shallower return loss over a wider frequency range. Oppositely, decreasing the gap height and thus the coupling strength resulted in dual-band with two distinct  $S_{11}$  troughs or narrow-band operation in the extreme case. A very low return loss resulted in a poor axial ratio as primarily the dominant mode was activated. It was found through HFSS simulation that the optimal airgap height was 12.7mm for achieving the outlined impedance bandwidth and low axial ratio.

### 7.2.4 Corner Truncation

Corner truncation was applied to opposite corners of both the top and bottom patch (See Figure 7.5) acting as the main stimulus for dual orthogonal mode activation to achieve circular polarization. Increasing the truncated area promotes stronger dual-mode behaviour reducing the axial ratio but at the expense of decreased impedance bandwidth and poorer overall return loss. A trade off was made between axial ratio bandwidth and impedance bandwidth, with a lower return loss being prioritized over the frequency range. Through HFSS simulations it was determined that the optimal corner truncation was 20% (of the patch area) for the direct fed patch and 25% for the coupled patch. The direct fed patch showed a greater impact on the return loss when trimming the corners which is why its truncation area was scaled back compared to the top patch.

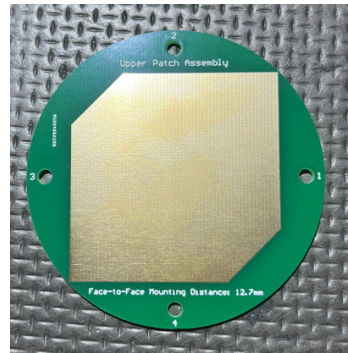


Figure 7.5: Top Board of Physical Prototype

## **7.2.5 Substrate Material**

FR4 ( $\epsilon_r = 4.4$ ) was chosen as the antenna substrate for both the upper and lower patches. In the original project constraints, Rogers 4003C ( $\epsilon_r = 3.55$ ) substrate was specified to be used as the antenna substrate due to its lower electrical permittivity, low-loss tangent, higher efficiency, and overall greater stability for RF applications. However, as the antenna operating frequency range is relatively low in the microwave realm it was found that the antenna performed similarly with FR4 and Rogers 4003C in HFSS simulations. Therefore, FR4 was selected to decrease the overall antenna cost by a significant factor (10x) and reduce the manufacturing time.

## **7.2.6 Mechanical Considerations**

The following mechanical design features were implemented to ensure compliance with CubeSat standards and create a manufacturable product.

### **7.2.6.1 Tuna Can Volume**

To ensure the manufactured patch antenna is compatible with the largest range of CubeSat launch providers, the top patch was modified into a circular shape (diameter of 64mm) within the allowable tuna can height and radius. This allowed the original mechanical height constraint of maximum 5mm to be extended to facilitate a larger air gap.

### **7.2.6.2 SMA Connection Method**

A through-hole female SMA connector was chosen as it was the simplest and cheapest option to solder the center pin of the SMA to the top patch. Using concealed methods such as a blind-via with a surface mount SMA was not feasible given increased manufacturing cost and complexity. A non-plated through hole for the SMA center pin was chosen to ensure isolation between the bottom ground plane and direct-fed radiating patch.

### **7.2.6.3 Copper Surface Finish**

Electroless Nickel Immersion Gold (ENIG) was selected as the copper surface finish for the PCB over the base option Hot Air Solder Leveling (HSAL). ENIG has a superior surface flatness, better corrosion resistance, and a more stable RF performance than HSAL. Though HSAL is widely used for low-frequency standard PCBs, it is common to use ENIG for high-frequency and patch antenna applications.

### **7.2.6.4 Standoff Material**

Non-conductive nylon standoffs were chosen to mechanically distance the upper and lower patch from one another. This non-conductive material was chosen to ensure no effect on the antenna radiation pattern was caused. Nylon was used to keep prototype costs down but should be swapped for a ceramic equivalent for space deployment.

### **7.2.6.5 Mounting to CubeSat**

The exact board outline with precisely placed mounting holes was created in alignment with the mechanical constraints outlined in section 3.

### 7.3 Final Design Parameters

Table 7.1 below summarizes the dimensions and specifications of the prototype.

*Table 7.1: Prototype Design Parameters*

Design Parameter	Value
Direct Patch Dimensions	33.3mm x 33.3mm
Coupled Patch Dimensions	44.8mm x 44.8mm
Copper thickness (both patches)	35µm (1 ounce copper)
Upper Substrate Height	1.6mm
Lower Substrate Height	1.6mm
Upper Substrate Radius	32mm (or 64mm diameter)
Lower Substrate Length x Width	100mm x 100mm
Probe Feed Location (X,Y)	(-15mm, 2.5mm)
Air Gap Height	12.7 mm
Copper Surface Finish	ENIG
Direct Patch Corner Truncation	20% of patch area
Coupled Patch Corner Truncation	25% of patch area
Antenna Substrate	FR4 TG 150-160 ( $\epsilon_r = 4.4$ )
Electrical Interface	Female SMA Connector: SMA-J-P-H-ST-TH1

### 7.4 Performance Parameters

The performance of the prototype described in sections 7.1 and 7.2 was tested either using HFSS simulations, or through use of a VNA in an anechoic chamber. Table 7.2 summarizes and compares these results to the specifications found in Table 3.1 through Table 3.3. It should be noted that all results shown are given for the specified bandwidth of 2025 – 2290 MHz. Further clarification for performance outside the specified band is given in the notes section below.

*Table 7.2: Prototype Performance Parameters*

ID	Parameter	Result	Test Method	Constraint Met?
EE-1	Bandwidth	1.9229 – 2.1786 GHz	VNA	No <sup>1</sup>
EE-2	Substrate Material	FR-4	N/A	Yes
EE-3	Input Impedance	Average: 23.3Ω Spread: 20.54 ±	VNA	No <sup>2</sup>
EE-4	Connector Type	Female SMA	N/A	Yes
EE-5	VSWR	5.51 or better	VNA	No <sup>3</sup>
EE-6	Power	With 5W of RF power, ~22°C of heat is generated	HFSS	Yes
EE-7	HPBW	Average: 83.6°	VNA & Anechoic Chamber	Yes <sup>4</sup>

EE-8	Polarization	Prototype: LHCP	HFSS	Yes
EE-9	Configurable Polarization	PCB was not made to be configurable	N/A	No <sup>5</sup>
EE-10	Gain	6.31 dBi	VNA & Anechoic Chamber	Yes <sup>6</sup>
EE-11	Axial Ratio	Average: 4.58 dB	VNA & Anechoic Chamber	No <sup>7</sup>
EE-12	Efficiency	42%	VNA	No <sup>8</sup>
ME-1	Size	Antenna meets mechanical constraints	3D Model Export	Yes
ME-2	Material Requirements	Antenna contains nylon which does not meet outgassing requirements	N/A	No <sup>9</sup>
ME-3	Weight	46 g	Scale	Yes

- 1 Bandwidth has been shifted down but is 256 MHz wide
- 2 Across the measured bandwidth the impedance is an average of  $28.6 \Omega$  or a spread of  $27.47 \pm 16.66 \Omega$  which is closer to the specifications
- 3 The measured bandwidth from EE-1 was defined by the -10dB crossings of the return loss. This corresponds to a VSWR of 1.92 or better within the band
- 4 Estimated using gain measurements instead of directivity. As such this is a conservative estimate which will be investigated in more detail in section 8.3.2.
- 5 While the actual PCB manufactured is not configurable for LHCP and RHCP. The same design can achieve this requirement by adding another pad for SMA mounting by rotating the position of the SMA connector 90°
- 6 Within the specified band, the gain was as high as 7.8 dBi and as low as 4.8 dBi. For the measured bandwidth, the maximum and minimum gain was 5.87 and 4.63 dBi respectively.
- 7 The axial ratio matched the results of the HFSS simulation at the corner frequencies. Matching the results to a curve like that found from the simulations, the average reduces to 3.32 dB. This axial ratio cannot be claimed in full confidence without extensive testing.
- 8 Efficiency was estimated using the measured  $S_{11}$  parameter multiplied by the simulated radiation efficiency from HFSS. Within the measured band, the measured efficiency was 90% and the radiation efficiency was 79% for a total efficiency of 71%
- 9 The prototype used nylon for cost savings. For deployment in space, ceramic should be used. This topic is covered in more detail in section 6.9.1

## 7.5 Design Shortcomings – Contributing Factors

### 7.5.1 EE-1: Bandwidth

The measured -10 dB bandwidth was centered slightly (~100MHz) lower than the required bands. This downward frequency shift is likely due to fabrication tolerances, addition of

solder mask and copper plating as well as small dimensional deviations in the driven and coupled patch geometry. The solder mask changes the effective dielectric constant and height of the substrate from simulated values which changes the effective electrical length and lowers the resonant frequency.

### 7.5.2 EE-11: Axial Ratio

The antenna did not achieve  $\leq 3$  dB axial ratio across the full operating band. HFSS results show the degradation at the lower band edge is due to the narrow axial-ratio bandwidth inherent to single-feed corner-truncated patches, where orthogonal mode frequencies diverge away from the design point. In the stacked proximity-coupled configuration, frequency-dependent coupling further limits modal overlap, while the FR-4 substrate's higher and less controlled dielectric constant shifts mode balance unfavorably. The chosen probe-feed location was optimized for return-loss bandwidth rather than polarization purity, contributing to the trade-off. At the lower band edge, higher-order and surface-wave effects also disrupt circularity. In practice, manufacturing tolerances, misalignment of the stacked layers, and a solder bump at the probe feed further degraded the measured axial ratio compared to simulation.

### 7.5.3 EE-12: Efficiency

Measured efficiency was 42 %, with an alternate estimate of 71 %. The lower-than-required efficiency is likely due to the higher dielectric loss tangent of FR-4, conductor losses in the feed and patch surfaces, and mismatch losses outside the center of the measured band. The discrepancy between the two reported efficiency values suggests that the measurement setup and calibration contributed to uncertainty, requiring a more controlled test procedure.

## 7.6 Parts Required for Fabrication

This section outlines the parts required for fabrication of one S-band patch antenna prototype unit and breaks down each parts' characteristics.

*Table 7.3: S-band Patch Antenna Required Parts for Manufacturing*

Item	Part	Manufacturer	Manufacturer Part #	Quantity	Description
1	Upper PCB	N/A	N/A	1	1-layer pcb for upper radiating patch. Designed in Altium
2	Lower PCB	N/A	N/A	1	2-layer pcb for lower radiating patch. Designed in Altium
3	Female SMA	Samtec Inc.	SMA-J-P-H-ST-TH1	1	Female Socket SMA Connector, 50 Ohms, Through-hole

					solder PCB, 20GHz Freq limit, threaded
4	Nylon Standoff	Essentra Components	15TSP003	4	Round Female Nylon Standoff Threaded #4/40 12.7mm Length
5	Nylon Machine Screws	Essentra Components	010440F025	8	Nylon Pan-Head Machine Screws, Slotted, #4/40, $\frac{1}{4}$ " length below head

It should be noted that any typically sized  $50\Omega$  THT Female SMA connector would likely be compatible for this design. The standoff height is chosen to meet the air gap height design parameter, and a #4 threaded hole was chosen to match the 3mm hole geometry of the bottom pcb. The nylon machine screws were chosen based on the standoff length and hole size.

## 8 Testing & Validation

This section outlines the physical and simulated tests that were performed to validate the performance of the prototype antenna. Test plans and the results of the tests are presented and compared to the desired results outlined in the design specifications sections.

### 8.1 Physical Test Plans

The following subsections outline the physical tests that were performed using a vector network analyzer (VNA) in the anechoic chamber to determine the performance of our physical prototype antenna.

#### 8.1.1 Bandwidth, Input Impedance, VSWR, and Efficiency Test Plan

Requirement ID(s)	EE-1, EE-3, EE-5, EE-12
Summary Description	Bandwidth shall be 2025 – 2110 and 2200 – 2290 MHz Input Impedance shall be a nominal $50\Omega$ VSWR shall be 1.92:1 or better within bandwidth Efficiency shall be 90% or better within bandwidth
Test Method	VNA One Port
Equipment	Vector Network Analyzer (VNA), Coaxial Cable with SMA Connector, Standard VNA Calibration Kit

#### Setup Procedure:

- Connect the patch antenna SMA connector to port one of the VNA.

- Do a full measurement one port calibration (open, short, and load standard) of the VNA. This is performed to remove systematic errors caused by cables losses or impedance mismatches from the test setup. The indicated calibration standards are terminators or couplers with precisely known magnitude and response. Perform the calibration over a frequency range a few hundred MHz from 1800 – 2300 MHz. This calibration is done via standard VNA Calibration Kit.

#### Test Procedure:

- Measure the device under test's  $S_{11}$  parameter across the frequency range.
- Measure  $Z$  of the device under test
- Convert  $S_{11}$  to VSWR and compare it to the required VSWR.

$$S_{11} = -RL = 20 \log(|\Gamma|) \quad (11)$$

$$VSWR = \frac{1 + |\Gamma|}{1 - |\Gamma|} \quad (12)$$

- Convert  $S_{11}$  to mismatch efficiency and multiply by radiation efficiency from HFSS

$$e_o = e_{cd}e_r = e_{cd(sim)} * (1 - |S_{11}|^2) \quad (13)$$

#### 8.1.2 Half-Power Beamwidth, Gain, and Axial Ratio Test Plan

<b>Requirement ID(s)</b>	EE-7, EE-10, EE-11
<b>Description</b>	Half-Power Beamwidth (HPBW) shall be $60^\circ$ or greater Gain along boresight shall be 6 dBi or greater Axial Ratio within HPBW shall be a nominal 3 dB
<b>Test Method</b>	Anechoic Chamber Measurement, Substitution Method, VNA Two Port
<b>Equipment</b>	Anechoic Chamber, Vector Network Analyzer (VNA), Rotating Positioner, Reference Antenna, Standard VNA Calibration Kit, Coaxial Cable with SMA connector

#### Setup Procedure:

- Mount the antenna under test on a rotating positioner in an anechoic test chamber's test zone.
- Place the receiving antenna at a known fixed distance in the antenna's far-field region within the anechoic chamber.
  - $R > \frac{2D^2}{\lambda}$  where  $D$  = largest dimension of the antenna and  $\lambda$  = wavelength.
- Connect the reference antenna to port one and the antenna under test to port two of the VNA.
- Do a full measurement two port calibration (open, short, load, and through standard). Perform the calibration over the required 2025-2110 MHz and 2200-2290 MHz frequency range.

#### Test Procedure:

- Connect a EMCO 3164-05 antenna to Port 1 of the VNA

- Transmit a known signal with a reference antenna for which the gain is known
- Receive said signal with the antenna under test
- Measure the power received ( $S_{21}$ ) by the antenna under test, transmitting using the reference antenna
- Estimate the antenna gain by reversing the calculation for  $S_{21}$ :

$$S_{21} = G_{ref} - FSPL - \text{Polarization Loss} + G_{ant} [dB] \quad (14)$$

$$\Rightarrow G_{ant} = S_{21} - G_{ref} + FSPL + \text{Polarization Loss} [dB] \quad (15)$$

- Repeat above steps over different orientations of the test antenna
  - $\Theta = [0^\circ, \pm 10^\circ, \pm 20^\circ, \dots, \pm 180^\circ]$
- To estimate HPBW, identify at which angle the gain drops by 3 dB
- Estimate is to be refined later using  $D = \eta G$  where  $\eta$  is the estimated efficiency
- From the measured power received determine the maximum and minimum values and calculate the axial ratio

$$AR = \frac{V_{max}}{V_{min}} = S_{21,max} - S_{21,min} [dB] \quad (16)$$

### 8.1.3 Mass Measurement

<b>Requirement ID(s)</b>	ME-3
<b>Description</b>	The antenna weight shall not exceed 100 grams.
<b>Test Method</b>	Weighing with Scale
<b>Equipment</b>	Calibrated Precision Scale

#### Setup Procedure:

- Stabilize the calibrated scale and tare it.
- Ensure antenna is complete with all components attached.

#### Test Procedure:

- Place the antenna on scale and measure its weight.
- Ensure that the weight of the antenna is below the 100-gram requirement, accounting for the error of the scale.

### 8.1.4 Anechoic Chamber Setup

For many of these tests, the use of an anechoic chamber was mentioned. To measure the parameters of the antenna as accurately and consistently as possible, the antenna, and reference antenna were positioned as shown in Figure 8.1 and Figure 8.2

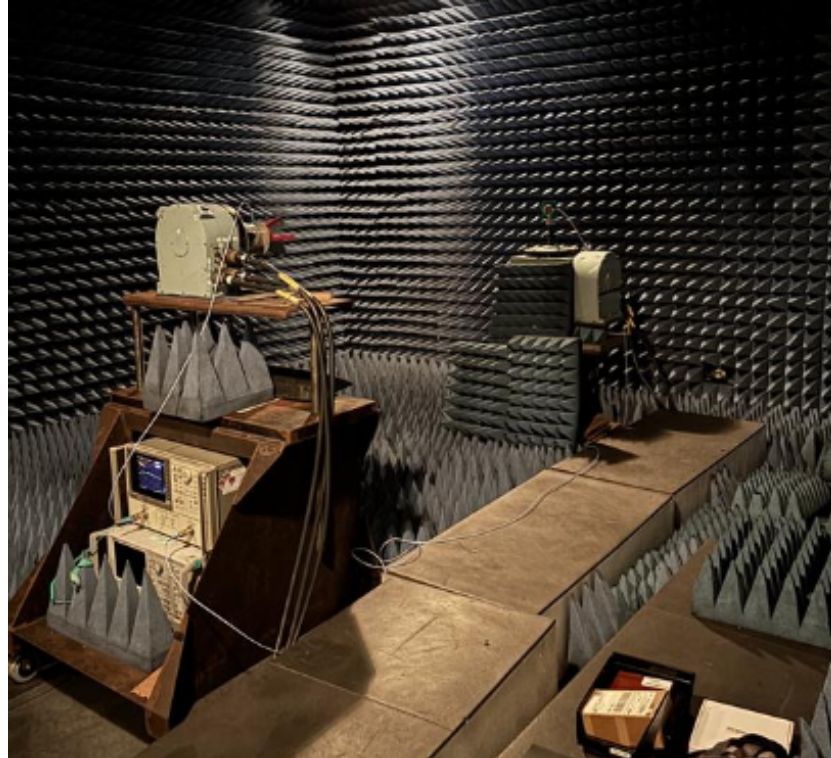


Figure 8.1: Anechoic Chamber Setup Depicting Reference Antenna (Left) and Physical Prototype Antenna (Right) Mounted on Rotating Positioner

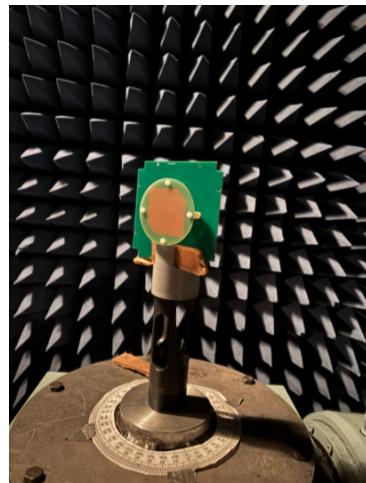


Figure 8.2: Physical Prototype Mounted to Rotating Positioner in Anechoic Chamber

It is important to note that to mount the prototype to the rotating positioner it was necessary to wedge the board in using pieces of cardboard. This made positioning the antenna accurately difficult and likely skewed the test results.

## 8.2 Software Simulations of Final Design

Before production of the PCBs and antenna, the following results of the antenna were obtained through HFSS simulations. Each plot corresponds to a specification from section 3.

Figure 8.3 shows the simulated bandwidth spanning from 1986 – 2303 MHz achieving a 317.5 MHz bandwidth with a minimum return loss at 2215 MHz.

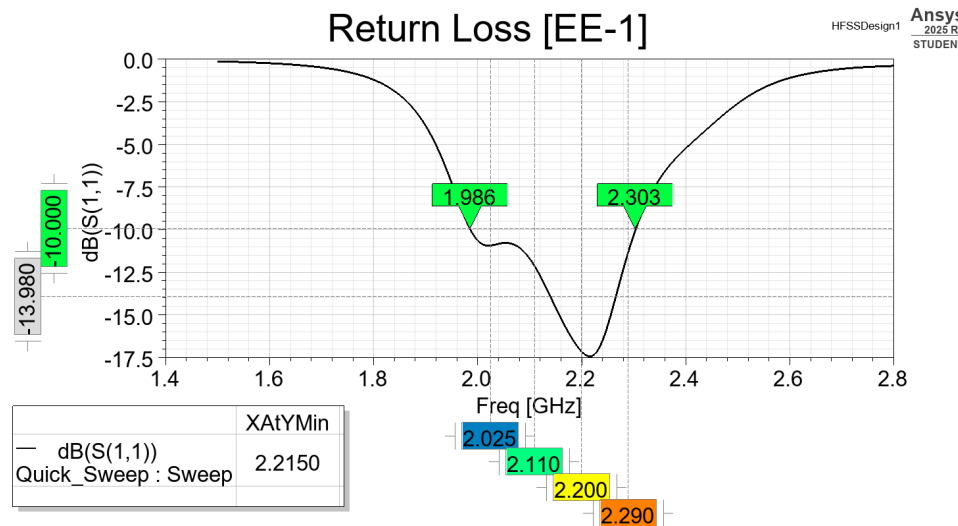


Figure 8.3: Simulated Return loss of Final Design

Figure 8.4 shows that simulated the input impedance of the antenna spans  $52 \pm 18.5 \Omega$  within the operation band.

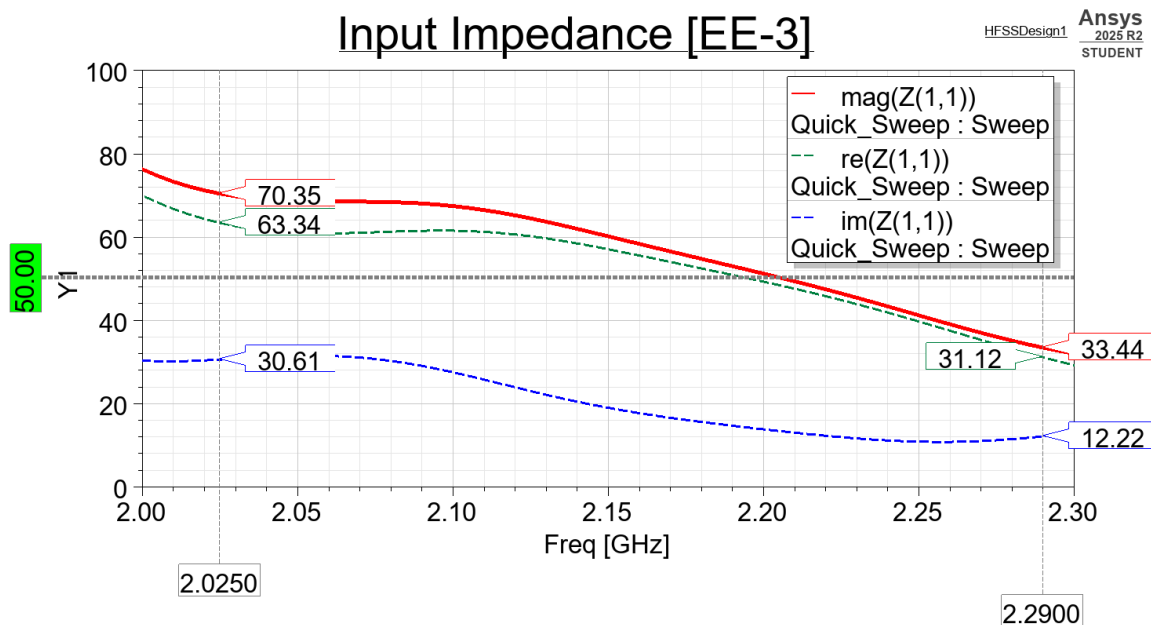


Figure 8.4: Simulated Input Impedance of Final Design

Figure 8.5 shows that within the operation band, the VSWR is 1.8142:1 or better.

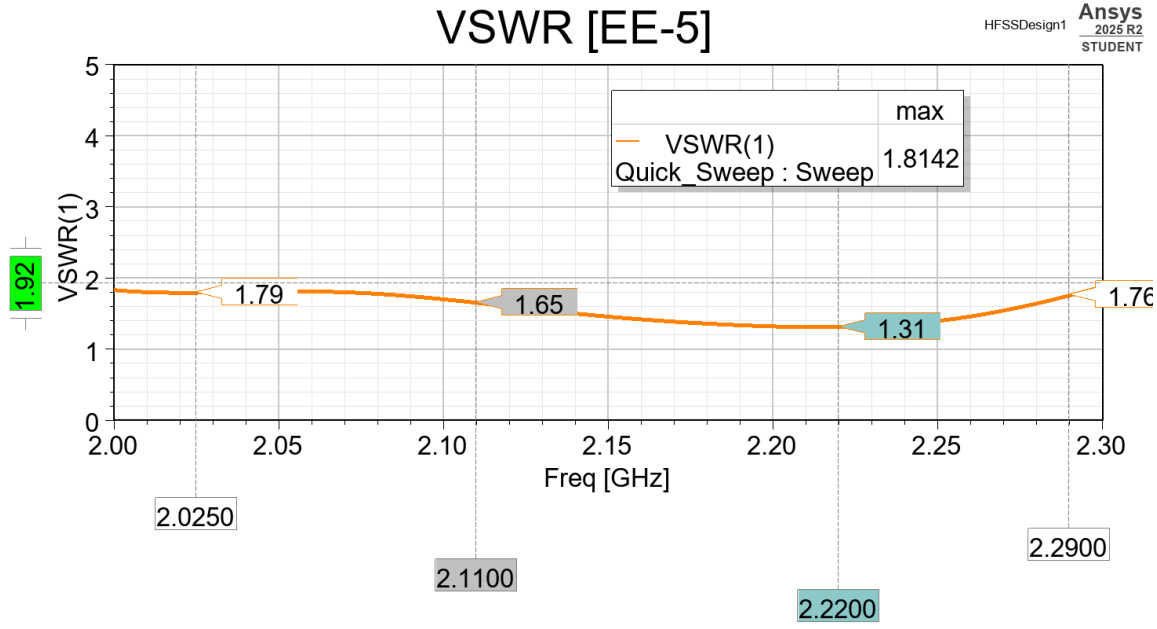


Figure 8.5: VSWR of Final Design

Figure 8.6 shows how the power is dissipated throughout the antenna. In HFSS power is normalized (1 W). The analysis of the power flow was done using the following equations [2]:

$$P_{accepted} = P_{incident} \times (1 - S_{11}) \quad (17)$$

$$P_{radiated} = P_{accepted} - P_{loss} \quad (18)$$

Any heat in the antenna is a result of  $P_{loss}$  being dissipated in the dielectric. Thus, by plotting  $P_{accepted} - P_{radiated}$ , we can infer the amount of power dissipated into the dielectric. Estimating the thermal resistance of FR-4 to be [14]:

$$R_{Th} = \frac{t}{k \times A} = \frac{1.6[m\text{m}]}{0.5 \left[ \frac{W}{mK} \right] \times (100[m\text{m}])^2} = 32 \left[ \frac{W}{K} \right] \quad (19)$$

Thus, we can calculate our worst-case heating using:

$$\Delta T = P_{loss} \times R_{Th} \quad (20)$$

Within the band our worst-case of heating was found to be 22.45°C. This heat is deemed as worst-case as it does not consider convection and radiation of the heat.

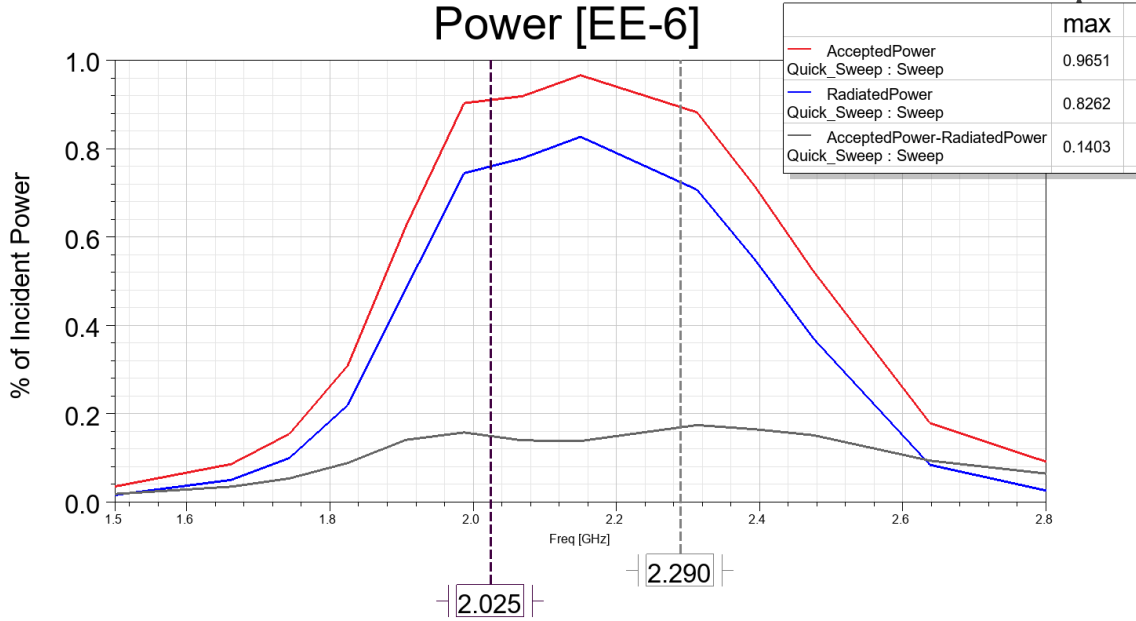


Figure 8.6: Simulated Radiated Power of Final Design

Figure 8.7 shows the directivity over the propagation angle. By taking the maximum directivity and identifying where it reduces by 3 dB, we can measure the simulated half-power beamwidth.

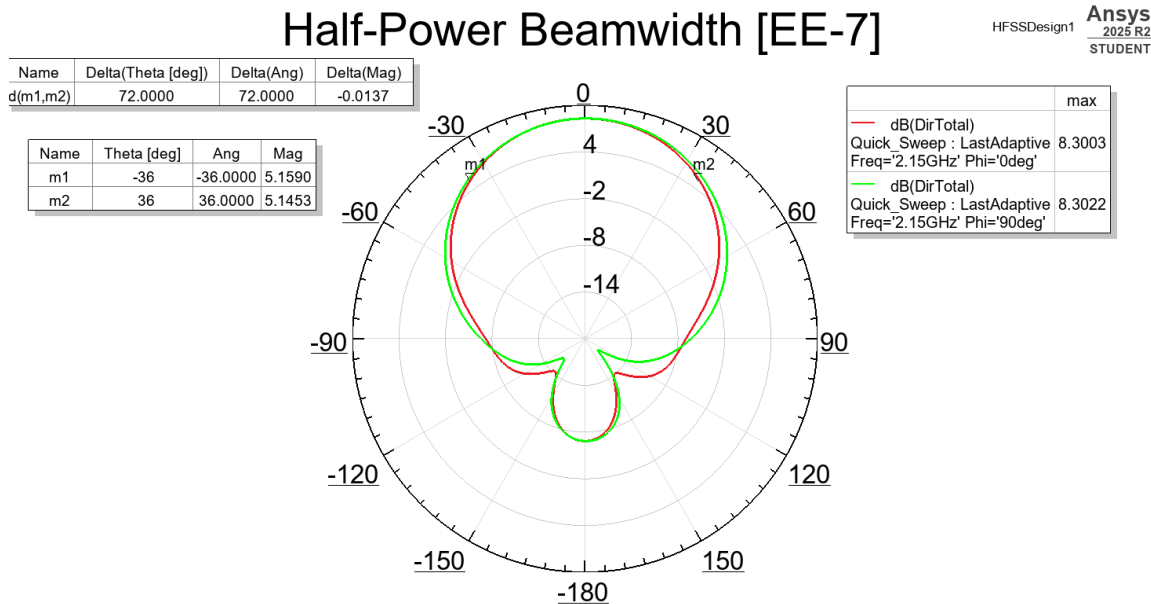
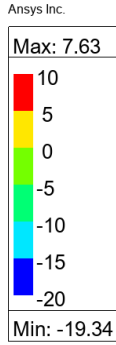


Figure 8.7: Polar Plot of Radiation Pattern Showing HPBW of Final Design

Figure 8.8 and Figure 8.9 show the 3D gain pattern and the 2D gain plot at low, center, and high frequency of the operation band.



## 3D Gain Plot [EE-10]

Ansys  
2025 R2  
STUDENT

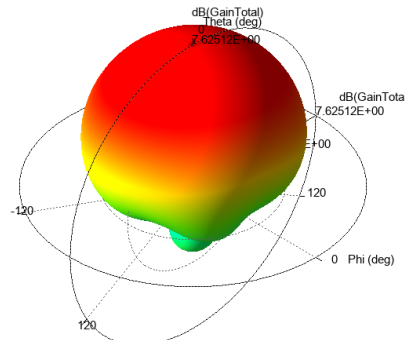


Figure 8.8: 3D Gain Plot of Final Design

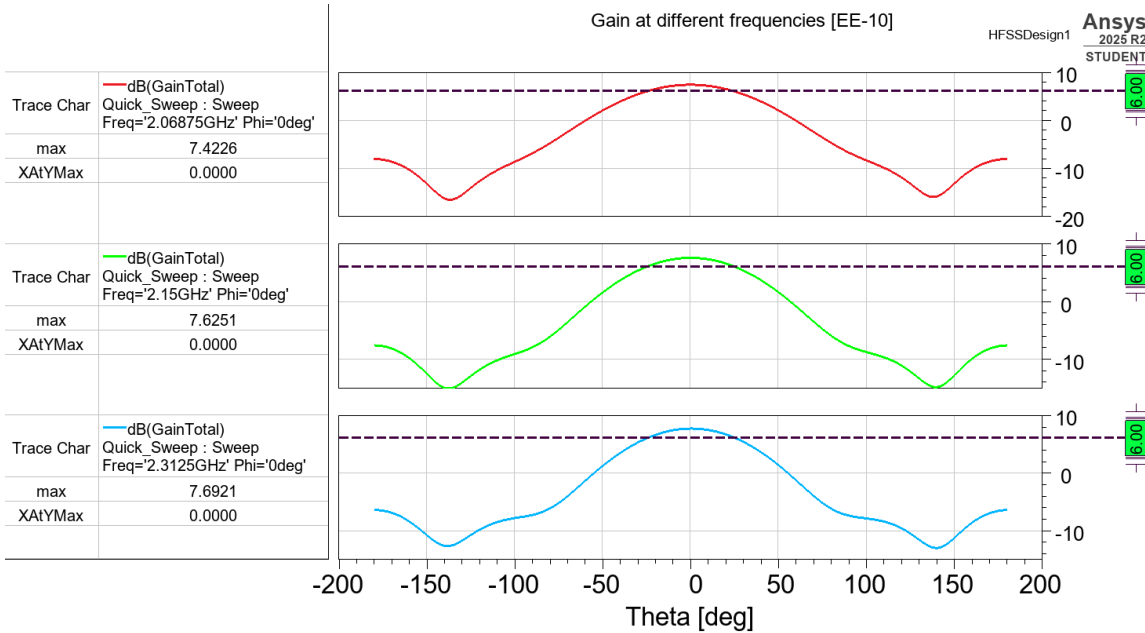


Figure 8.9: 2D Gain Plot of Final Desing at Different Frequencies

Figure 8.10 through Figure 8.12 investigate the polarization of the antenna through the measurement of axial ratio.

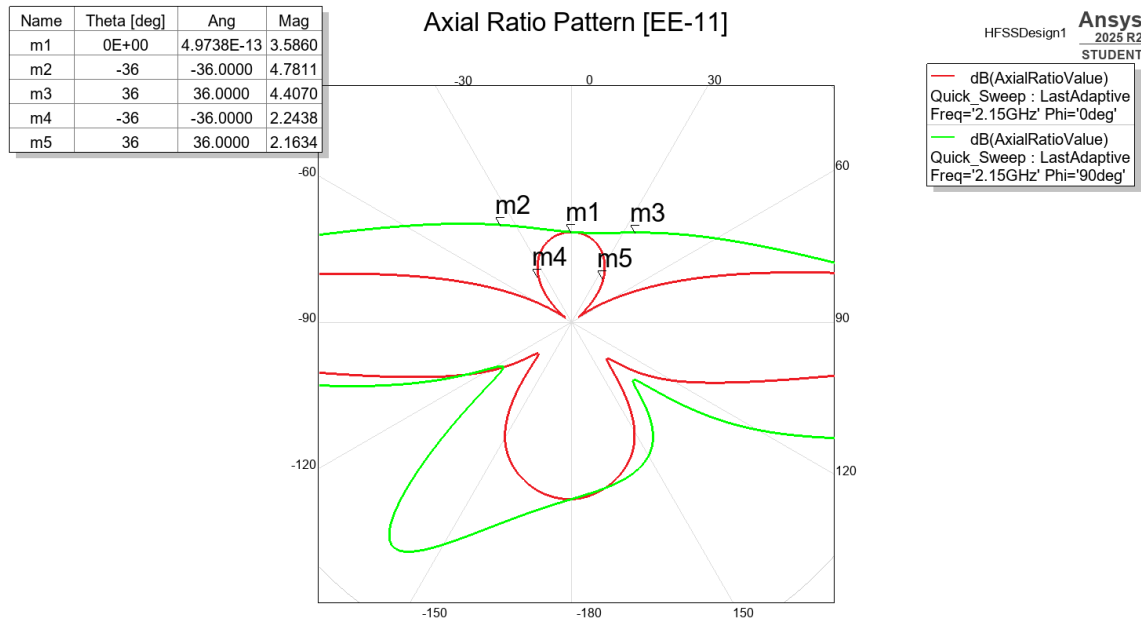


Figure 8.10: Zoomed-In Polar Plot of Axial Ratio of Final Design at 2.15 GHz

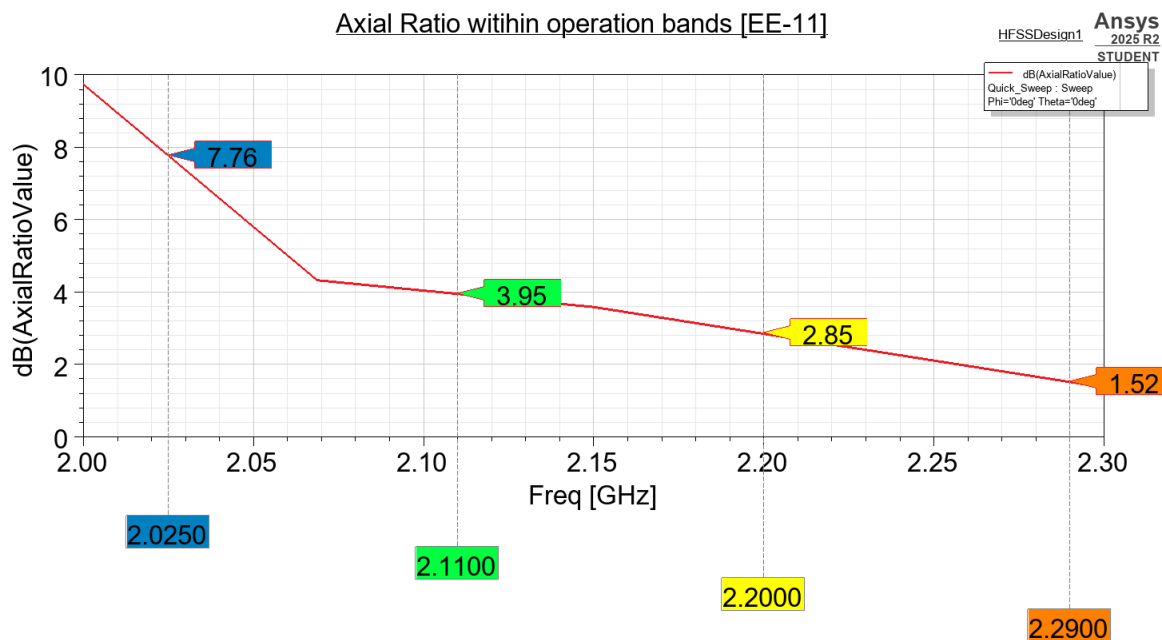


Figure 8.11: Axial Ratio vs Frequency Plot of Final Design

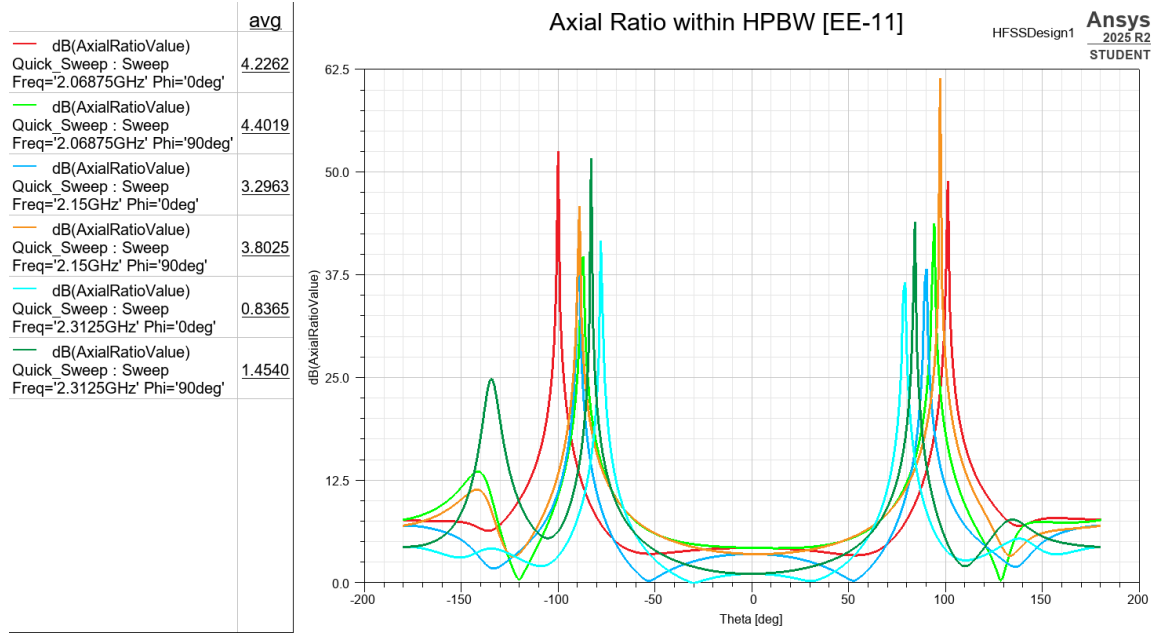


Figure 8.12: Axial Ratio vs Theta Angle Plot of Final Design

## 8.3 Physical Test Results

The following sections present the physical tests results that were performed as per the tests plans outlined in 8.1.

### 8.3.1 Bandwidth, Input Impedance, VSWR, and Efficiency Results

The following results were obtained using the Nanovna V2 Plus4 vector network analyzer outside of the anechoic chamber.

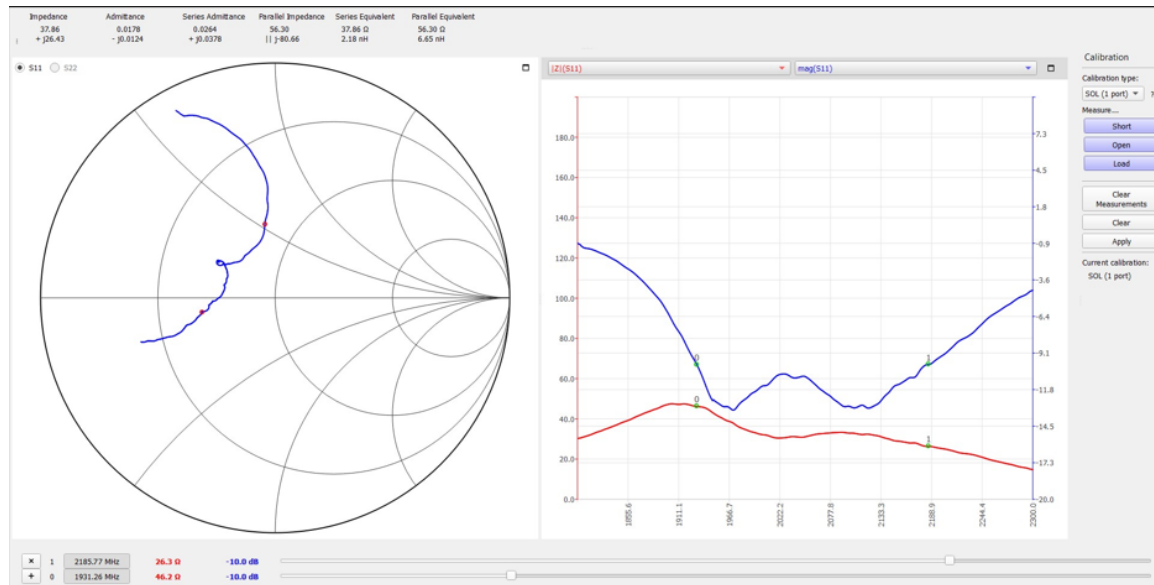


Figure 8.13: Return Loss and VSWR Plots of Physical Prototype

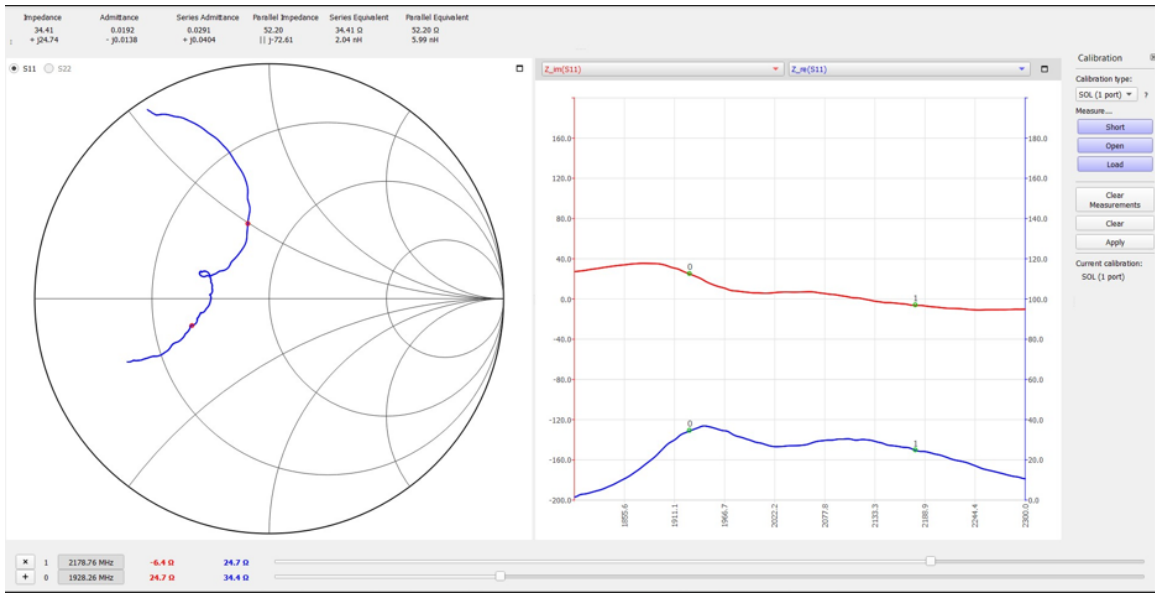


Figure 8.14: Real and Imaginary Parts of Input Impedance of Physical Prototype

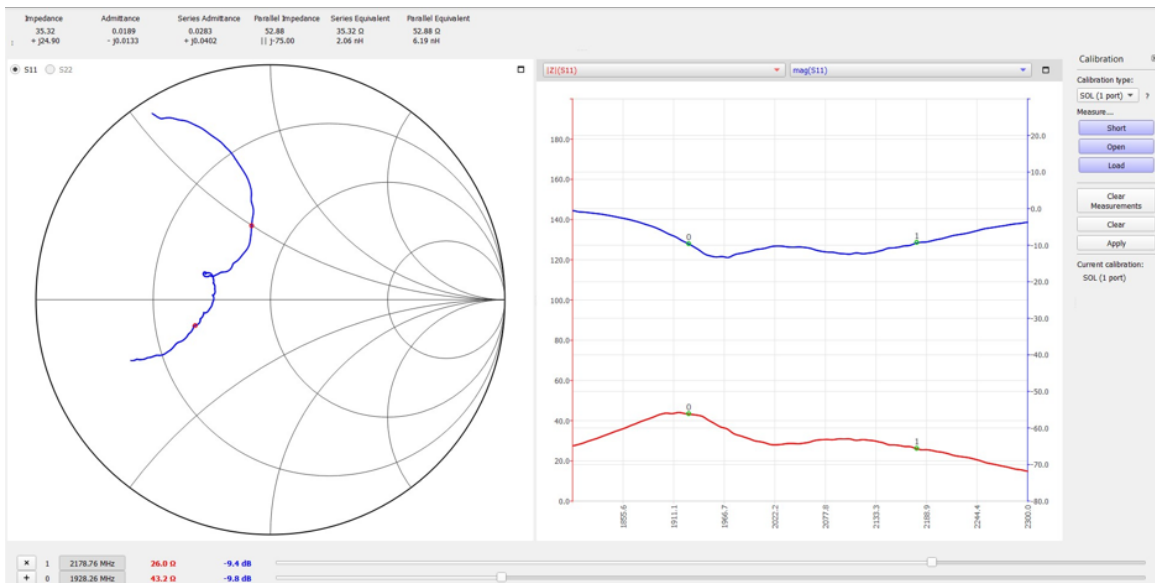


Figure 8.15: Return Loss and Magnitude of Input Impedance of Physical Prototype

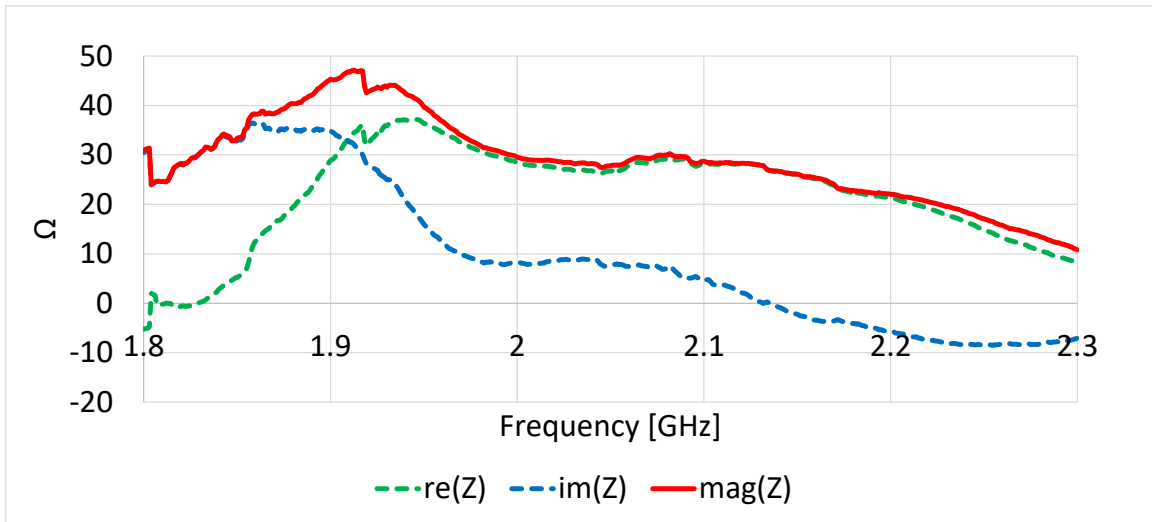


Figure 8.16: Measured Input Impedance of Prototype vs Frequency

Figure 8.17 depicting the return loss was obtained through the use of a separate vector network analyzer in the anechoic chamber.

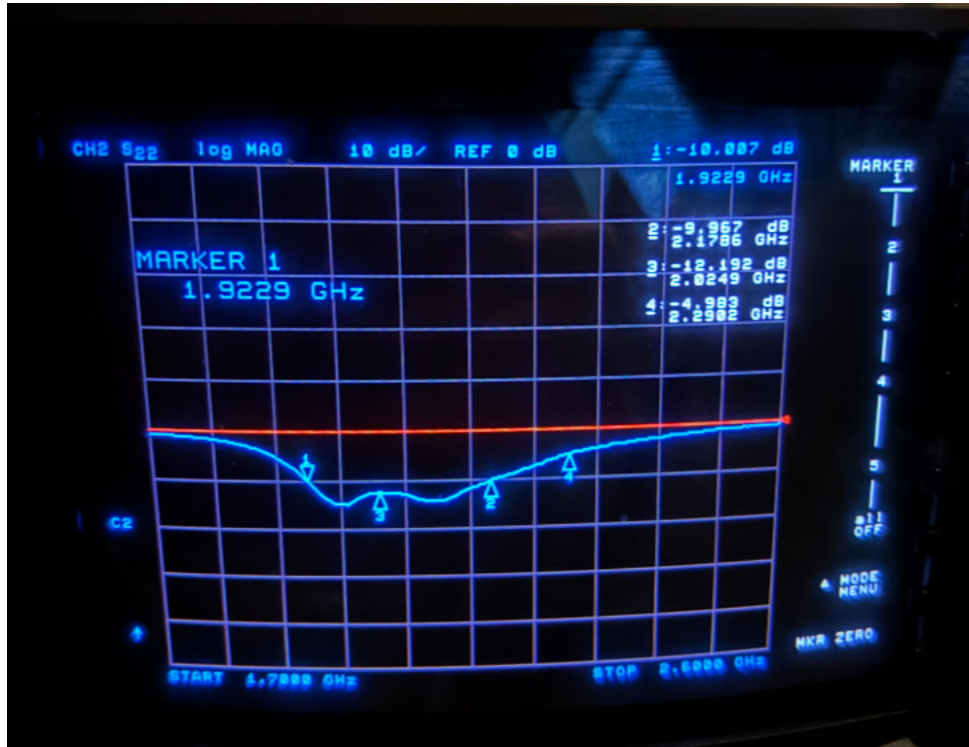


Figure 8.17: Return Loss of Physical Prototype Taken in Anechoic Chamber

Figure 8.18 shows the comparison of the measure bandwidth and the simulated bandwidth. The green area is the desired -10 dB bandwidth while the measured -10 dB bandwidth is indicated with black markers.

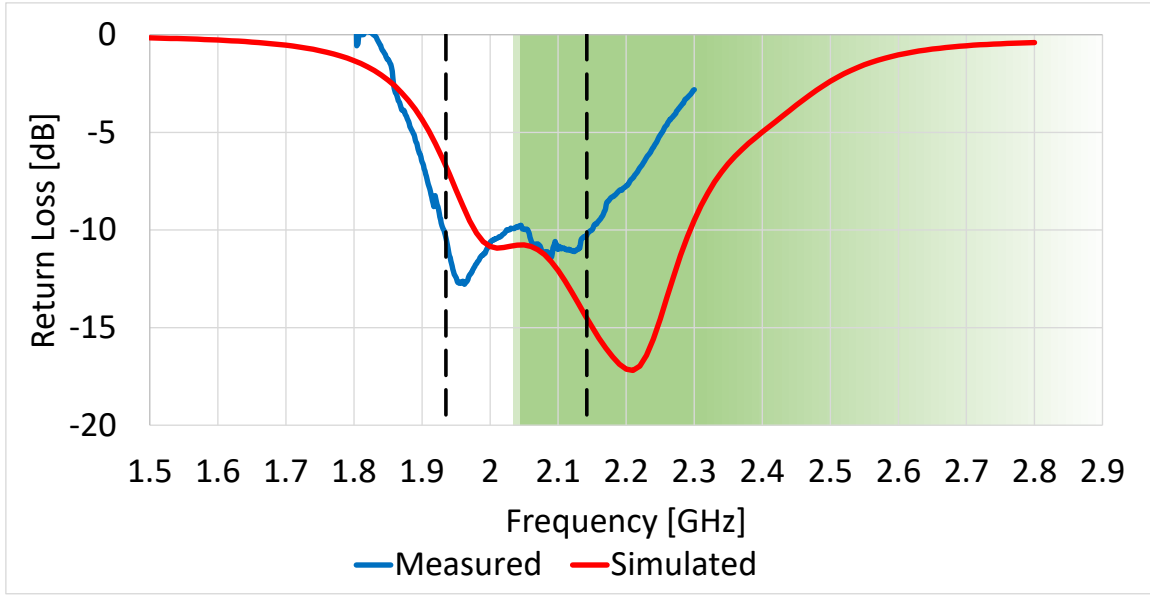


Figure 8.18: Measured and Simulated Return Loss vs Frequency

As mentioned in section 8.1.1, we can determine the mismatch efficiency the measured  $S_{11}$  parameter. However, to get the total efficiency simulation data from section 8.2. After measuring and calculating the efficiencies, the datasets were plotted to create Figure 8.19.

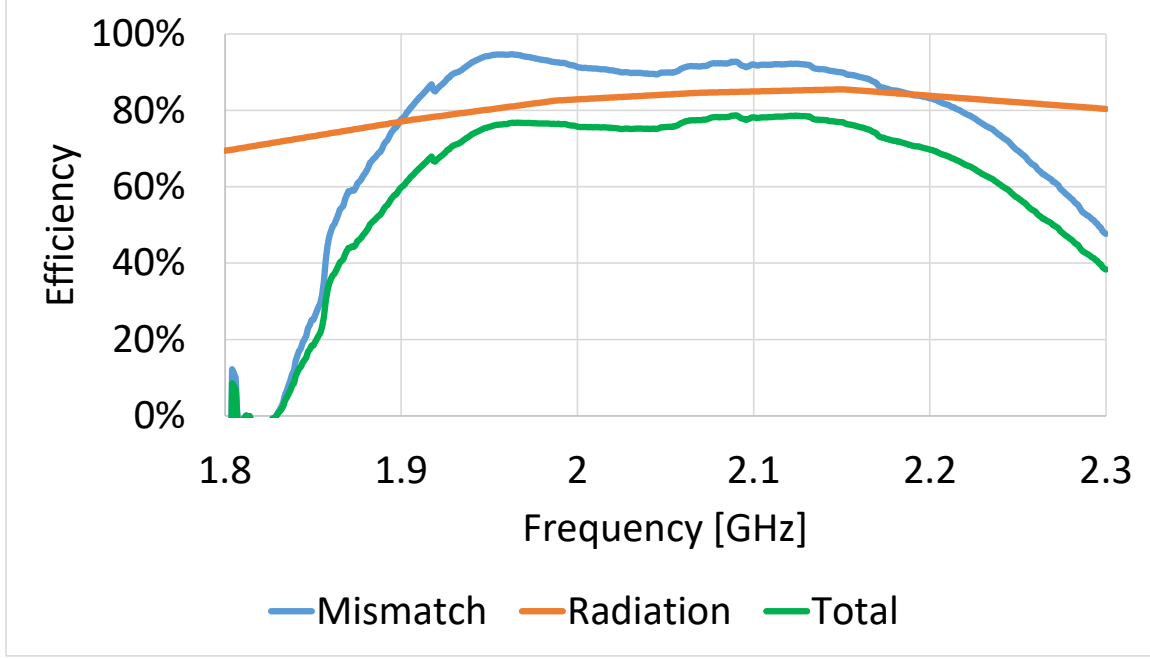


Figure 8.19: Efficiencies vs Frequency of the Prototype

Since the root cause of the difference between the simulated and measured results is the impedance mismatch, the cause of such a drastic mismatch were investigated. Quality issues regarding the SMA connection and the soldering are suspected to have played a role

in this phenomenon. Additionally, it was observed that the input impedance over the entire band was  $< 50 \Omega$  which differs significantly to the simulation data. The un-tested hypothesis for this result is that HFSS underperforms when simulating the impact of capacitive coupling between the two conductors especially at the gap height the prototype was manufactured with.

### 8.3.2 Half-Power Beamwidth, Gain, and Axial Ratio Results

Following the process outlined in section 8.1.2 the following results were obtained. The frequencies of interest were the corner frequencies of the desired bandwidth (2.025 and 2.29 GHz) and the corner frequencies of the measured bandwidth (1.923 and 2.179 GHz).

After measuring the  $S_{21}$  parameter using the VNA, the FSPL needed to be estimated using:

$$FSPL = 20 \log(D [km]) + 20 \log(f[MHz]) + 32.44 \quad (21)$$

at the frequencies of interest. The distance between the reference antenna and the antenna under test was measured to be  $D = 2.2 \text{ m} = 0.0022 \text{ km}$ . Since the transit distance was closer to 3 m than 1 m, the 3 m gain at 2000 and 2500 MHz per

Appendix A: EMCO 3164-05 Calibration Certificate was considered. Using an initial estimate of 3 dB for polarization loss, the gain could now be calculated using the equation from section 8.1.2.

Figure 0.1 and Figure 0.2 show the 2D gain pattern for the measured and desired corner frequencies with the 6 dB goal indicated as well.

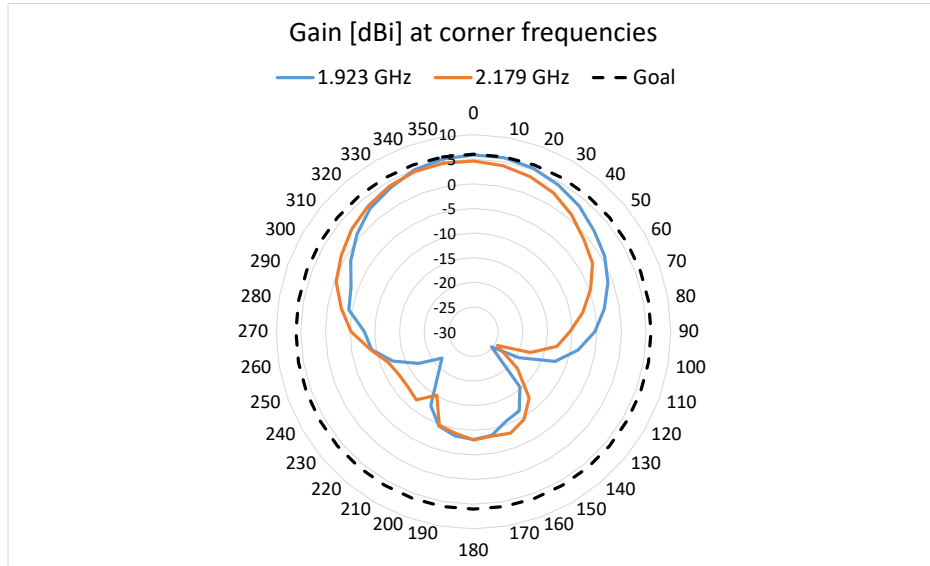
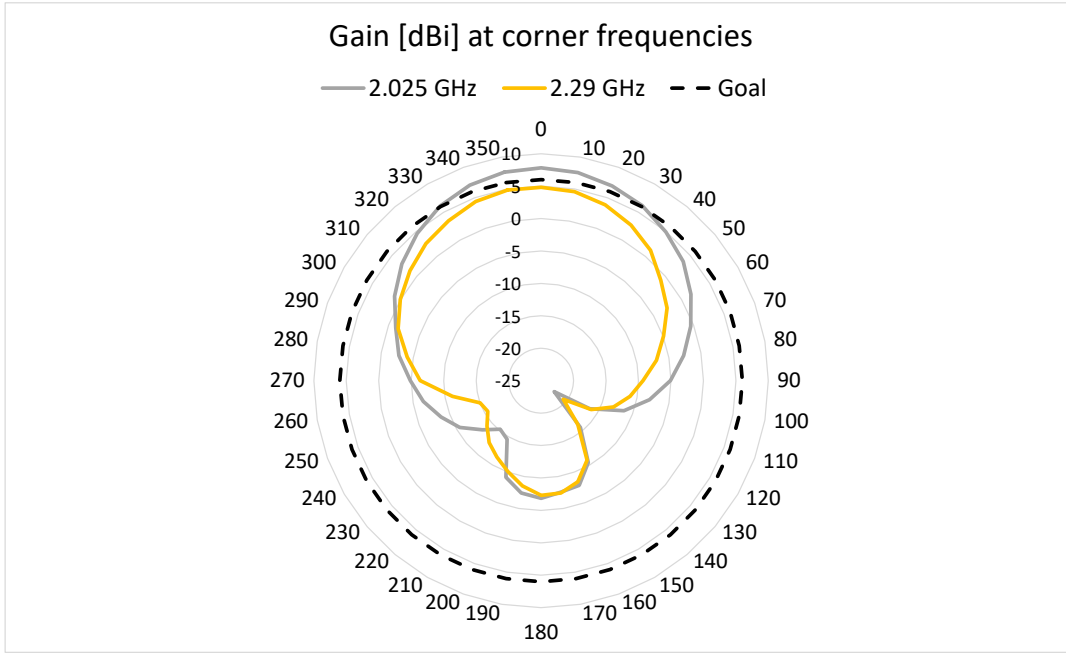


Figure 0.1: Polar Gain Plots for Achieved 10dB Bandwidth Limits



*Figure 0.2: Polar Gain Plots for Desired 10dB Bandwidth Limits*

While in the anechoic chamber, angles at which the gain decreased by 3 dB were recorded yielding the HPBWs found in Table 0.1.

*Table 0.1: Initial HPBW of Prototype*

	3 dB Limits	HPBW
1.923 GHz	43° to -43.5°	86.5°
2.179 GHz	45° to -37.5°	82.5°
2.025 GHz	36° to -49.5°	85.5°
2.290 GHz	34° to -46°	80°

Using the simulated radiation efficiency data of section 8.2 and the  $S_{11}$  data gathered in section 8.3.1, the total efficiency could be calculated and multiplied by gain to determine a directivity estimate and a more accurate HPBW calculation.

Figure 0.3 through Figure 0.6 show the 2D polar directivity plot with each of their half-power circles indicated. Such results were analysed to get a refined measurement of the HPBWs shown in Table 0.2.

Estimated Directivity [dB] at corner frequencies

— 1.923 GHz - - Half-Power

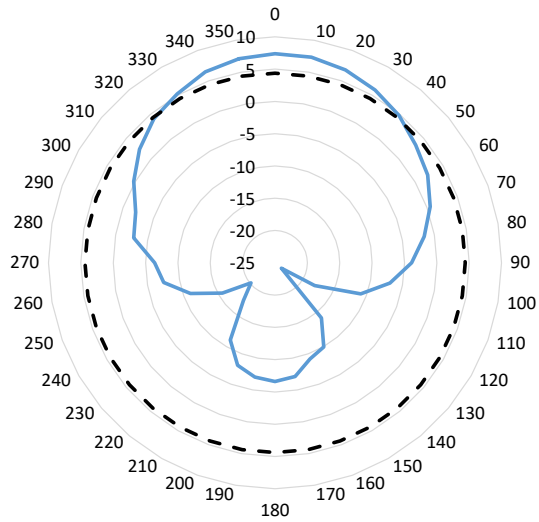


Figure 0.3: Polar Directivity Plot at 1.923 GHz

Estimated Directivity [dB] at corner frequencies

— 2.179 GHz - - Half-Power

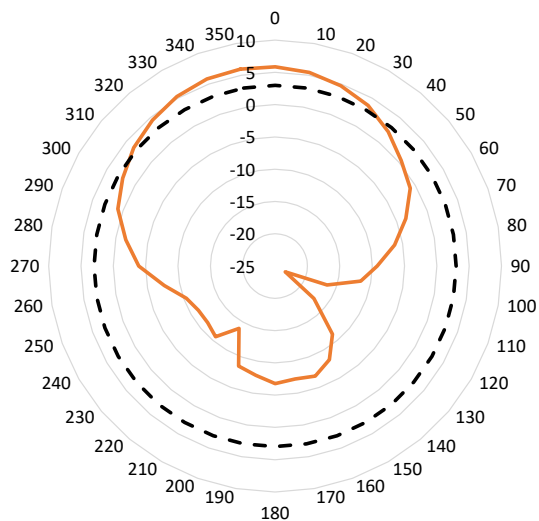


Figure 0.4: Polar Directivity Plot at 2.179 GHz

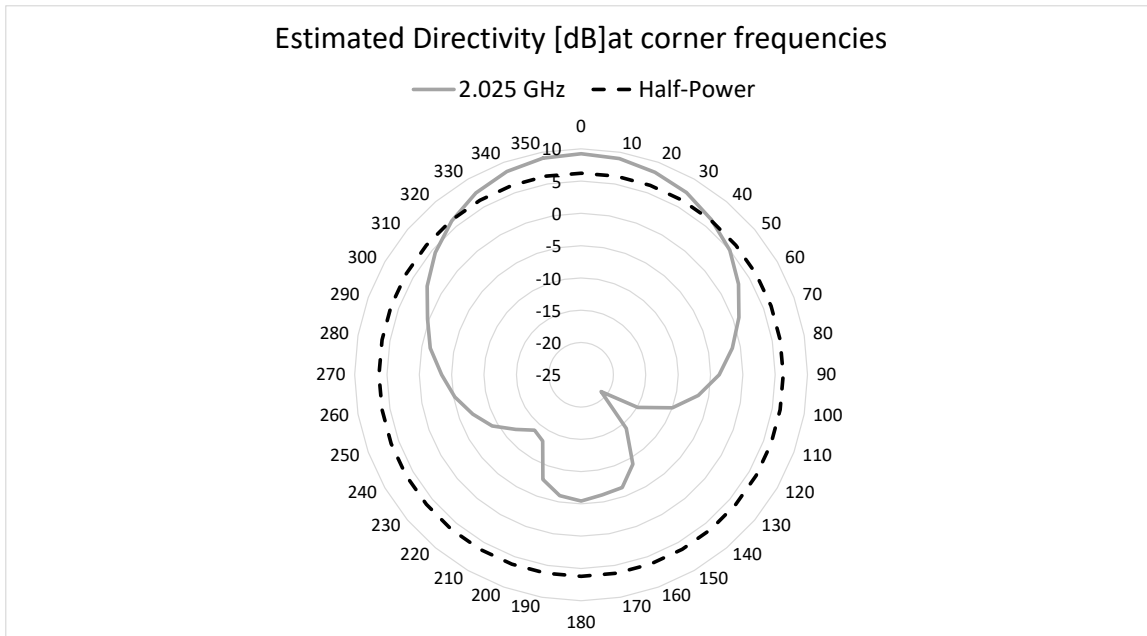


Figure 0.5: Polar Directivity Plot at 2.025 GHz

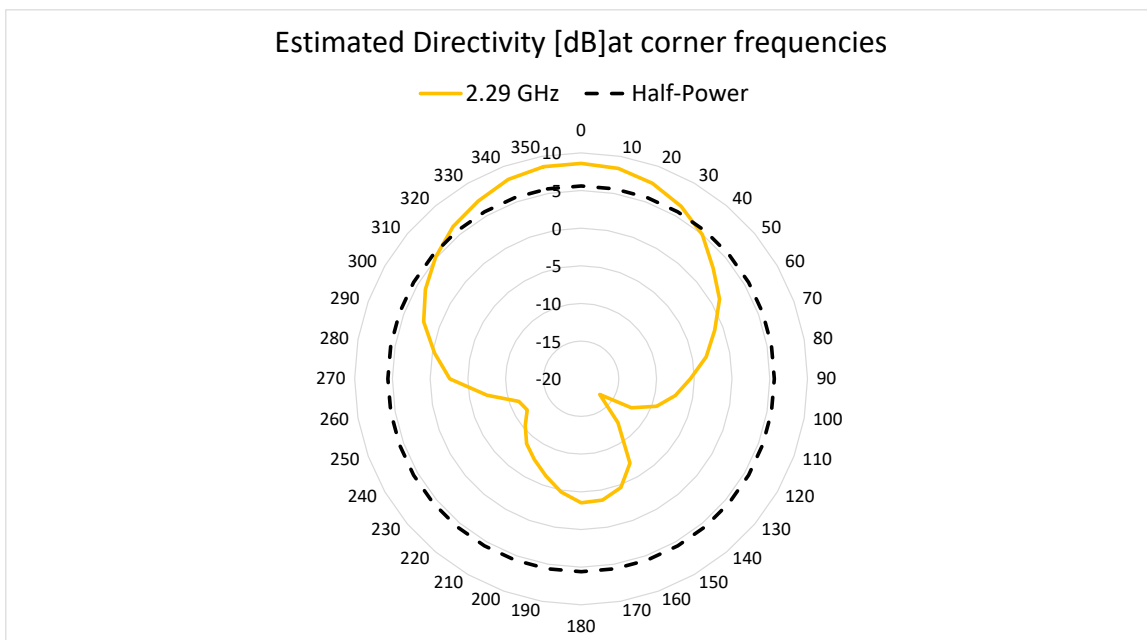


Figure 0.6: Polar Directivity Plot at 2.29 GHz

Table 0.2: Refined HPBW of Prototype

	3 dB Limits	HPBW
1.923 GHz	40° to -35°	75°
2.179 GHz	30° to -50°	80°
2.025 GHz	38° to -38°	76°
2.290 GHz	32° to -44°	76°

Since the reference antenna is linearly polarized, rotating it along its axis allows us to find the maximum, and minimum field strengths from which axial ratio is derived. To compute this, the derivation from section 8.1.2 is used. Results of such calculations have been tabulated in Table 0.3 and plotted in Figure 0.7.

*Table 0.3: Axial Ratio of the Prototype*

	S <sub>21</sub> max [dB]	S <sub>21</sub> min [dB]	Axial Ratio [dB]
1.923 GHz	-32.959	-54.421	21.462
2.179 GHz	-34.329	-40.667	6.338
2.025 GHz	-34.655	-42.421	7.766
2.290 GHz	-37.211	-38.605	1.394

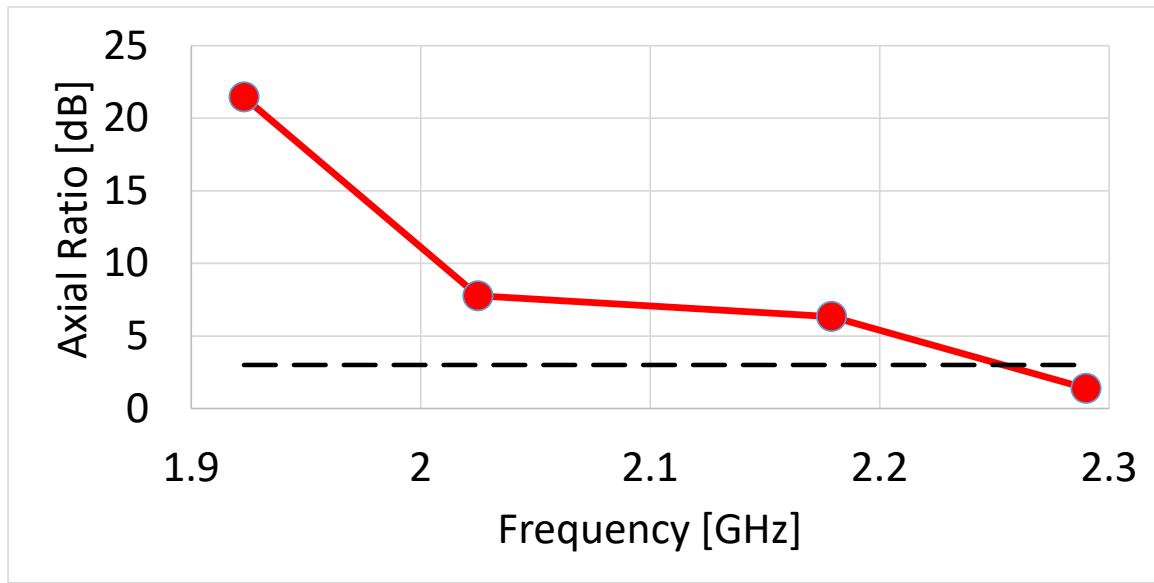


*Figure 0.7: Axial Ratio vs Frequency of the Prototype*

Similar to the simulated results, axial ratio decreases as frequency increases. However, the axial ratio is larger on average than the expected results. This most likely, stems from the geometry chosen. Simply trimming the corners of the patch at 45° does not produce the same quality polarization that complex geometries are able to accomplish.

With the exception of axial ratio, which was discussed above, the results measured in this section reasonably agreed with our simulated data. It was observed that parameters such as gain were minimally impacted by frequency in the simulations, so it stands to reason that the results remained consistent despite the impedance differences mentioned in the previous section.

### 8.3.3 Antenna Weight

The antenna weight in its final assembly was verified with a household mass scale. The overall weight was measured at 46g, shown in Figure 0.8 below, which is well under the maximum antenna weight of 100g outlined in the project mechanical constraints (Section 3).

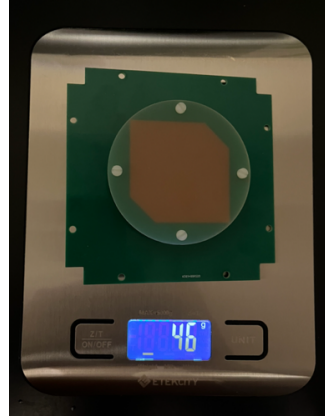


Figure 0.8: Physical Prototype Placed on Scale

## 9 Cost Analysis

The cost analysis for the CubeSat S-band patch antenna project includes both direct costs (purchased materials and fabrication) and indirect costs (labor, facility usage, and other overheads).

### 9.1 Direct Cost Breakdown

Direct costs cover physical materials, manufacturing expenses, and purchased components necessary to design, fabricate, and assemble the antenna prototype. All components were purchased graciously for the project by UVic CFAR.

Item	Quantity	Description	Price per Unit (CAD)	Price Total (CAD)
Lower PCB	5	2-layer FR-4 PCB containing ground plane and driven patch	\$12.16	\$60.81
Upper PCB	5	1-layer FR-4 PCB containing parasitic patch	\$12.16	\$60.81
Standoffs	5	Round Standoff Threaded #4-40 Nylon 0.500" (12.70mm) 1/2" Natural	\$0.57	\$2.87
SMA Connector	10	Female board mount 50Ω SMA connector	\$2.08	\$20.83
Screws	10	#4-40 1/8"long, Slotted Panhead Screws	\$0.09	\$0.87

**Total Direct Costs:** \$146.19

## 9.2 Indirect Cost Breakdown

Indirect costs include labor, consultation, facility use, and other non-material project expenses. Labor costs are estimated at \$50/hour for all standard engineering work. All consultation, anechoic chamber time, and VNA equipment was generously provided free of charge by the University of Victoria and UVic CFAR.

Item	Description	Hours/Qty	Rate (CAD)	Total Cost (CAD)
Labor – Research & Current Market Analysis	Review of academic literature and commercial CubeSat antenna products to identify performance benchmarks, cost targets, and competitive design approaches.	40	\$50.00/hr	\$2,000.00
Labor – Antenna Modelling	Time spent creating initial and refined HFSS patch antenna models within dimensional constraints.	50	\$50.00/hr	\$2,500.00
Labor – Simulation & Optimization	Parametric sweeps and optimization in HFSS to meet bandwidth and circular polarization targets.	125	\$50.00/hr	\$6,500.00
Labor – PCB Design	Translation of the optimal simulated design into a manufacturable Altium PCB layout.	25	\$50.00/hr	\$1,250.00
Labor - Testing	Measurement and analysis using VNA and anechoic chamber; comparing data with simulations.	25	\$50.00/hr	\$1,250.00
Consultation	Specialist guidance on RF simulation parameters and PCB layout best practices.	10	\$150.00/hr	\$1,500.00
Anechoic Chamber Rental	Facility access for antenna gain, radiation pattern, and polarization testing.	8	\$50.00/hr	\$400.00
VNA Rental	Use of high-frequency Vector Network Analyzer for return loss and impedance measurements.	8	\$25.00/hr	\$200.00

**Total Indirect Costs:** \$15,600.00

## 9.3 ROI Calculation

Assuming a conservative per-unit sale price of the completed S-Band Patch Antenna design of \$3,000.00 and an initial batch of 5 antennas the following ROI calculation was performed:

$$\begin{aligned} \text{Total Revenue} &= \$2,500.00 \times 5 = \$12,500.00 \text{ CAD} \\ \text{Total Project Cost} &= \$146.19 + \$15,600.00 = \$15,746.19 \text{ CAD} \end{aligned}$$

$$ROI = \frac{\text{Total Revenue} - \text{Total Project Cost}}{\text{Total Project Cost}}$$

$$ROI \text{ of Initial Production} = \frac{\$12,500.00 - \$15,746.19}{\$15,746.19} = -20.62\%$$

The resulting ROI from the initial production run would be negative due to the bulk of the costs being from research & development. Once the initial indirect costs are accounted for subsequent production runs would have a total manufacturing cost of \$146.19 CAD for the production of 5 antennas yielding a much larger ROI highlighting long term profitability assuming there is a demand.

$$ROI \text{ of Subsequent Production} = \frac{\$12,500.00 - \$146.19}{\$146.19} = 8450.52\%$$

## 9.4 Cost-Reduction Strategies

Throughout the design and prototyping process of the CubeSat S-band patch antenna, several cost-conscious decisions were made to ensure the project remained within the set out by UVIC CfAR without compromising critical performance objectives. The following measures were implemented:

### Through-Hole Vias Instead of Blind/Buried Vias

While blind or buried vias can offer minor layout advantages, they significantly increase PCB manufacturing costs. Through-hole vias were chosen for interlayer connectivity, maintaining manufacturing simplicity and keeping per-board costs low without negatively affecting antenna performance.

### FR-4 Substrate Instead of Rogers

High-Frequency Laminates Rogers substrates are known for their superior dielectric properties at microwave frequencies but are substantially more expensive. For the purposes of this prototype, FR-4 was selected due to its low cost and wide availability. The design was carefully optimized in HFSS to account for FR-4's dielectric constant and loss tangent, ensuring acceptable performance while avoiding the higher cost of specialized substrates.

By employing these strategies, the team was able to achieve a direct cost of only \$146.19 for materials, making the prototype highly cost-effective and supporting a strong projected return on investment (ROI) in future production.

## 10 Conclusion & Recommendations

### 10.1 Conclusion

The project produced a proximity-coupled stacked patch antenna for CubeSat S-band communications. The final prototype met most of the updated electrical and mechanical requirements. It achieved an average measured gain of 6.31 dBi in the main lobe (EE-10) and a half-power beamwidth of 83.6° (EE-7). The design met the CubeSat 1U mechanical interface (ME-1) and mass limit of 100 g, with a measured weight of 46 g (ME-3). It also satisfied the revised impedance and VSWR requirement (EE-3, EE-5) of  $\leq 1.92:1$  (-10 dB return loss) across its measured operating band.

The measured -10 dB bandwidth was 1.9229–2.1786 GHz, corresponding to a fractional bandwidth of approximately 12%. While this meets the updated VSWR requirement, the band is centered below the mission frequencies of 2025–2110 MHz and 2200–2290 MHz resulting in EE-1 not being met. The antenna produced left-hand circular polarization but had an average axial ratio of 4.58 dB, exceeding the  $\leq 3$  dB limit outlined by EE-11. The Measured efficiency was 42 %, with an alternate estimate of 71 %, both below the 90 % requirement of EE-12. Moreover, the prototype used nylon standoffs, which do not comply with NASA outgassing standards for flight hardware (ME-2).

The results confirm the viability of the stacked patch configuration for CubeSat S-band use under revised constraints. Further work is required to shift the operating band to the mission frequencies, reduce axial ratio, improve efficiency, and use flight-qualified materials

### 10.2 Recommendations

To improve upon the current design and prepare it for operational deployment, the following recommendations are proposed:

1. **Enhanced Substrate Selection:** Use of low-loss substrates such as Rogers RT/duroid series to reduce dielectric losses, improve bandwidth, and enhance polarization purity.
2. **Frequency Alignment and Bandwidth Improvement** – Adjust driven patch dimensions, coupled patch dimensions, and air-gap height based on parametric sweep results to shift the operational band upward and achieve full coverage of the specified frequency ranges.
3. **Polarization Enhancement** – Improve axial ratio performance through refined corner truncation geometry or by adopting dual-feed or hybrid-coupler techniques to increase polarization bandwidth without excessive return-loss degradation.

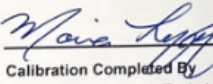
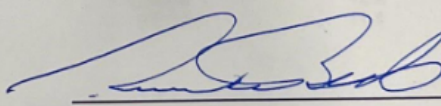
4. **Impedance Matching** – Optimize probe-feed position or incorporate a compact matching network to achieve  $50 \Omega$  nominal input impedance across the target bands.
5. **Efficiency Verification** – Repeat calibrated anechoic chamber measurements with standardized procedures to reconcile the efficiency discrepancy and verify repeatability.
6. **Flight-Compatible Mechanical Design** – Replace nylon standoffs with low-outgassing materials such as ceramic and validate any material changes through simulation and measurement.
7. **Environmental Qualification** – Conduct thermal-vacuum, vibration, and thermal cycling tests to ensure mechanical integrity and compliance with CubeSat launch and space environment standards.

By addressing these recommendations, the antenna design can be transitioned from a proof-of-concept prototype to a fully qualified flight-ready system, capable of supporting reliable S-band communication in CubeSat missions.

## 11 References

- [1] C. A. Balanis, Antenna Theory: Analysis and Design, Hoboken: John Wiley & Sons, 2016.
- [2] D. M. Pozar, Microwave Engineering 4th ed., John Wiley & Sons, Inc..
- [3] D. R. J. a. N. G. Alexopoulos, "Simple approximate formulas for input resistance, bandwidth, and efficiency of a resonant rectangular patch," *IEEE Transactions on Antennas and Propagation*, vol. 39, no. 3, pp. 407-410, Mar. 1991.
- [4] J.-M. Z. P.-F. L. a. L.-X. X. Jun-Yi Lv, "A Dual-Band Patch Antenna with Combined Self-Decoupling and Filtering Properties and Its Application in Dual/Squad-Band Two-Element MIMO Array," *Sensors*, vol. 24, no. 21, p. 6833–6833, Oct. 2024.
- [5] A. T. a. R. S. C. Chen, "Broadband two-layer microstrip antenna," *1984 Antennas and Propagation Society International Symposium*, vol. 22, pp. 251-254, 1984.
- [6] W. L. S. a. G. A. Thiele, Antenna Theory and Design, Hoboken, NJ: Wiley, 2013.
- [7] K. C. a. J. Mink, "Microstrip Antenna Technology," *IEEE Transactions on Antennas and Propagation*, vol. 29, no. 1, pp. 2-24, Jan. 1981.
- [8] "RO4003C Laminates," [Online]. Available: <https://www.rogerscorp.com/advanced-electronics-solutions/ro4000-series-laminates/ro4003c-laminates>. [Accessed 30 May 2025].
- [9] A. HFSS, "Ansys HFSS 3D high frequency simulation software," 23 Jun 2025. [Online]. Available: <https://www.ansys.com/products/electronics/ansys-hfss>.
- [10] NASA, "State of the Art of Small Spacecraft Technology," NASA, 08 Mar. 2024. [Online]. Available: <https://www.nasa.gov/smallsat-institute/sst-soa/structures-materials-and-mechanisms/>. [Accessed 30 May 2025].
- [11] L. Qian, X. Chen, X. Liu, H. Zhou, H. Wang and M. Hou, "Low-Profile Wideband Patch Antenna Using Even and Odd Modes for 5G Terminal Applications," *IEEE Antennas Wireless Propagation*, vol. 23, no. 8, pp. 2476-2480, 2024.
- [12] J. A. King, "AMSAT-UK," January 2013. [Online]. Available: <https://iaru.amsat-uk.org/spreadsheet.htm>. [Accessed 9 July 2025].
- [13] "Outgassing Database," NASA, 11 July 2025. [Online]. Available: <https://etd.gsfc.nasa.gov/capabilities/outgassing-database/>. [Accessed 15 July 2025].
- [14] PCBONLINE Team, "PCBONLINE," 15 September 2022. [Online]. Available: <https://www.pcbonline.com/blog/pcb-thermal-conductivity.html#2>. [Accessed 10 August 2025].
- [15] K.-L. W. a. T.-W. C. F.-S. Chang, "Low-cost broadband circularly polarized patch antenna," vol. 51, p. 3006–3009, Oct. 2003.

## Appendix A: EMCO 3164-05 Calibration Certificate

	<b>ETS-LINDGREN™</b> An ESCO Technologies Company 1301 Arrow Point Drive Cedar Park, Texas 78613 (512) 531-6498	 Track# J124568 Ltd Cal <input type="checkbox"/> By ML Date 28-Sep-07 Next Cal Due _____ <a href="http://www.ets-lindgren.com">www.ets-lindgren.com</a>
<b>Certificate of Calibration Conformance</b> Page 1 of 5		
<b>The instrument identified below has been individually calibrated in compliance with the following standard(s):</b> SAE, ARP-958 - 2003, Electromagnetic Interference Measurement Antennas; Standard Calibration Method, Society of Automotive Engineers, Aerospace Recommended Practice. Fixed height, three antenna rotation, 1 meter separation. Vertical calibration performed per above listed methodology.		
<b>Environment:</b> Laboratory MTE is maintained in a temperature controlled environment with ambient conditions from 18 to 28 C, relative humidity less than 90%. The instrument under test has been calibrated on an open air test site (OATS) with environment temperature conditions ranging from 0 to 40 C which has no known influences on measurement quality.		
<b>Manufacturer:</b>	EMCO	<b>Operating Range:</b> 2 - 18 GHz
<b>Model Number:</b>	3164-05	<b>Instrument Type:</b> Quad Ridge Horn (Small)
<b>Serial Number / ID:</b>	00066133	
<b>Tracking Number:</b>	J124568	
<b>Date Completed:</b>	28-Sep-07	
<b>Test Type:</b>	1 and 3 meter, Horizontal and Vertical	
<b>Calibration Uncertainty:</b> k=2, (95% Confidence Level)	01m	2 - 18 GHz, +/-0.3 dB
	03m	Horizontal/Vertical - 2000-18000MHz, +/- 1.78/1.73 dB
<b>Test Remarks:</b>	Special calibration: 3 meter horizontal and vertical.	
<b>Calibration Traceability:</b> All Measuring and Test Equipment (M/TE) Identified below are traceable to the National Institute for Standards and Technology (NIST). Calibration Laboratory and Quality System controls are compliant with ISO/IEC 17025-2005.		
<b>Standards and Equipment Used:</b> Make / Model / Name / S/N / Recall Date		<b>Condition of Instrument</b> On Release:
Rohde & Schwarz ZVK Vector Network Analyzer	1127.8651.60	In Tolerance to Internal Quality Standards
Agilent 8722ES Network Analyzer	US39175458	08-Aug-08
	 Attested and Issued on 28-Sep-07 Ronald W. Bethel, Calibration Manager	
<small>This document provides traceability of measurements to recognized national standards using controlled processes at the ETS-Lindgren Calibration Laboratory. Uncertainties listed are derived from the methods described by NIST Tech Note 1297. This certificate and report may not be reproduced, except in full, without the written approval of ETS-Lindgren Calibration Laboratory in accordance with ISO/IEC 17025-2005, QAF 1107 (06/07)</small>		


**Gain and Antenna Factors for Quad Ridged Guide Antenna**

Manufactured by EMC Test Systems

Model Number: 3164-05 Serial Number: 00066133

3.0 Meter Calibration Polarization: Horizontal

1.0 Meter Transmit Height

Frequency (MHz)	Antenna Factor (dB/m)	Gain Numeric	Gain dBi
2000	31.4	3.04	4.8
2500	31.6	4.49	6.5
3000	32.1	5.84	7.7
3500	32.5	7.21	8.6
4000	34.3	6.18	7.9
4500	35.3	6.25	8.0
5000	37.7	4.45	6.5
5500	37.9	5.13	7.1
6000	37.8	6.22	7.9
6500	39.6	4.82	6.8
7000	40.6	4.51	6.5
7500	40.0	5.87	7.7
8000	39.8	6.98	8.4
8500	40.5	6.81	8.3
9000	40.3	8.00	9.0
9500	39.9	9.71	9.9
10000	40.0	10.58	10.2
10500	40.2	11.00	10.4
11000	40.8	10.46	10.2
11500	41.0	10.98	10.4
12000	40.6	13.06	11.2
12500	41.2	12.32	10.9
13000	41.7	12.05	10.8
13500	43.1	9.45	9.8
14000	42.7	10.96	10.4
14500	42.2	13.23	11.2
15000	42.3	13.79	11.4
15500	42.5	14.08	11.5
16000	43.5	11.92	10.8
16500	44.6	9.83	9.9
17000	44.7	10.24	10.1
17500	45.1	9.97	10.0
18000	45.2	10.32	10.1

Specification compliance testing factor (3.0 meter spacing) to be added to receiver meter reading in dB $\mu$ V to convert to field intensity in dB $\mu$ V/meter. Calibrated 19 Sep 07 (DD/MM/YYYY). Calibration per SAE/ARP 958.



## Gain and Antenna Factors for Quad Ridged Guide Antenna

Manufactured by EMC Test Systems

Model Number: 3164-05 Serial Number: 00066133

3.0 Meter Calibration

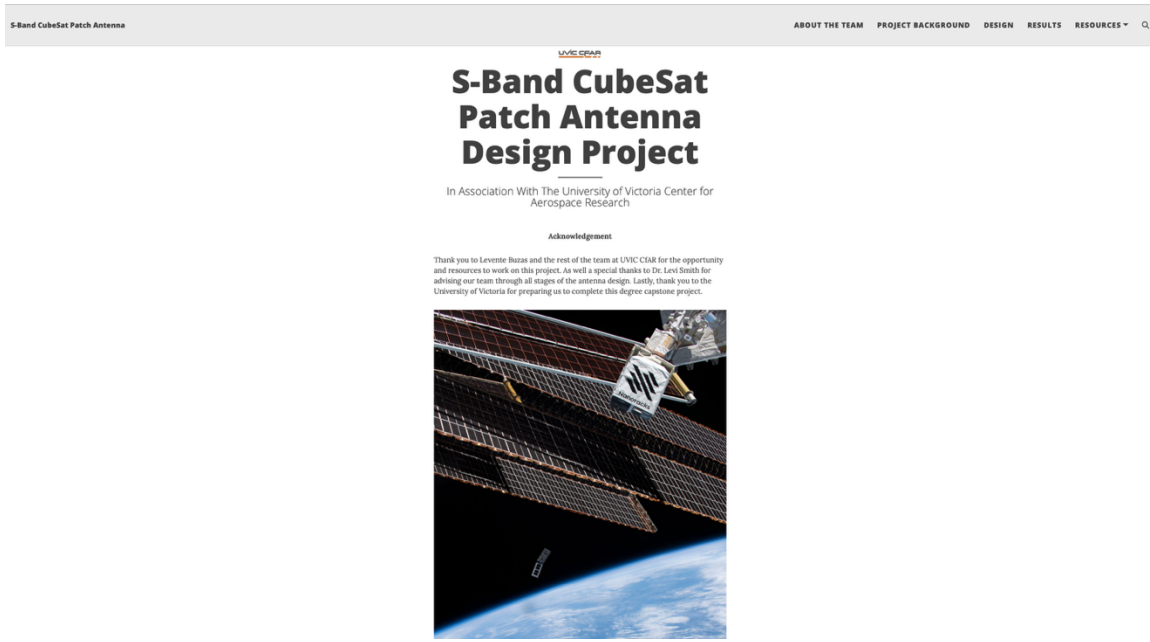
Polarization: Vertical

1.0 Meter Transmit Height

Frequency (MHz)	Antenna Factor (dB/m)	Gain Numeric	Gain dBi
2000	31.5	2.99	4.8
2500	32.5	3.68	5.7
3000	33.2	4.56	6.6
3500	33.8	5.32	7.3
4000	35.3	5.01	7.0
4500	35.6	5.81	7.6
5000	37.2	4.98	7.0
5500	37.5	5.60	7.5
6000	37.3	7.08	8.5
6500	38.1	6.89	8.4
7000	38.5	7.24	8.6
7500	39.6	6.48	8.1
8000	40.4	6.20	7.9
8500	39.7	8.10	9.1
9000	40.0	8.46	9.3
9500	39.2	11.42	10.6
10000	39.6	11.41	10.6
10500	39.9	11.92	10.8
11000	40.3	11.88	10.7
11500	40.7	11.92	10.8
12000	40.4	13.70	11.4
12500	40.7	14.03	11.5
13000	41.0	13.94	11.4
13500	41.9	12.43	10.9
14000	41.7	13.79	11.4
14500	41.8	14.58	11.6
15000	41.7	15.80	12.0
15500	42.5	14.31	11.6
16000	43.2	12.81	11.1
16500	43.9	11.69	10.7
17000	43.6	13.35	11.3
17500	43.9	13.24	11.2
18000	44.6	11.86	10.7

Specification compliance testing factor (3.0 meter spacing) to be added to receiver meter reading in dB $\mu$ V to convert to field intensity in dB $\mu$ V/meter. Calibrated 19 Sep 07 (DD/MM/YYYY). Calibration per SAE/ARP 958.

## Appendix B: Project Website



The project website can be accessed via the following link:

<https://cubesatpatchantenna.github.io>